1. Report No.	2. Government Accession No.	3. Recipient's Catalog No.
FHWA/TX-06/0-1707-4		

4 Title and Subtitle	5. Report Date
QUANTIFY SHAPE, ANGULARITY AND SURFACE TEXTURE OF AGGREGATES USING IMAGE ANALYSIS AND STUDY THEIR EFFECT ON PERFORMANCE	October 2003
	6. Performing Organization Code

7. Author(s)	8. Performing Organization Report No.
Dallas Little, Joe Button, Priyantha Jayawickrama, Mansour Solaimanian, Barry Hudson	Report 0-1707-4

9. Performing Organization Name and Address	10. Work Unit No. (TRAIS)
Texas Transportation Institute The Texas A&M University System College Station, Texas 77843-3135	11. Contract or Grant No. Project 0-1707

12. Sponsoring Agency Name and Address	13. Type of Report and Period Covered
Texas Department of Transportation Research and Technology Implementation Office P. O. Box 5080 Austin, Texas 78763-5080	Technical Report: August 2001 – July 2003
	14. Sponsoring Agency Code

15. Supplementary Notes

Project performed in cooperation with the Texas Department of Transportation and the Federal Highway Administration.

Project Title: Long-Term Research on Bituminous Coarse Aggregate

url:http://tti.tamu.edu/documents/0-1707-4.pdf

16. Abstract

There is a consensus among researchers that the aggregate shape properties affect performance, but a debate has a risen over the suitability of physical tests to quantify the related shape property. Most of the current physical tests are indirect methods of measuring the shape property of aggregates. Also, some of the current physical test methods are laborious and time-consuming, and there is a need for better methods that are accurate and rapid in measuring the aggregate shape properties.

Recent improvements in acquisition of digital images and their analysis provide unique opportunities for describing shape and texture of particles in an automated fashion. Two independent systems are presented for capturing angularity and texture images and are analyzed with the help of the aggregate imaging system (AIMS). The goal is to measure surface properties of both coarse and fine aggregates and relate these properties to performance. In addition, AIMS shape analysis results are compared to other physical tests.

17. Key Words	18. Distribution Statement
Aggregate Shape, Aggregate Texture, Flat and Elongation, Aggregate Angularity	No Restrictions. This document is available to the public through NTIS: National Technical Information Service 5285 Port Royal Road Springfield, Virginia 22161 http://www.ntis.gov

19. Security Classif.(of this report)	20. Security Classif.(of this page)	21. No. of Pages	22. Price
Unclassified	Unclassified	144	

Form DOT F 1700.7 (8-72) **Reproduction of completed page authorized**

QUANTIFY SHAPE, ANGULARITY AND SURFACE TEXTURE OF AGGREGATES USING IMAGE ANALYSIS AND STUDY THEIR EFFECT ON PERFORMANCE

by

Dallas Little
Senior Research Fellow
Texas Transportation Institute

Joe Button
Senior Research Engineer
Texas Transportation Institute

Priyantha Jayawickrama
Associate Professor
Texas Tech University

Mansour Solaimanian
Research Engineer
Center for Transportation Research

and

Barry Hudson
Consultant
Svedala

Report 0-1707-4
Project Number 0-1707
Project Title: Long-Term Research on Bituminous Coarse Aggregate

Performed in cooperation with
Texas Department of Transportation
and the
Federal Highway Administration

October 2003

TEXAS TRANSPORTATION INSTITUTE
The Texas A&M University System
College Station, Texas 77843-3135

Disclaimer

The contents of this report reflect the views of the authors, who are responsible for the opinions, findings, and conclusions presented herein. The contents do not necessarily reflect the official views or policies of the Texas Department of Transportation (TxDOT) or the Federal Highway Administration (FHWA). This report does not constitute a standard, specification or regulation. Additionally, this report is not intended for construction, bidding, or permit purposes. Dr. Dallas N. Little (TX # 40392) is the principal investigator for the project.

Acknowledgments

Special thanks are given to Ms. Caroline Herrera of TxDOT's Construction Division for her assistance in the development of this strategy selection process. We also extend our thanks to the representatives of the Texas Department of Transportation for their assistance in conducting the research and development of this literature review. Thanks also go to the FHWA for its support.

TABLE OF CONTENTS

Page

TABLE OF CONTENTS (CON'T)

Page

TABLE OF CONTENTS (CON'T)

Page

LIST OF FIGURE

Figure **Page**

LIST OF FIGURE

LIST OF FIGURE (CON'T)

LIST OF TABLES

CHAPTER I
INTRODUCTION

A key aspect to the performance of any asphalt mixture is the selection of the materials that will be used in the mixture. Superpave, which is a product of the Strategic Highway Research Program (SHRP), is an acronym for Superior Performing Asphalt Pavements. One of the key components of Superpave is materials selection. Aggregate characteristics are a major factor in the performance of an asphalt mixture. In the Superpave mixture design system several aggregate criteria were included to assure the performance of the asphalt mix (*1*). These criteria included coarse aggregate angularity (ASTM Standard D-5821), uncompacted voids in fine aggregate (Method A of AASHTO Standard T-304), flat and elongated particles (ASTM Standard D-4791), clay content, and gradation parameters. SHRP set the recommended limits on these aggregate criteria which were established based on experience and research.

There is a consensus among researchers that the aggregate shape properties affect performance, but a debate has arisen over the ability of the tests to quantify the related shape properties. Coarse aggregate angularity is determined manually by counting the number of fractured faces. Fine aggregate angularity is obtained from a simple test in which a sample of fine aggregate is poured into a small, calibrated cylinder by flowing through a standard funnel. Gradation is determined through sieve analysis, and clay content must be determined through hydrometer testing.

A proportional caliper is normally used to determine the shape of the aggregate particles: flatness and elongation. Recent experience shows that the fine aggregate angularity test cannot discern quality among aggregates. This is due to the fact that the packing properties of aggregate are not only a function of the angularity, but are also affected by several aggregate properties including surface texture, form, and gradation. Furthermore, Superpave tests for measuring coarse aggregate properties are laborious and limited to the ability to test a representative sample. These tests are also subjective, as they are based on all visual inspection. In addition, the current flat-elongation

determination yields a single index reflecting the proportion of aggregates that exceeds a predetermined average dimension ratio. This method is far less descriptive than a probabilistic method for summarizing the results. Another limitation to the current Superpave aggregate shape tests is that two distinct and unrelated tests are required to measure the angularity of coarse and fine aggregates.

Recently, there have been a number of developments in the field of visual imaging. Also, software has been developed to calculate important aggregate image properties. Electronic, computerized imaging offers a great opportunity to speed aggregates characterization, especially for critical use in Superpave asphalt mixes. Video image-analysis techniques for determining aggregate properties are now viewed as a more viable and cost-effective alternative. They are fast, dependable, and accurate methods. There is an initial cost involved in setting up a system; however, benefits could recover the initial costs (*2*).

OBJECTIVE OF THE PROJECT

The main objective of this project is to evaluate the efficacy of image analysis. Three different systems were used for capturing images, and images were analyzed with the help of Automated Imaging System (AIMS) software (*3*). The researchers identified the following objectives:

1. Quantify angularity, form, and surface texture of both fine and coarse aggregates.
2. Correlate aggregate shape properties as classified by image analysis techniques with performance.
3. Determine whether surface properties characterized with the help of image analysis techniques are superior to physical tests such as fine aggregate angularity, coarse aggregate angularity, and flat and elongated values in terms of their correlation to performance with the goal of eliminating cumbersome and time-consuming tests.

CHAPTER II
LITERATURE REVIEW

INTRODUCTION

Aggregate shape, size and gradation have a great impact on the performance of asphalt concrete *(1)*. The chapter starts by summarizing the importance of aggregate shape in influencing the performance of hot mix asphalt (HMA). Then, it presents image analysis methods used to quantify aggregate shape characteristics. A description of the imaging systems available for capturing images is discussed with emphasis on their ability to analyze the different aspects of fine and coarse aggregate shape.

EFFECT OF AGGREGATE SURFACE PROPERTIES ON HMA PERFORMANCE

Aggregate particles suitable for use in HMA should be cubical rather than flat, thin, or elongated. In compacted mixtures, angular-shaped particles exhibit greater interlock and internal friction, and, hence, result in greater mechanical stability than do rounded particles. On the other hand, mixtures containing rounded particles, such as most natural gravels and sands, have better workability and require less compactive effort to obtain the required density. This ease of compaction is not necessarily an advantage, however, since mixtures that are easy to compact during construction may continue to densify under traffic, ultimately leading to rutting due to low voids and plastic flow *(4)*.

Surface texture also influences the workability and strength of HMA. A rough, sandpaper-like surface texture, such as found on most crushed stones, tends to increase strength and requires additional asphalt cement to overcome the loss of workability, as compared to a smooth surface found in many river gravels and sands. Voids in a compacted mass of rough-textured aggregate usually are higher also, providing

additional space for asphalt cement. Smooth-textured aggregates may be easier to coat with an asphalt film, but the asphalt cement usually forms stronger mechanical bonds with the rough-textured aggregates (*4*).

Thus angular and rough-textured aggregates are crucial to develop interlocking among aggregates in HMA, and accordingly, they are desirable to obtain HMA mixtures that resist permanent deformation and fatigue cracking. On the other hand, the presence of flat and elongated aggregate particles is undesirable in HMA mixtures. Such particles tend to break down during construction affecting durability of HMA.

Superpave identifies aggregate "consensus" properties as critical to the overall performance of HMA pavements. Therefore, these properties need to be carefully monitored while evaluating aggregate quality and performance (*5*).

Consensus properties represent aggregate characteristics that play a key role in the performance of an HMA pavement. Criteria for the consensus properties are based on the anticipated traffic level and aggregate position within the pavement structure. Aggregates near the pavement surface are subjected to high traffic levels and require stringent consensus properties. Critical values for these properties have been recommended based on performance history and field experience. Though the criterion for consensus properties is proposed for an aggregate blend, many consensus aggregate requirements are applied to individual aggregates to identify undesirable elements. The consensus properties include (*5*)*:*

- coarse aggregate angularity,
- fine aggregate angularity,
- flat and elongated particles, and
- clay content in fine aggregate.

Table 1 illustrates aggregate consensus properties that affect performance parameters.

Table 1. Aggregate Properties Influencing Performance (*6*).

HMA Performance Parameter	Aggregate Property
Permanent Deformation Stripping	• Fine aggregate particle shape, angularity, and surface texture • Coarse aggregate particle shape, angularity, and surface texture • Deleterious fines and organic material • Properties of P200 material
Fatigue Cracking	• Fine aggregate particle shape, angularity, and surface texture • Coarse aggregate particle shape, angularity, and surface texture • Properties of P200 material
Frictional Properties	• Coarse aggregate particle shape, angularity, and surface texture • Properties of P200 material • Aggregate gradation (blend)

PHYSICAL TEST PROCEDURES FOR MEASURING THE CONSENSUS PROPERTIES

Uncompacted Void Content of Fine Aggregates (UVC)(ASTM C-1252) (*7*)

Uncompacted Void Content test is an indirect method for measuring fine aggregate angularity (FAA). The test determines percent air voids present in loosely compacted fine aggregate when a sample of fine aggregate is allowed to flow into a small calibrated cylinder through a standard funnel. The diameter of the funnel orifice is approximately 12.5 mm (0.5 inch), and its tip is located 114 mm (4.5 inch) above the top of the

cylinder. This test relates uncompacted void content to the number of fractured faces in an aggregate (*8*).

Air voids present in loosely compacted or uncompacted aggregates are calculated as the difference between the volume of the calibrated cylinder and the absolute volume of the fine aggregate collected in the cylinder. The volume of the cylinder is calibrated and is approximately 100 ml. Absolute volume of the collected fine aggregate is calculated using the dry bulk specific gravity of the fine aggregate. The dry bulk specific gravity of samples is calculated using ASTM C-128. The uncompacted void content of fine aggregate is calculated from the following formula:

$$U = \frac{V - (F / G_b)}{V} \times 100 \qquad (1)$$

Where:

U = uncompacted void content in fine aggregate, %;

V = volume of a calibrated cylinder, ml;

F = mass of fine aggregate in the cylinder; and

G_b = dry bulk specific gravity of fine aggregate.

Uncompacted void content in coarse aggregates can be found similarly as described above (ASTM C-252 or AASHTO T-304) for fine aggregates.

Compacted Aggregate Resistance (CAR) Test (*8*)

This test is an indirect method for evaluating fine aggregate angularity and texture. It measures shear resistance of compacted fine aggregates passing the 2.36 mm sieve in an "as received" condition (*8*). The test evaluates the stability of combined fine aggregate

materials used in a paving mixture. A high stability fine aggregate blend is observed to have a uniform distribution of fines within the sample.

Aggregate samples oven dried to a constant weight passing the No. 8 sieve are used for the test. A 1200 g sample of aggregate is mixed with 1.75 percent water by weight and then placed in a 102 mm (4 inch) diameter Marshall HMA mold. It is then compacted using 50 blows from a Marshall Hammer to prepare a sample approximately 63.5 mm (2.5 inch) high. The sample is subjected to an unconfined compressive load at a rate 50.8 mm/min (2 inch/minute) transmitted through a 37.5 mm (1.5 inch) diameter flat faced steel cylinder on the plane surface of the compacted sample through the Marshall HMA test machine. A plotter plots a graph of sample stability versus flow that is used for interpretation of the stability of the fine aggregate sample. This test is a performance-based test for measuring fine aggregate angularity and is similar to the California Bearing Ratio test (AASHTO T-193) *(8)*.

Flat and Elongated Particles in Coarse Aggregates (ASTM D 4791-99) (*9*,*10*)

ASTM D 4791-99 test method determines percent flat and elongated particles within aggregate samples retained on the No. 4 sieve (4.75 mm) or higher sieves. The test quantifies aggregate particles with a ratio of length to thickness greater than a specified value *(9)*. A proportional caliper device with different sets of openings (2:1, 3:1, and 5:1) is used for measuring aggregate size ratios. Either aggregate mass or a particle count method can determine percentages of flat and elongated particles.

Superpave specifies this aggregate property as a consensus property and has specified guidelines for the maximum percent of flat and elongated (5:1 ratio) acceptable based on traffic conditions. Table 2 illustrates Superpave criteria for maximum flat and elongated particles.

Table 2. Superpave Flat and Elongated Criteria (*2*).

Traffic Million ESALs	Maximum Percent < 100 mm
<0.3	-
< 1	-
< 3	10
< 10	10
< 30	10
< 100	10
> 100	10

Flat and elongated particles tend to break up during construction and under traffic and weaken the aggregate blend, making it susceptible to shear failure, resulting in permanent deformation of the mix. Restricting the percentage of flat and elongated particles in HMA ensures a high degree of internal friction in the aggregate blend, resulting in high shear strength and resistance to rutting (*11*).

A particle count method is used for measuring the amount of flat and elongated particles for a 5:1 ratio to check coarse aggregate shape parameters based on Superpave specifications. The larger opening in the proportional caliper is set equal to the length of the particle. If the particle, when oriented to measure its thickness, can pass completely through the smaller opening of the caliper, it is classified as flat and elongated. The number of flat and elongated particles is counted for each aggregate, and the percentage of flat and elongated particles is then calculated (*9*).

Automated Testing for Flat and Elongated Particles

Automated testing and analysis techniques are versatile tools for characterizing shape parameters of aggregates. Several new automated techniques have been developed and are being used for determining aggregate shape, angularity, surface texture, and size distribution of fines that influence HMA performance parameters (*12*).

Superpave tests for measuring the coarse aggregate shape properties are laborious and their ability to test a representative sample of aggregate is limited (*12*). Moreover, Superpave criterion for flat and elongated coarse aggregate is based only on a 5:1 size ratio and does not represent the various ratios found within aggregate samples (*13*). Thus, it may not be possible to quantify the overall effect of aggregate shape and angularity on pavement performance through this test.

Multiple Ratio Analysis (MRA) Digital Caliper

This device developed by Martin Marietta Aggregates can effectively measure multiple size ratios found within an aggregate sample. Determining various aggregate ratios within an aggregate sample is critical, as it enables proper blending of angular and cubical particles to ensure that the resulting combined gradation passes close to the maximum density line.

The MRA Digital Caliper can evaluate multiple aggregate size ratios at the same time and it restricts flat and elongated aggregate particle in an aggregate blend (*13*). The experimental setup consists of a digital caliper interfaced with an Excel® spreadsheet. The largest and smallest dimension of an aggregate particle can be measured by orienting it in the caliper and these data are entered into the spreadsheet by pressing a foot switch.

The spreadsheet then calculates the ratio and informs the operator which one of the five ratios (<2:1, 2:1 to 3:1, 3:1 to 4:1, 4:1 to 5:1, and >5:1) the particle falls within. Dimension ratios are color coded on the Excel spreadsheet to prevent any errors during evaluation. Once the aggregate sample is separated into the five ratios, the number of aggregates in each fraction is determined and weighed. A weighted average for the total sample is then calculated to determine the proportion of different aggregate sizes in the sample (*13*).

IMAGE ANALYSIS METHODS FOR MEASURING AGGREGATE SHAPE *(3)*

Imaging technology was used recently to quantify aggregate shape characteristics and their relationship to the behavior of HMA. Image analysis looks promising in providing precise data for aggregate shape characteristics *(14)*. A number of parameters have been used to describe aggregate shape, like angularity, form, and texture. Various methods exist, such as Surface Erosion-Dilation Techniques, Fractal Behavior Technique, Hough Transform for analysis of angularity, and Intensity Histogram Method and Fast Fourier Transform Method for analysis of texture. There are some direct measurements of particle dimensions, which will be discussed in this project later. Also, there are several computer-automated systems available commercially for capturing and analyzing images and a handful of others that have developed at research institutions. Some such systems are VDG-40 Videograder, developed by the French LCPC (Laboratorie Ventral des Ponts et Chaussees); Georgia Tech Digital Imaging System; WipFrag and WipShape Systems; Camsizer (German companies of Jenoptik Laser Optik Systeme (GnbH); and Retsch Technology (GmbH) developed this system); and Illinois Image Analyzer (University of Illinois at Urbana Champaign) *(2)*. Also, the researchers in this project used scanning electron microscopy for capturing texture images.

Methods for describing aggregate shape have been categorized into direct and indirect methods *(4)*. Direct methods are those where particle characteristics are measured, described qualitatively, and possibly quantified through direct measurement of individual particles. Indirect methods use measurements of bulk properties to determine geometric irregularities in the particle sample analysis. Indirect methods usually lump aggregate properties together, and are limited in separating the different characteristics of shape.

A summary of direct and indirect methods used in state highway agencies and research studies is shown in Table 3 *(3)*.

Table 3. A Summary of Methods for Measuring Aggregate Characteristics (*3*).

Test or System Name	**References for the Test Method**	Direct (D) or Indirect (I) Method	**Field (F) or Central (C) Laboratory Application**	**Applicability to Fine (F) or Coarse (C) Aggregate**
Uncompacted Void Content of Fine Aggregates	AASHTO T-304	I	F, C	F
Uncompacted Void Content of Coarse Aggregates	AASHTO TP56, NCHRP Report 405, Ahlrich (1996)	I	F, C	C
Index for Particle Shape and Texture	ASTM D-3398	I	F, C	F, C
Compacted Aggregate Resistance	Report FHWA/IN/JTRP-98/20, Mr. David Jahn (Martin Marietta, Inc.)	I	F, C	F
Florida Bearing Ratio	Report FHWA/IN/JTRP-98/20, Indiana Test Method No. 201-89	I	F, C	F
Rugosity	Tons and Goetz (1968), Ishai and Tons (1971)	I	F, C	F
Time Index	Quebec Ministry of Transportation, Janoo (1998)	I	F, C	F
Angle of Internal Friction from Direct Shear Test	Chowdhury et al. (2001)	I	C	F
Percentage of Fractured Particles in Coarse Aggregate	ASTM D-5821	D	F, C	C
Flat and Elongated Coarse Aggregates	ASTM D-4791	D	F, C	C
Imaging Systems				
Multiple Ratio Shape Analysis	Mr. David Jahn (Martin Marietta, Inc.)	D	F, C	C
VDG-40 Videograder	Emaco, Ltd. (Canada), Weingart and Prowell (1999)	D	F, C	C
Computer Particle Analyzer	Mr. Reckart (W.S. Tyler Mentor Inc.), Tyler (2001)	D	C	F, C
Micromeritics OptiSizer PSDA	Mr. M. Strickland (Micromeritics OptiSizer)	D	C	F, C
Video Imaging System (VIS)	John B. Long Company	D	C	F, C
Buffalo Wire Works PSDA	Dr. Penumadu, University of Tennessee	D	C	F, C
Particle Parameter Measurement System	Scientific Industrial Automation Pty. Ltd. (Australia), Bourke et al. (1997)	D	C	F, C
WipShape	Maerz and Zhou (1999)	D	C	C
University of Illinois Aggregate Image Analyzer (UIAIA)	Tutumluer et al. (2000), Rao (2001)	D	C	C
Aggregate Imaging System (AIMS)	Masad (2001b)	D	C	F, C
Laser-Based Aggregate Analysis System	Kim et al. (2001)	D	C	C

DESCRIPTION OF AIMS-AGGREGATE SHAPE INDICES *(3)*

The shape of a particle can be fully expressed in terms of three independent properties: form, roundness (or angularity), and surface texture. The difference between these properties is illustrated in the schematic diagram (Figure 1).

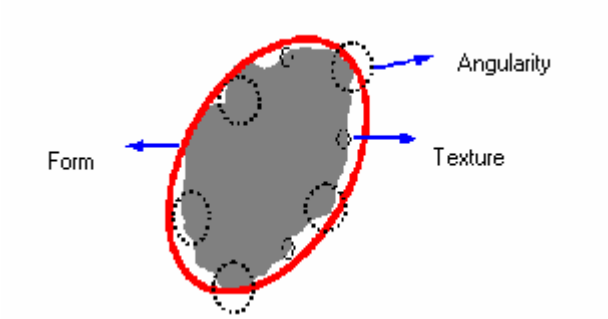

Figure 1. Aggregate Shape Properties: Form, Angularity, and Texture.

Particle Form

Particle form is an index, which is measured by incremental changes in the particle radius in all directions (Masad et al. *(14)*). Radius is defined as the length of the line that connects the particle center to points on the boundary. The form index (FI) is described as the sum of the changes in radius:

$$FI = \sum_{\theta=0}^{\theta=355} \frac{\left| R_{\theta+5} - R_{\theta} \right|}{R_{\theta}} \qquad (2)$$

Where:

R = the radius of the particle in different directions, and

θ = the angle in different directions.

As shown in equation (2), the change in radius is measured every 5 degrees. This increment is selected in order to separate the FI from angularity variations at the surface.

A change on a particle surface that represents angularity has been found to be on the order of 0.075 mm. Based on the analysis, measuring changes in particle radii every 5 degrees minimizes the influence of boundary variations smaller than 0.075 mm on the FI (*14*).

Form factor correlates well with the aspect ratio, which is influenced by overall proportion of a particle (*14*).

Particle Angularity

Angularity is defined as the difference between a particle radius in a certain direction and that of an equivalent ellipse. The equivalent ellipse has the same aspect ratio as the particle, but has no angularity. By normalizing the measurements to the aspect ratio, the effect of form on this angularity index is minimized. Angularity index is expressed as:

$$\mathrm{AI} = \sum_{\theta=0}^{\theta=355} \frac{\left|R_{p\theta} - R_{EE\theta}\right|}{R_{EE\theta}} \qquad (3)$$

Where:

$R_{p\theta}$ = the radius of the particle at a directional angle θ, and

$R_{EE\theta}$ = the radius of an equivalent ellipse at a directional angle θ.

Particle Texture

Available methods for measuring texture rely on measuring particle boundary irregularity captured on a black and white image at high resolution. However, texture details are best captured by analyzing the image in its original gray–scale format (*14*) the surface irregularities range from 0 to 255. This definition allows detailed representation of particle surface texture. Large variation in gray-level intensity is representative of

rough surface texture, whereas a smaller variation in gray-level intensity is representative of a smooth particle.

Fast Fourier Transform is one of the methods by which aggregate texture can be measured.

AGGREGATE SELECTION

The researchers select aggregates that covered almost the entire spectrum of physical test results for image analysis as shown in Table 4. We performed physical tests by Harpreet Bedi and obtained results of these tests from his dissertation "*Development of Statistical Wet Weather Model to Evaluate Frictional Properties at the Pavement-Tire Interface on Hot Mix Asphalt Concrete*" (*6*).

Table 4. Aggregates Selected for Image Analysis Based on Physical Test Results.

Agg #	Producer	Pit	District	Type
1	Marock, Inc.(Now Martin Marietta)	Chambers	Fort Worth	Limestone
2	Valley Caliche	Beck	Pharr	Gravel1
3	Trinity Materials, Inc	Luckett	Waco	Gravel2
4	Brazos River Gravel	Brazos	Brazos	Gravel3
5	Meridian Aggregate (Granite)	Mill Creek, Ok	Paris	Granite1
6	Western Rock Products	Davis, Ok	Childress	Granite2
7	Georgia Granite	Georgia	Georgia	Granite3

PERFORMANCE TESTS

Permanent deformation, physically visible as ruts on the pavement surface, is a primary concern of asphalt mix designers, materials engineers, contractors, and federal, state, and local highway agencies. Permanent deformation problems usually show up early in the mix life and typically result in the need for major repair whereas other distresses take much longer to develop. During the implementation phase of Superpave, wheel-tracking devices have gained a great deal of attention as potential candidates for proof-testing the ability of HMA to resist permanent deformation. There are several different wheel-

tracking devices that are commercially available today. These include the French Pavement Rutting Tester, the German Hamburg Wheel-Tracking Device, (HWTD) and the Asphalt Paving Analysis (APA). These devices are somewhat similar in concept with slight differences in design and operation.

The researchers considered the APA and the Hamburg Wheel-Tracking Device in this project. The Asphalt Pavement Analyzer simulates field traffic and temperature conditions, whereas the Hamburg Wheel-Tracking Device simulates moisture-induced damage along with traffic and temperature conditions. Thus the Hamburg test is more severe and is not for light-duty mixes.

CHAPTER III
IMAGE ANALYSIS SYSTEM

The aggregate imaging system consists of hardware and software. Hardware consists of the image acquisition system, which is different for angularity and texture images. The software used in this project is Aggregate Imaging System *(15)*.

IMAGE ACQUISITION SYSTEM FOR ANGULARITY AND FORM INDEX

The system is a part of the image analysis laboratory in the veterinary school of Texas A&M University and was used for capturing aggregate images for determining surface properties such as angularity index and form index of 0.6 mm sized aggregates. The setup consists of the following components as shown in Figure 2:

- Zeiss Axioplan 2 Microscope with motorized z-stage and DAPI, FITC, Rhodamine, and Texas Red fluorescence filters;
- Ziess Axiophot 2 Camera Module supporting a Hammamatsu C5810 3 chip CCD camera and dual film cameras;
- Macintosh G3 computer;
- Epson Expression 636 scanner; and
- Kodak 8650 PS "photographic quality" thermal dye printer.

Images were captured in a tif format with a resolution of 640 x 480 pixels under a magnification of 2.5 x. These images were captured in gray scale and were then converted to binary images for finding angularity and form index.

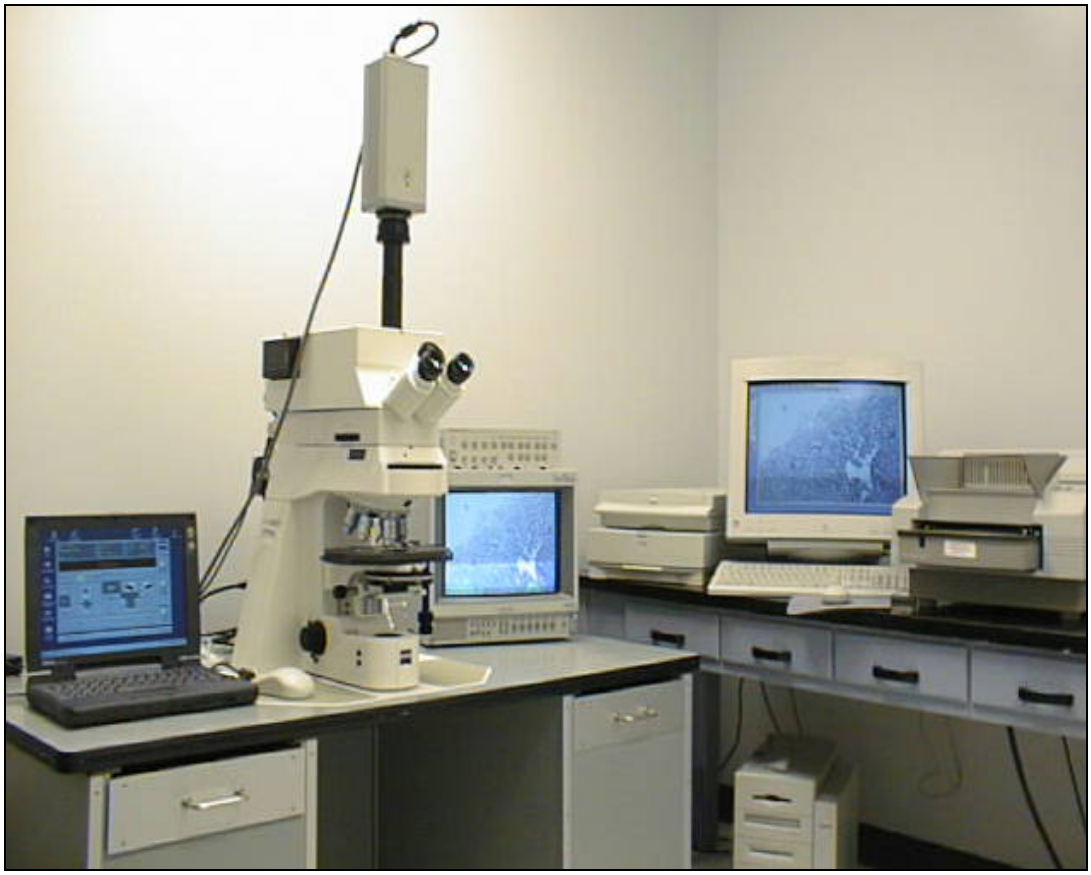

Figure 2. Image Acquisition System for Angularity and Form Index.

IMAGE ACQUISITION SYSTEM FOR TEXTURE INDEX

Scanning Electron Microscope (SEM): The system is a part of the Microscopy and Imaging Center at Texas A&M University. The SEM was selected to measure texture index. The particle size chosen for measuring fine aggregate shape properties was 0.6 mm, which is very small, and it was difficult to study texture of the whole particle under ordinary microscope.

JEOL JSM-6400: This software-oriented, analytical-grade SEM, is capable of acquiring and digitizing images. Acceleration voltages from 0.2 to 40 kV, a magnification range

of 10 to 300,000 x, and a resolution of 3.5 mm allow an operator to achieve excellent results on a wide variety of samples (Figure 3).

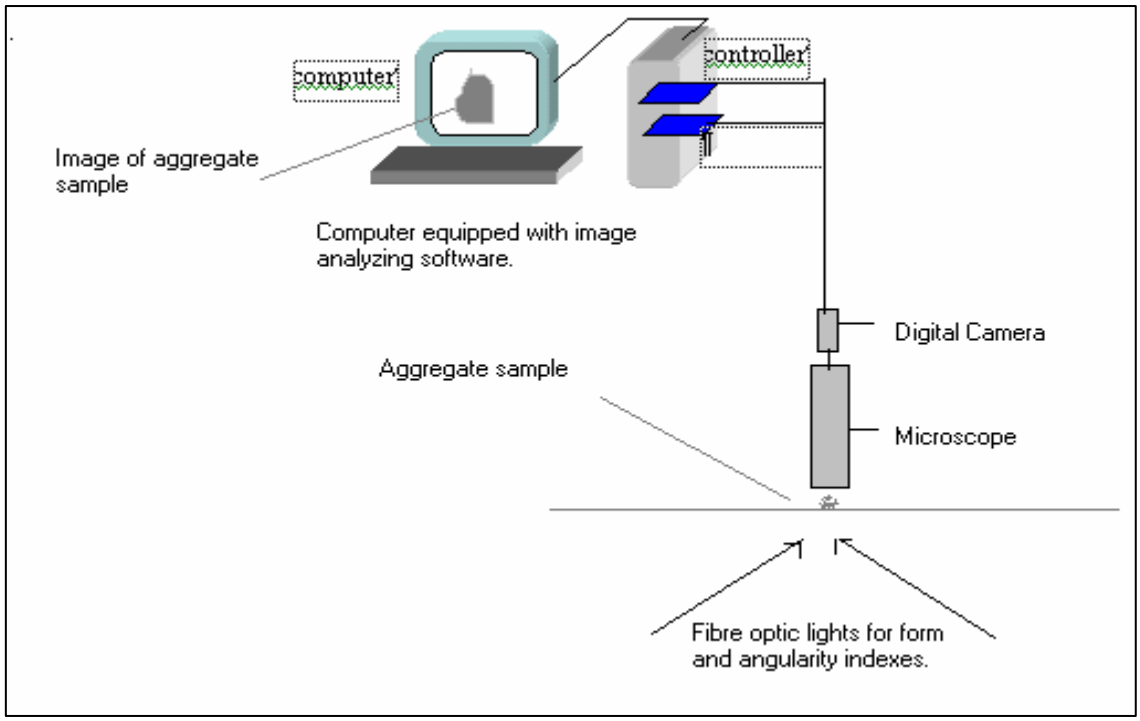

Figure 3. Schematic Diagram of System Used for Texture Index.

Scanning Electron Microscopy (*16*)

The SEM is one of the most versatile instruments available for the examination and analysis of the microstructural characteristics of solid objects. The primary reason for the SEM's usefulness is the high resolution that can be obtained when bulk objects are examined: values on the order of 2 to 5 nm (20 to 50 Å) are now usually quoted for commercial instruments, while advanced research instruments are available that have achieved resolutions of better than 1 nm (10 Å). Another important feature of the SEM is the three-dimensional appearance of the specimen image, a direct result of the large depth of field.

The basic components of the SEM are the lens system, electron gun, electron collector, visual and recording cathode ray tubes, and the electronics associated with them. In this instrument, the area to be examined or the microvolume to be analyzed is irradiated with a finely focused electron beam, which may be static or swept in a raster across the surface of the specimen. The types of signals produced when the electron beam impinges on a specimen surface include secondary electrons, backscattered electrons, Auger electrons, characteristic x-rays, and photons of various energies. In the scanning electron microscope, the signals of greatest interest are the secondary and backscattered electrons, since these vary according to differences in surface topography as the electron beam sweeps across the specimen.

Zworykin et al. described the first SEM used to examine thick specimens (*17*), working at the RCA Laboratories in the United States. The authors recognized that secondary-electron emission would be responsible for topographic contrast, and they accordingly constructed the design shown in Figures 4 and 5.

In its current form, the SEM is both competitive with and complementary to the capabilities offered by other microscopes. It offers much of the use and image interpretation found in the conventional light microscope while providing an improved depth of field and the benefits of image processing. The SEM is, thus, a versatile and powerful machine and consequently a major tool in research and technology.

Figure 4. Image Acquisition System for Texture Index.

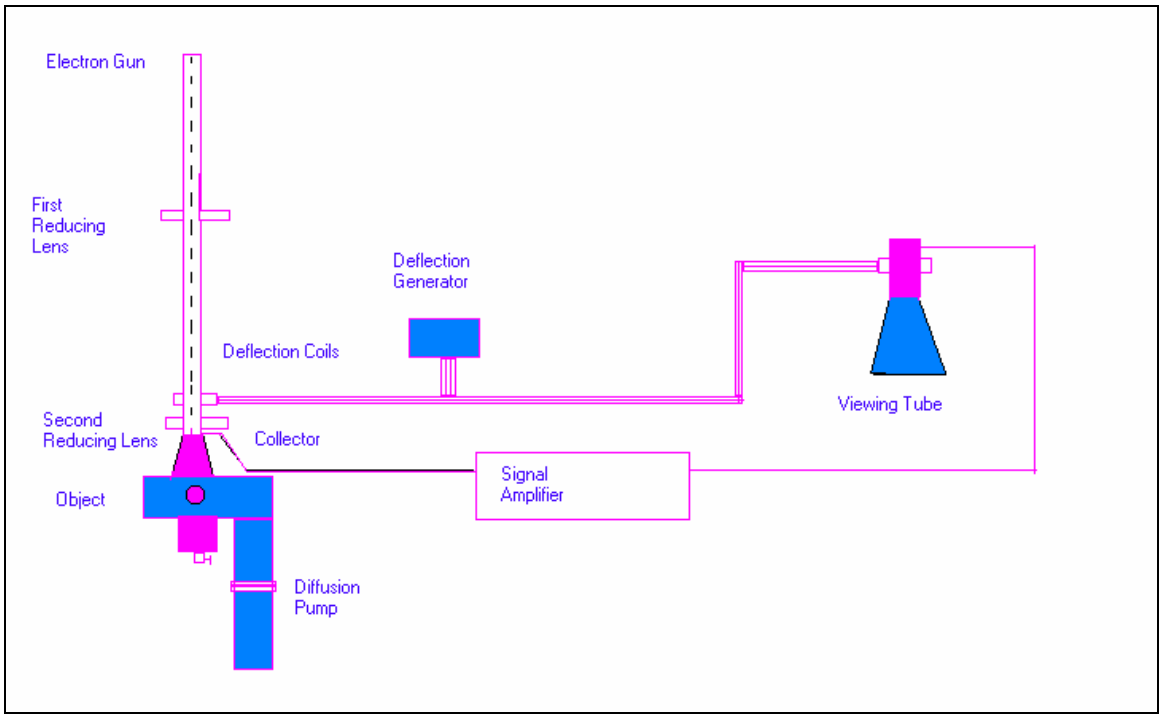

Figure 5. Schematic Diagram of an Early SEM.

AGGREGATE IMAGING SYSTEM SOFTWARE (*15*)

This software is developed under LabVIEW and IMAQ Vision. LabVIEW is a graphical (G) based programming language. This software is designed for data acquisition and instrument control, and comprises libraries of functions and development tools. The Aggregate Imaging System is as shown in Figure 6.

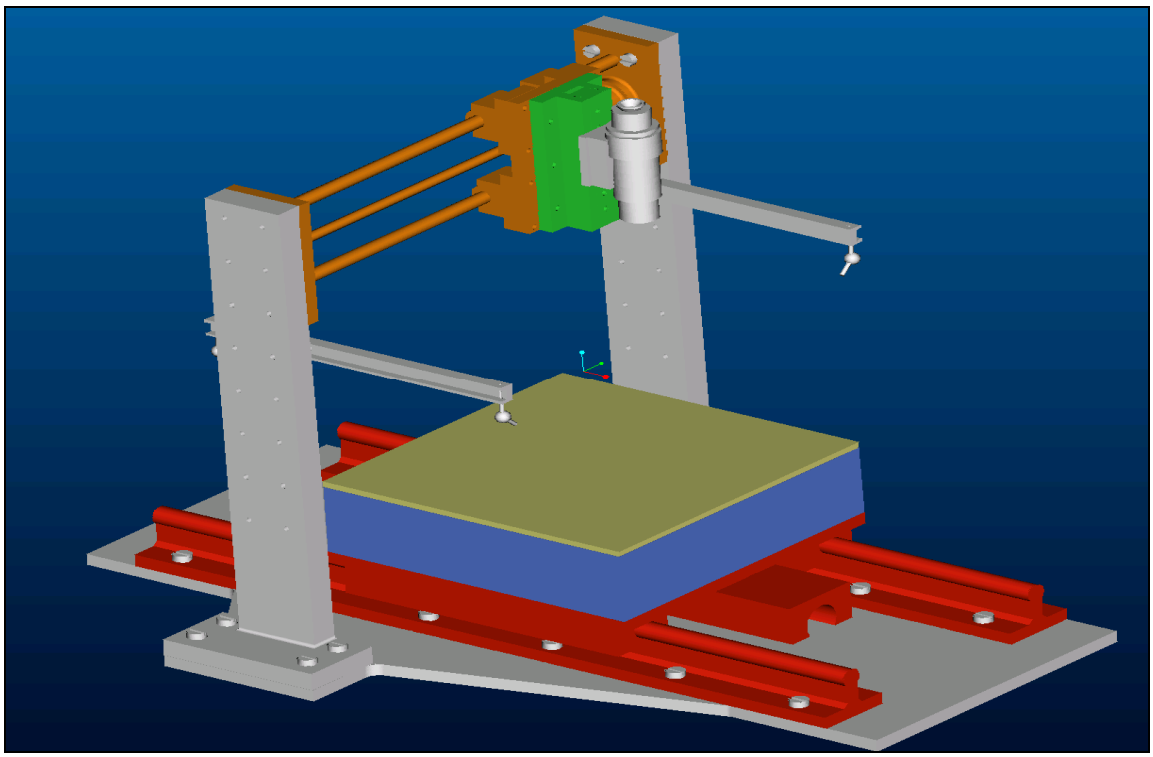

Figure 6. AIMS (Aggregate Imaging System) (*3*).

Texture Analysis

This project presents a multi-scale analysis of textural variation on aggregate images. Wavelet theory offers a mathematical framework for multi-scale image analysis of texture.

What is Wavelet Analysis?(*18*)

The fundamental idea behind wavelets is to decompose a signal or an image at different resolutions. Wavelets are special functions that satisfy certain mathematical conditions and are used in representing data, and could be one-dimensional signals (speech) or two-dimensional signals (images). Fourier transform, represents a given function in terms of sinusoidal functions. However, most of the transforms share a common weakness, fixed time and/or frequency resolution. For example, the sine and cosine functions used in Fourier analysis are not localized in time. These basic functions do not decay and have fixed amplitude for all time. In other words, it provides a fixed frequency resolution for all time. However, in wavelet analysis, the scale used in analyzing data plays an important role. The wavelet method, unlike other frequency transform methods, can be used to analyze data at different scales or resolutions. Wavelets have the advantage of producing resolution scalable signals with no extra effort.

The wavelet transform maps an image into a low-resolution image and a series of detailed images (Figure 7). The low-resolution image is obtained by iteratively blurring the images, and the detail images contain the information lost during this operation. The blurring operation eliminates fine details in the image while retaining the coarse details. The fine details are captured in the detail images. This produces a multiresolution representation of the original data (an image in our case). The resulting low-resolution and detail images help us in analyzing an image at different scales, which is not possible using a regular Fourier transform.

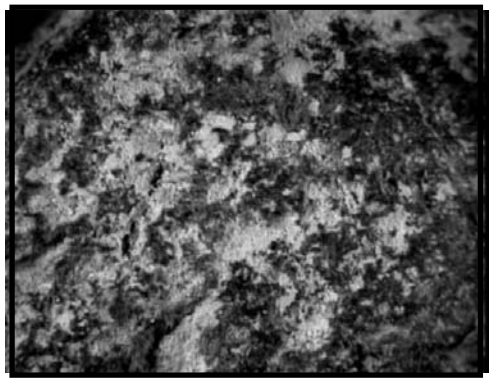

(a) Original Image.

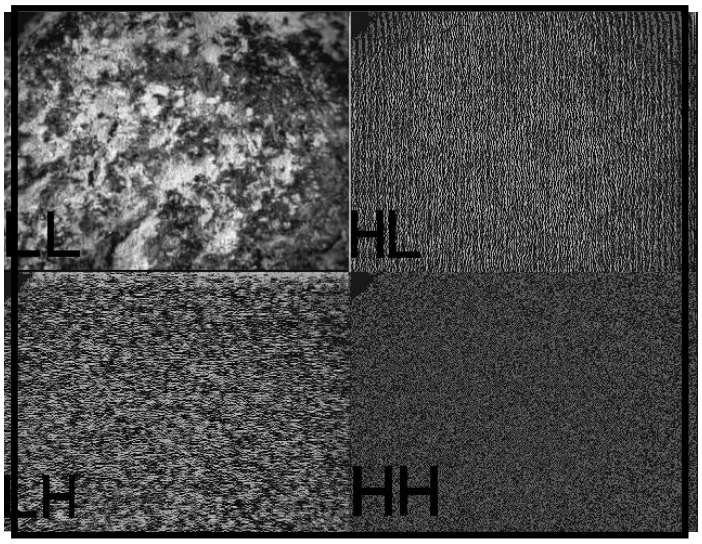

(b) One-Level Wavelet Decomposition.

Figure 7. One-Level Wavelet Decomposition.

Angularity Analysis

Angularity analysis can be done by radius method and gradient method. Radius method defines angularity as the difference between a particle radius in a certain direction and that of an equivalent ellipse. The equivalent ellipse has the same aspect ratio as the particle, but has no angularity. By normalizing the measurements to the aspect ratio, the

effect of form on this angularity index is minimized. Angularity index by radius method is expressed as

$$\mathrm{AI} = \sum_{\theta=0}^{\theta=355} \frac{\left| R_{p\theta} - R_{EE\theta} \right|}{R_{EE\theta}} \qquad (4)$$

Where:

$R_{p\theta}$ = the radius of the particle at a directional angle $\theta = 5$ degrees, and

$R_{EE\theta}$ = the radius of an equivalent ellipse at a directional angle θ.

The acquired image should be in the binary form in order to use this software.

A new, gradient-change approach has been adopted for angularity measurements of aggregates. The resulting angularity index has a bigger dynamic range, and hence is capable of fine distinction among particles with "almost-similar angularity." To measure angularity, we must adopt a method that can capture the sharp angular corners of a highly angular particle and, at the same time, assign an almost-zero angularity to particles that are rounded. The gradient method does possess these properties. At sharp corners of the edges of an image, the direction of the gradient vector for adjacent points on the edge changes rapidly. On the other hand, the direction of the gradient vector for rounded particles changes slowly for adjacent points on the edge.

The acquired image is the first threshold to get a binary image. This binary image then undergoes some pre-processing steps to get rid of noise and unwanted artifacts brought in during image acquisition and/or thresholding. The gradient-based method for angularity measurement is shown in Figure 8. Next, the gradient vectors at each edge-point are calculated using a Sobel mask, which operates at each point on the edge and its eight nearest neighbors. Based on the orientation of the gradient vectors at each edge-point, the angularity index is calculated for the aggregate particle, as described in the following paragraphs.

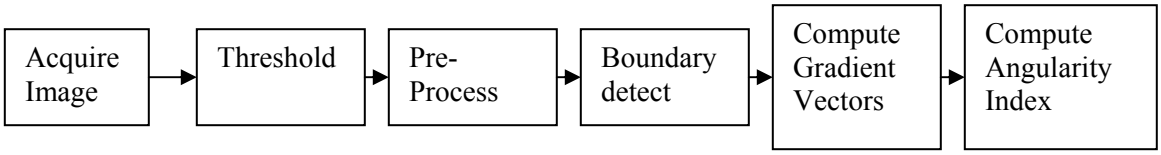

Figure 8. Gradient-Based Method for Angularity Measurement.

The magnitudes of the horizontal gradient G_x and vertical gradient G_y are found at each point on the edge. The gradient magnitude is given by $|G| = |G_x| + |G_y|$. The angle of orientation of the edge (relative to the pixel grid), which results in the spatial gradient, is given by:

$$\theta = \arctan\left(G_y / G_x\right) \tag{5}$$

Figure 9 shows the method of assigning angularity values to a corner point on the edge. Note that the change in the angle of the gradient vector α (for a rounded object) is much less compared to the change in the angle of gradient vector β (for an angular object). Angularity values for all the boundary points are calculated and their sum accumulated around the edge to finally form the angularity index of the aggregate particle.

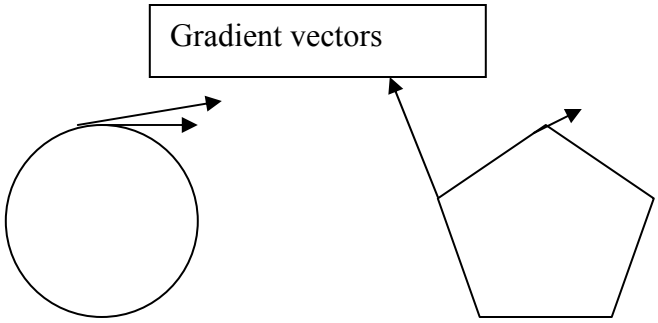

Figure 9. Comparing Angularity of Rounded Edges with Sharp Edges.

Erosion Levels

The gradient-based angularity analysis method is sometimes too sensitive with abrupt but insignificant angular corners. These localized corners tend to be over emphasized and hence, distort the true angularity index of the aggregate. To get rid of such bumps around the edge, the image is eroded until the unwanted tip disappears. As shown in Figure 10 levels of erosion are necessary, as well as sufficient, to achieve this. It also was found that three levels of erosion, in general, were sufficient to get rid of similar bumps in most of the images.

Figure 10. Erosion Cycle 1 to 3 from Right to Left.

Form Analysis

Particle form is an index that is measured by incremental changes in the particle radius in all directions. Radius is defined as the length of the line that connects the particle

center to points on the boundary. The form index is described as the sum of the changes in radius:

$$FI = \sum_{\theta=0}^{\theta=355} \frac{\left| R_{\theta+5} - R_{\theta} \right|}{R_{\theta}} \qquad (6)$$

Where,:

R = the radius of the particle in different directions, and

θ = the angle in different directions.

The above formula was used to compute form index in two dimensions. The three-dimensional form analysis is conducted for the coarse aggregates using AIMS. Information about the three dimensions of a particle {longest dimension, (d_L), intermediate dimension (d_I), and shortest dimension (d_S)} is essential for proper characterization of the aggregate form. Indices such as spherecity and shape factor are defined in terms of three aggregate dimensions as shown in equations (7) and (8) below:

$$\text{Sphericity} = \sqrt[3]{\frac{d_s d_I}{d_L^2}} \qquad (7)$$

$$\text{Shape Factor} = \frac{d_s}{\sqrt{d_L d_I}} \qquad (8)$$

The above two equations are used to calculate aggregate form based on three-dimensional analysis. A particle thickness is measured using the auto-focus microscope. The eigenvector method is used to find the two principal axes of the particle projection. These axes, along with a particle thickness, are used to calculate the shape indices.

PROTOCOL FOR MEASURING ANGULARITY AND FORM INDEX WITH AIMS

- For the present analysis of fines, three aggregate types– limestone, gravel, and granite– of size 0.6 mm were selected.
- Images of the above aggregates were taken with the help of the system as shown in Figure 2.
- Images were taken in Adobe Photo Shop® and stored in a .tif format.
- For the results shown in this project, an image size of 640 X 480 pixels and a canvas size of 960 X 720 pixels were kept.
- These images were then converted to binary form with the help of Scion-Image® software, which made them fit to be analyzed with AIMS software *(14)*.
- Analysis was done for three erosion cycles.
- The software converts the .tif extension to .pbm for analyzing images and the output is in the form of text files: Rad_Ang.txt, Grad_Ang.txt, and Form_2D.txt.

CAPTURING IMAGES WITH SEM

- Several individual particles (approximately four to six) of each sample were placed on a layer of double-stick carbon tape attached to the top of a SEM sample holder called a stub.
- Each stub is a small cylinder 10 mm high and 9.5 mm in diameter. The samples are then dried overnight in a dessicator jar (containing Drierite) and coated with 400 Å of gold or carbon-palladium with a Hummer sputter coating device.
- The coated samples were examined at 120 X magnifications using a JEOL JSM 6400 scanning electron microscope at 15 KeV (15 thousand electron volts) at working distances of 36 mm.
- The captured images were saved as a gray-scale image with a .tif extension.

CHAPTER IV
IMAGE ANALYSIS AND PHYSICAL TEST RESULTS

The aim of this project is to measure surface properties such as aggregate angularity, form, and texture with the help of image analysis and see how they affect performance as compared to physical tests.

This chapter discusses results of aggregate angularity by radius and gradient method, form, and texture. Angularity and form images of fine aggregates are captured with the help of an optical microscope shown in Figure 2, Chapter III whereas texture images are captured with the help of scanning electron microscope (shown in Figure 5, Chapter III). However, coarse aggregate images were obtained with AIMS (shown in Figure 6, Chapter III).

Results of fine and coarse aggregates are shown in the Tables 5 through 8. Aggregates are crushed to study the effect of crushing. Results of seven aggregates are presented in this chapter. The selected aggregates are one limestone, three gravels, and three granites. The researchers selected these aggregates based on the physical test results (6). The aggregates selected encompassed the entire spectrum of physical test results. Median values are shown in Tables 5, 6 and 7 representing 50 aggregate particles. Median values are considered as a representative of all 50 aggregates compared to average because of the presence of outliers.

The following abbreviations have been used:

- F = Fine aggregates,
- C = Coarse aggregates,
- C_{UN} = Uncrushed as delivered from field,
- C_{CF} = Crushed as delivered from field,
- F_{UN} = Uncrushed fine aggregates (as received), and

- F_{CF} = Crushed fine aggregates from field (as received).

Table 5. Image Analysis: Fine Aggregates – As Delivered.

Pit/ Supplier	Type	Size (0.6mm)	Radius Angularity	Gradient Angularity	Form_2D	Texture
Martin Marietta	Limestone	F^*	11.19	2652.38	6.59	192
Beck	Gravel-1	F_{CF}^*	12.80	2611.39	9.40	96.00
Trinity	Gravel-2	F_{CF}^*	14.83	3532.02	7.78	100.00
Brazos River Gravel	Gravel-3	F_{UN}^*	9.27	2044.5	5.95	93.00
Millcreek	Granite-1	F^*	17.04	5128.38	8.44	197.00
Davis	Granite-2	F^*	19.07	3157.37	9.73	126.80
Georgia Granite	Granite-3	F^*	17.99	4401.4	7.87	145.00

** F=fine aggregates, F_{CF}=crushed as delivered from field, F_{UN} = uncrushed as delivered from field.*

Table 6. Image Analysis: Fine Aggregates — Laboratory Crushed.

Pit/ Supplier	Type	Size (0.6mm)	Radius Angularity	Gradient Angularity	Form_2D	Texture
Martin Marietta	Limestone	F^*	13.51	2929.40	8.50	208.00
Beck	Gravel-1	F^*	16.41	2901.13	9.00	167.00
Trinity	Gravel-2	F^*	22.28	4404.91	9.30	140.50
Brazos River Gravel	Gravel-3	F^*	21.95	3904.50	8.68	128.00
Millcreek	Granite-1	F^*	15.89	3477.48	9.14	133.00
Davis	Granite-2	F^*	24.94	5431.89	8.46	218.00
Georgia Granite	Granite-3	F^*	18.43	4280.63	8.58	128.00

** F = fine aggregates*

Table 7. Image Analysis: Coarse Aggregates —As Delivered.

Pit/ Supplier	Type	Size (0.6mm)	Radius Angularity	Gradient Angularity	Form_2D	Texture
Martin Marietta	Limestone	C*	15.50	3041.00	7.15	245.50
Beck	Gravel-1	C_{CF}*	11.71	2926.85	6.30	110.00
Trinity	Gravel-2	C_{UN}*	9.90	1725.24	5.77	91.00
Brazos River Gravel	Gravel-3	C_{UN}*	10.09	1936.26	5.39	150.00
Millcreek	Granite-1	C*	13.96	2988.81	8.29	276.00
Davis	Granite-2	C*	14.59	2728.66	9.10	150.00
Georgia Granite	Granite-3	C*	12.77	3347.32	6.52	422.00

** C = coarse aggregates, C_{CF}= crushed as delivered from field C_{UN} = uncrushed as delivered from field.*

Table 8. Aggregate Properties-Physical Test Results.

Pit/ Supplier	Type	Size (0.6mm)	FAA (%) Fine Aggregate Angularity	CAR (lbs) Compacted Aggregate Resistance	Flat & Elongated Particles %.4.75 mm
Martin Marietta	Limestone	F*	45.53	4266.70	12.50
Beck	Gravel-1	F_{CF}*	47.81	5000.00	6.40
Trinity	Gravel-2	F_{CF}*	49.85	5000.00	3.30
Brazos River Gravel	Gravel-3	F_{UN}*	39.00	480.20	6.00
Millcreek	Granite-1	F*	50.02	4700.00	7.90
Davis	Granite-2	F*	47.39	4450.00	15.0
Georgia Granite	Granite-3	F*	48.00	2232.00	5.00

** F=fine aggregates, F_{CF}=crushed as delivered from field, F_{UN} = uncrushed as delivered from field.*

OBSERVATIONS

Results of the fine aggregates as received and crushed in the laboratory are as shown in Tables 5 and 6, respectively. Results indicate that all the aggregates became more

angular and elongated after crushing except two of the granites (Granite-1 and Granite-3). Table 7 shows the results of coarse aggregates.

Table 8 shows the fine aggregate angularity, compacted aggregate resistance, and flat and elongated values of all seven aggregates. Appendix A shows the correlation between physical test results and image analysis indices.

FAA results show some correlation with angularity indices of image analysis. Also, flat and elongated results correlate to some extent with the form index values. But the CAR value of Granite-3 is much lower compared to the rest of the aggregates. CAR values do not correlate with the image analysis values. The CAR and FAA results do not differentiate between crushed gravel and granite (Gravel-1, Gravel-2, Granite-1, and Granite-2).

Figure 11 shows the angularity, form, and texture index values of fine aggregates, and Figures 12 and 13 show the effects of crushing on the surface properties of aggregates. Figure 14 shows the surface properties of coarse aggregates.

Figures 11(a) and 11(b) below show radius and gradient angularity of fine aggregates. As shown in Figure 11(a) radius angularity of all aggregates is very close and it is very difficult to differentiate aggregate types, whereas in the case of gradient angularity (Figure (11b)) all aggregates can be easily distinguished. It can be seen that granites are the most angular of all aggregate types, and Gravel-3, which is river gravel, is least angular.

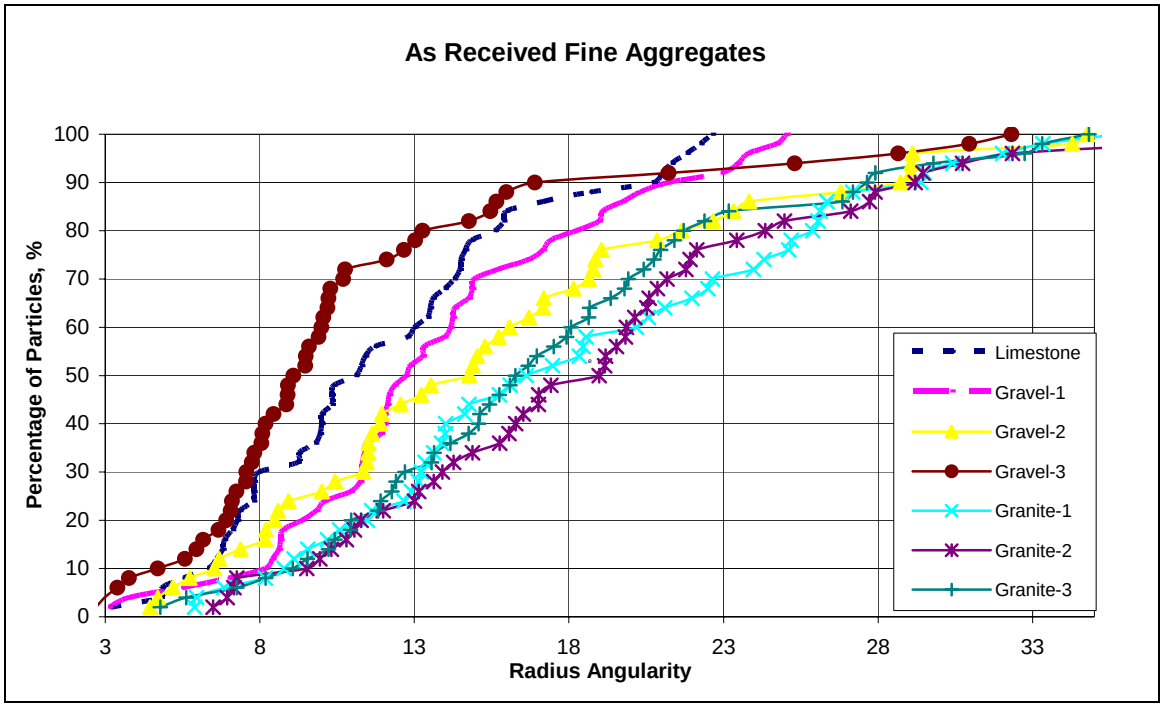

(a) Radius Angularity

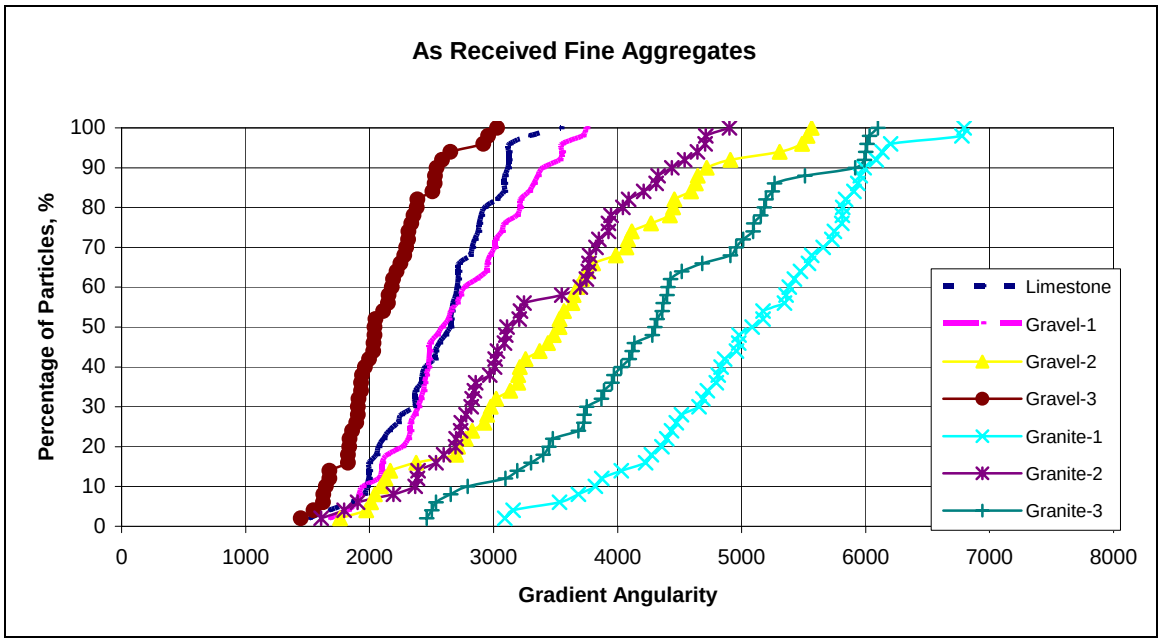

(b) Gradient Angularity

Figure 11. Image Analysis Results: Fine Aggregates — As Received.

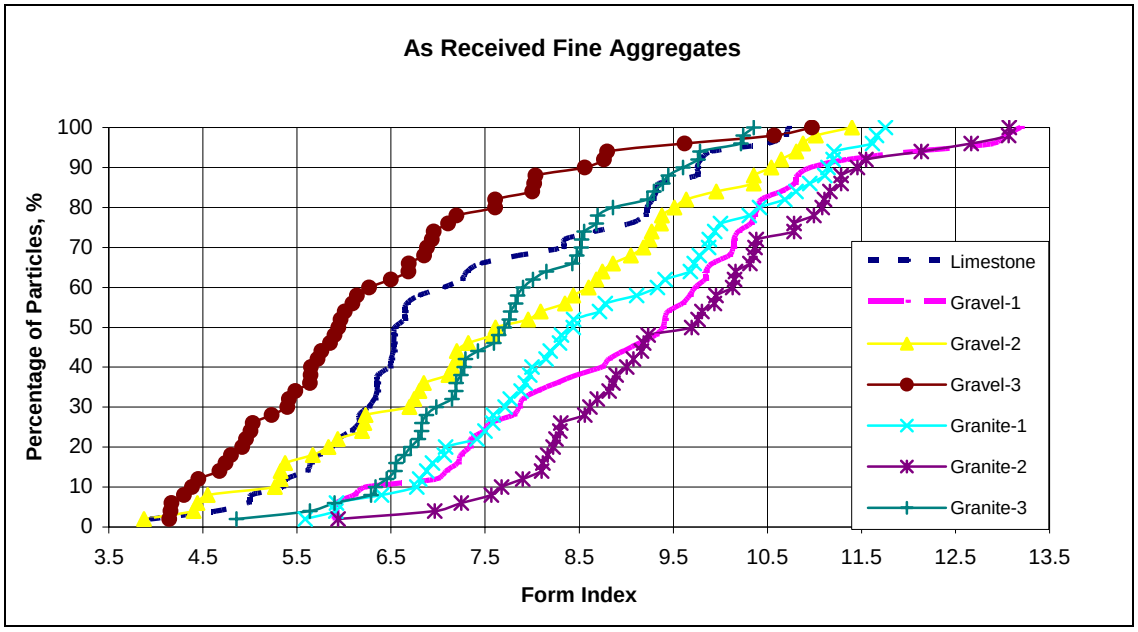

(c) Form Index

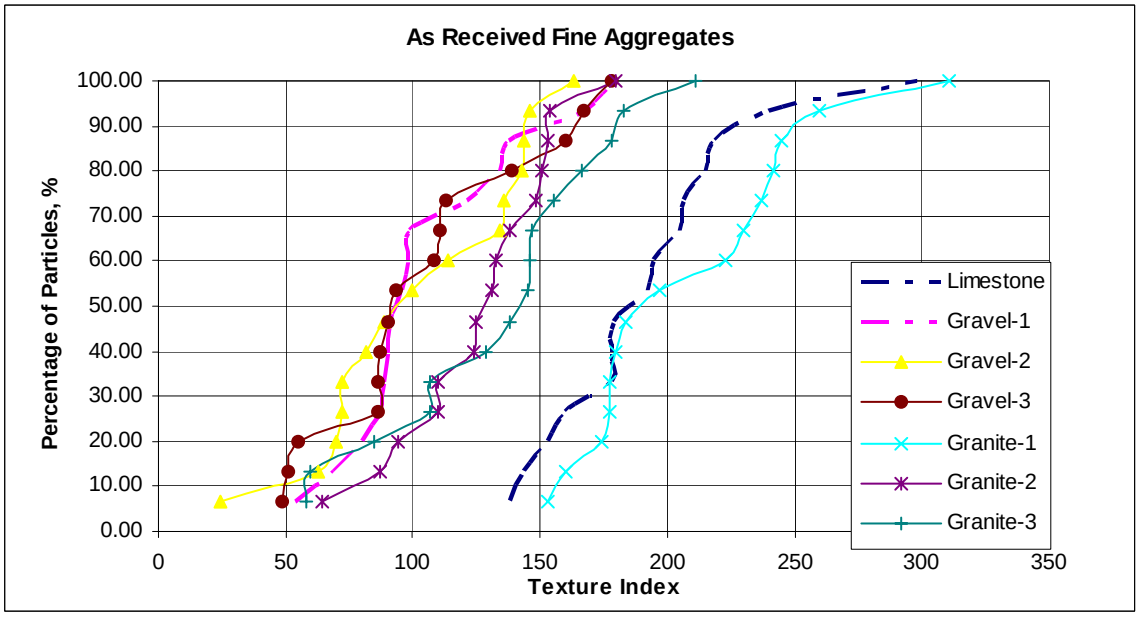

(d) Texture Index

Figure 11. Image Analysis Results: Fine Aggregates — As Received (Continued).

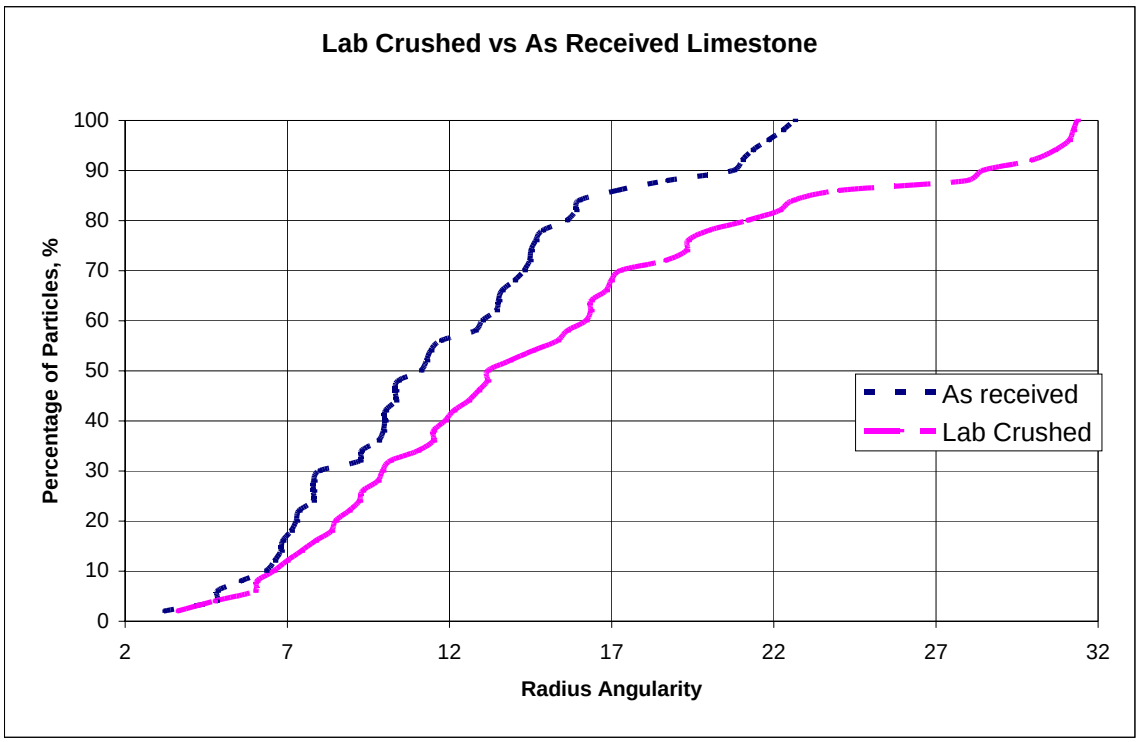

(a) Radius Angularity

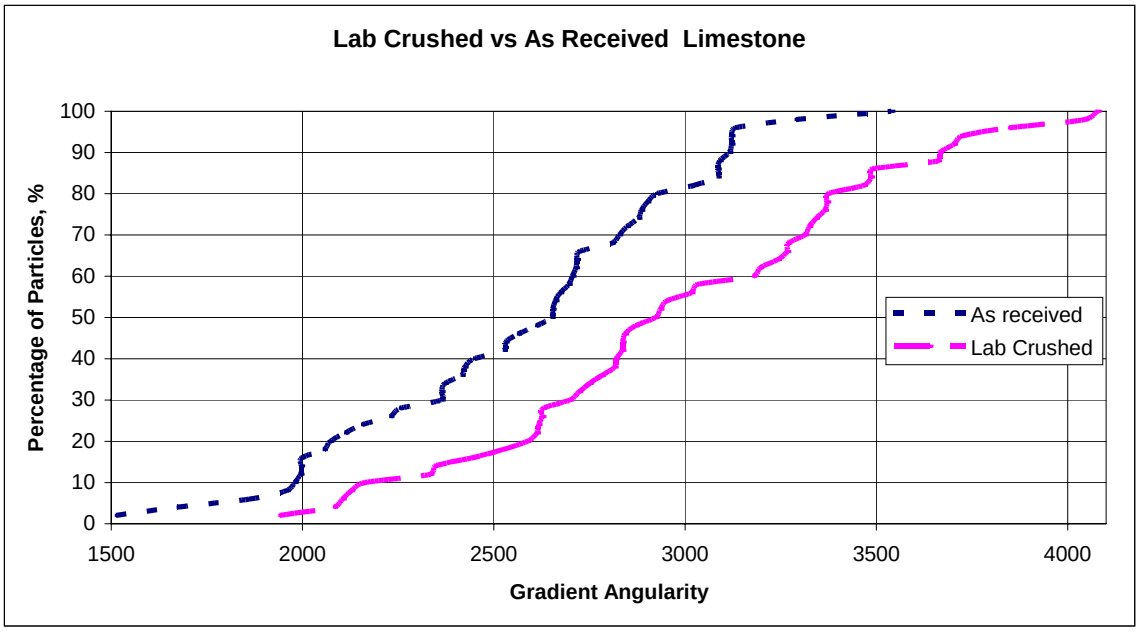

(b) Gradient Angularity

Figure 12. Effect of Crushing on Limestone Image Analysis Parameters.

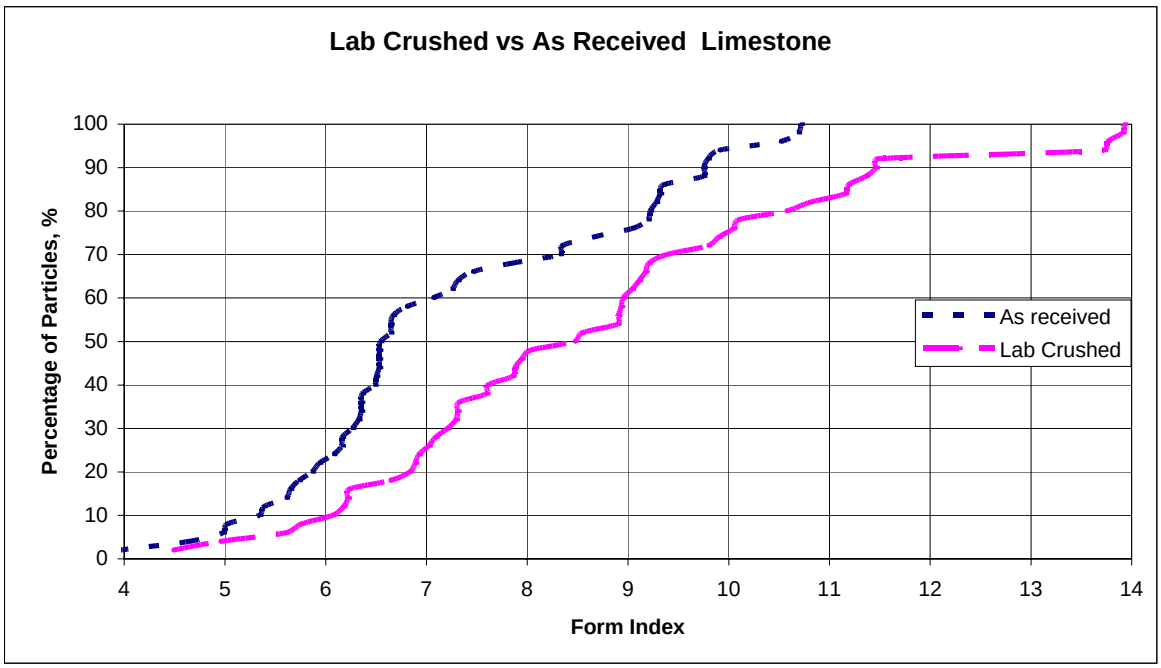

(c) Form Index

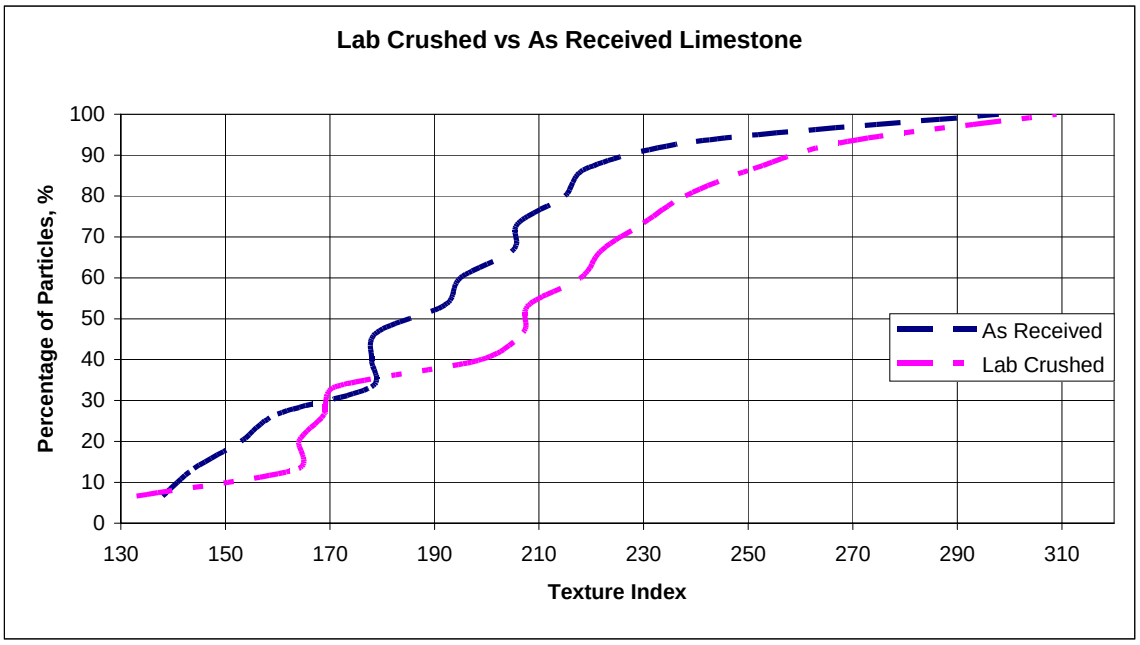

(d) Texture Index

Figure 12. Effect of Crushing on Limestone Image Analysis Parameters (Continued).

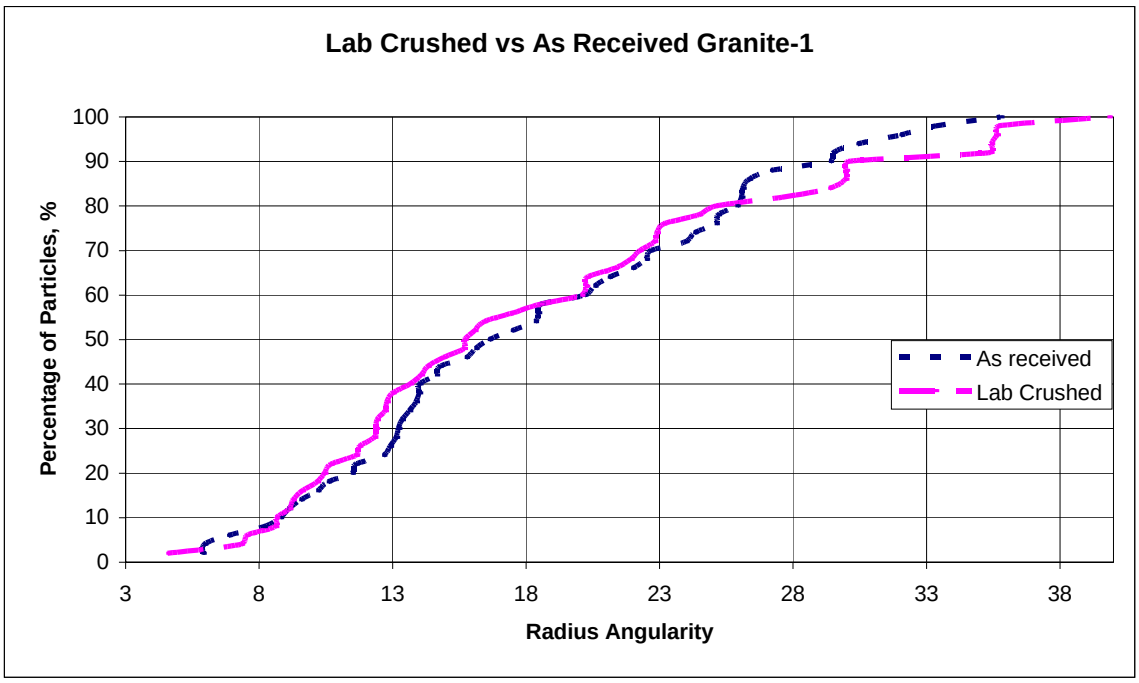

(a) Radius Angularity

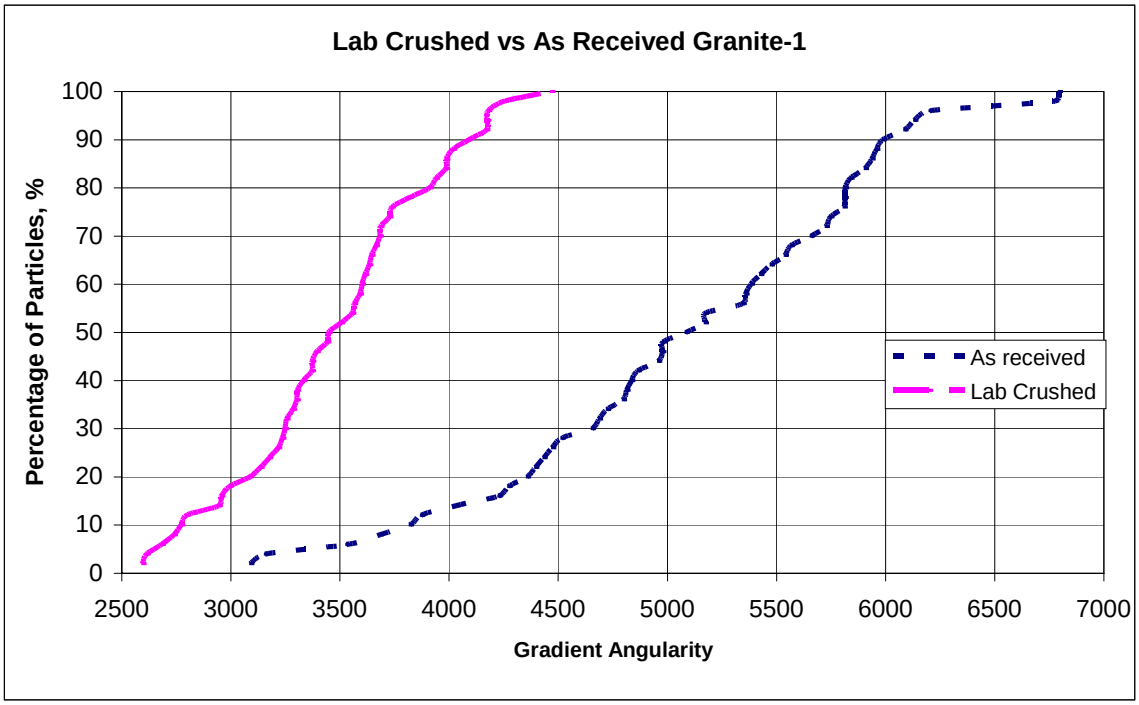

(b) Gradient Angularity

Figure 13. Effect of Crushing on Granite-1 Image Analysis Parameters.

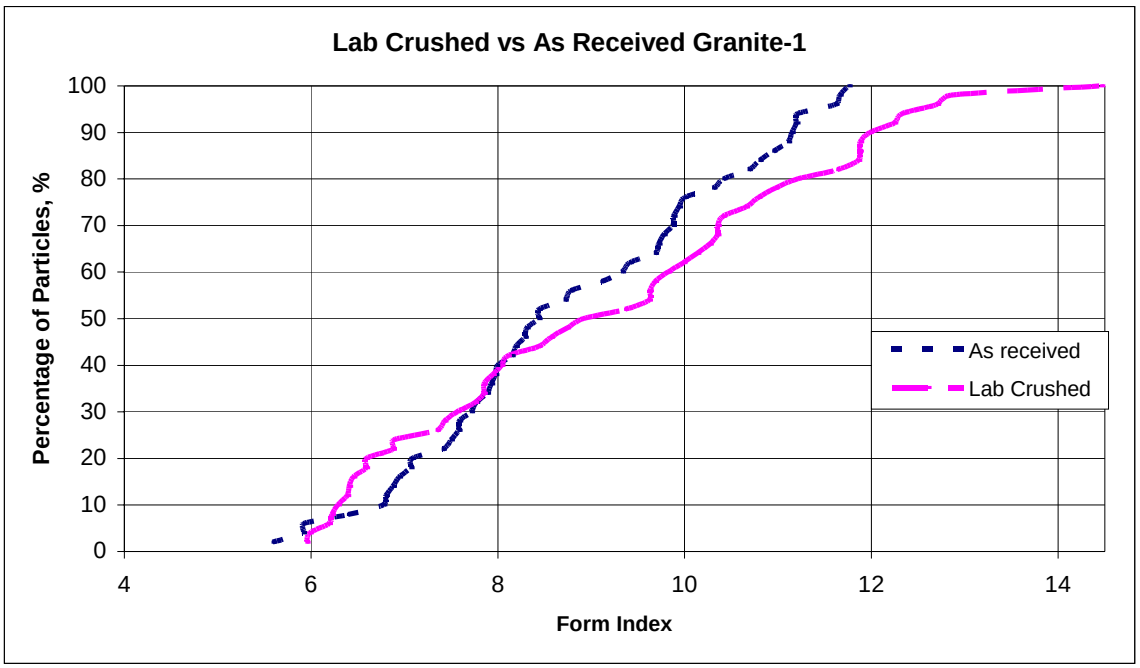

(c) Form Index

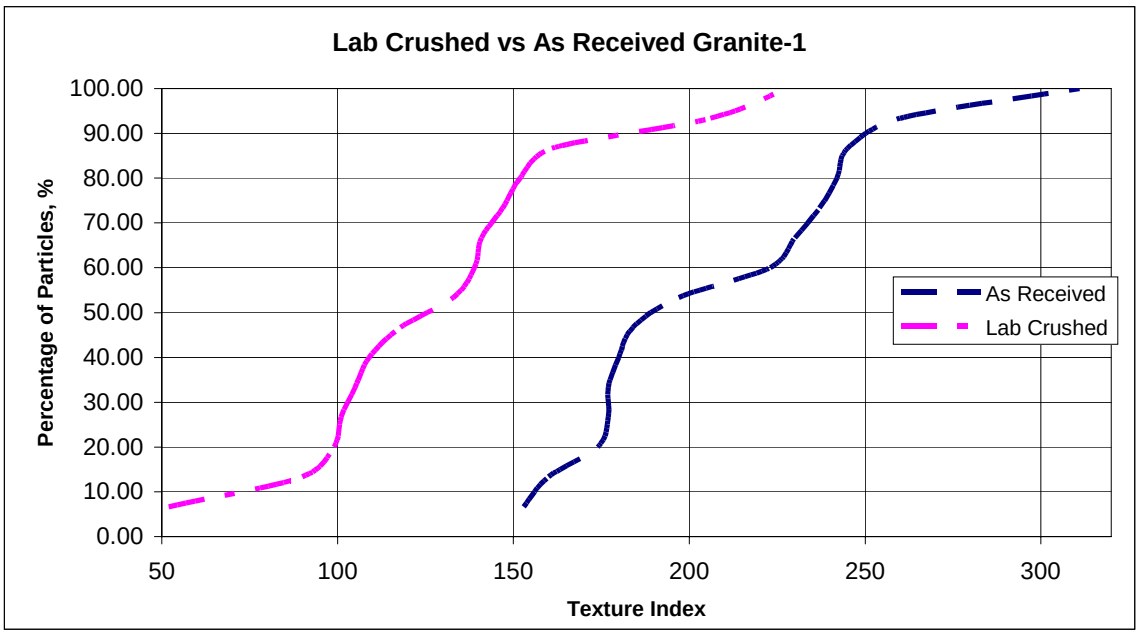

(d) Texture Index

Figure 13. Effect of Crushing on Granite-1 Image Analysis Parameters (Continued).

Form index of all fine aggregates is shown in Figure 11(c). Granite-2 and Gravel-1 had higher form values as compared to the other aggregates, and Gravel-3, river gravel, has the lowest value. Figure 11(d) shows texture index of all aggregates. Gravel-3 and Gravel-1 have almost the same distribution, and have a much lower texture value compared to the others, and Granite-1 has the maximum value.

All seven aggregates were crushed to see the effect of crushing on surface properties of aggregates such as angularity, form, and texture. An increase in the value of properties of these aggregates was observed, with the exception of Granite-1 and Granite-3, in which there was no increase in image indices. Also, a decrease in form value was observed in Granite-2. This can be attributed to the fact that granite is highly crushed in the field.

Figures 12 and 13 show the crushing effect on two of the seven aggregates. The remaining figures are given in Appendix B. Increase in image analysis parameters was observed in almost all the aggregates except granite. This is due to the fact that granite is crushed from the source itself so laboratory crushing does not increase surface properties of aggregates. No significant increase was observed in the case of Limestone and Gravel-3 texture indices.

Figure 14(a) shows radius angularity of all coarse aggregates. Limestone has the highest angularity values. We can observe that Gravel-2 and Gravel-3 are less angular compared to the other aggregates. Fine angularity of Gravel-2 was very high. This is because fine aggregates of Gravel-2 are not natural but crushed aggregates.

As seen in 14(b), angularity as measured by the gradient method shows that Granite-3 is the most angular followed by Limestone, and Gravel-2 and Gravel-3 are the least angular.

Figures 14(c) and 14(d) show form and texture values. A very good correlation is observed between the coarse aggregate and the fine aggregate textures.

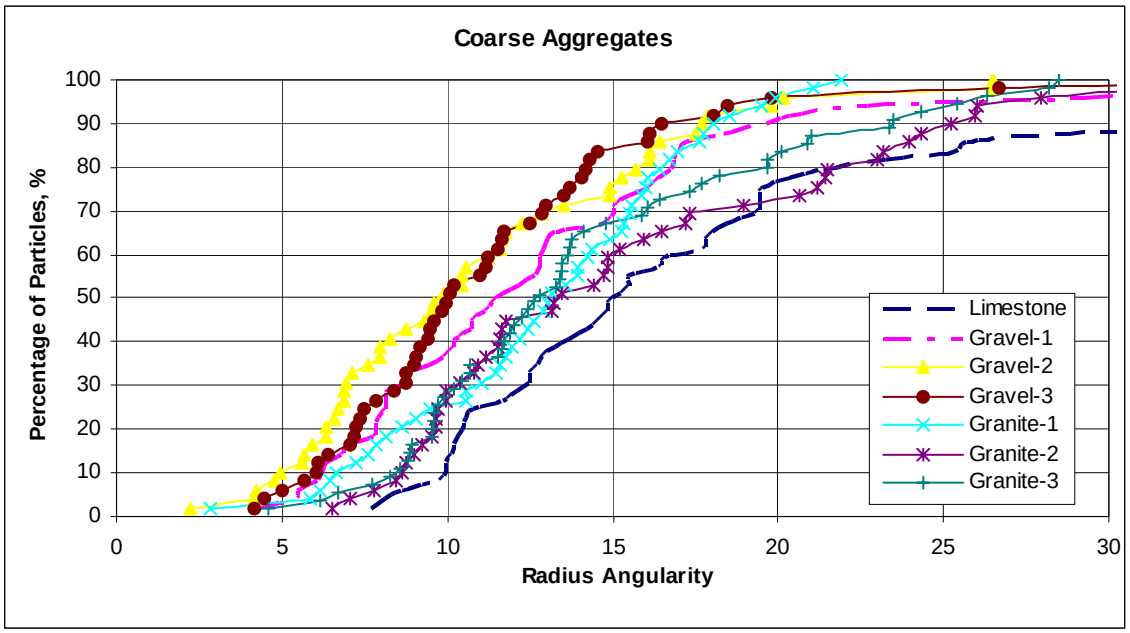

(a) Radius Angularity

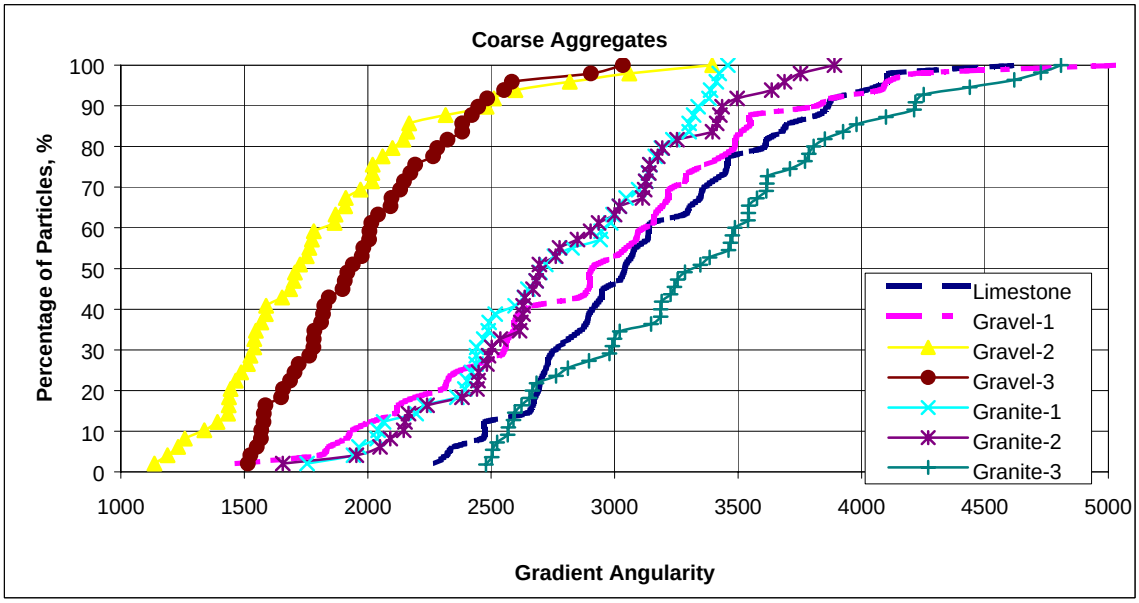

(b) Gradient Angularity

Figure 14. Image Analysis Results: Coarse Aggregates.

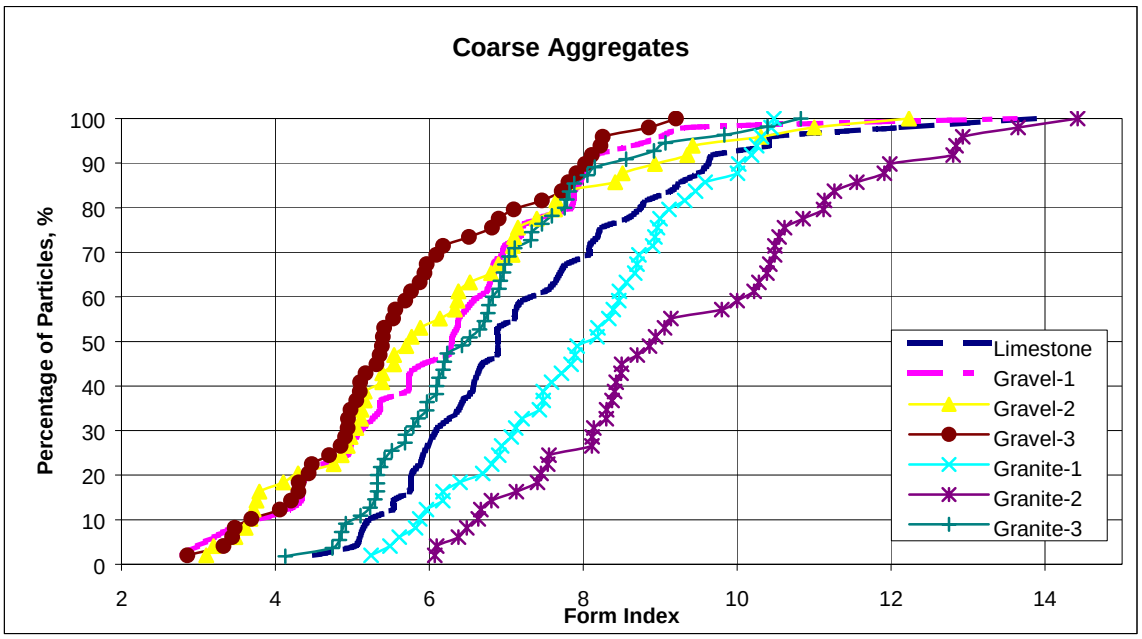

(c) Form Index

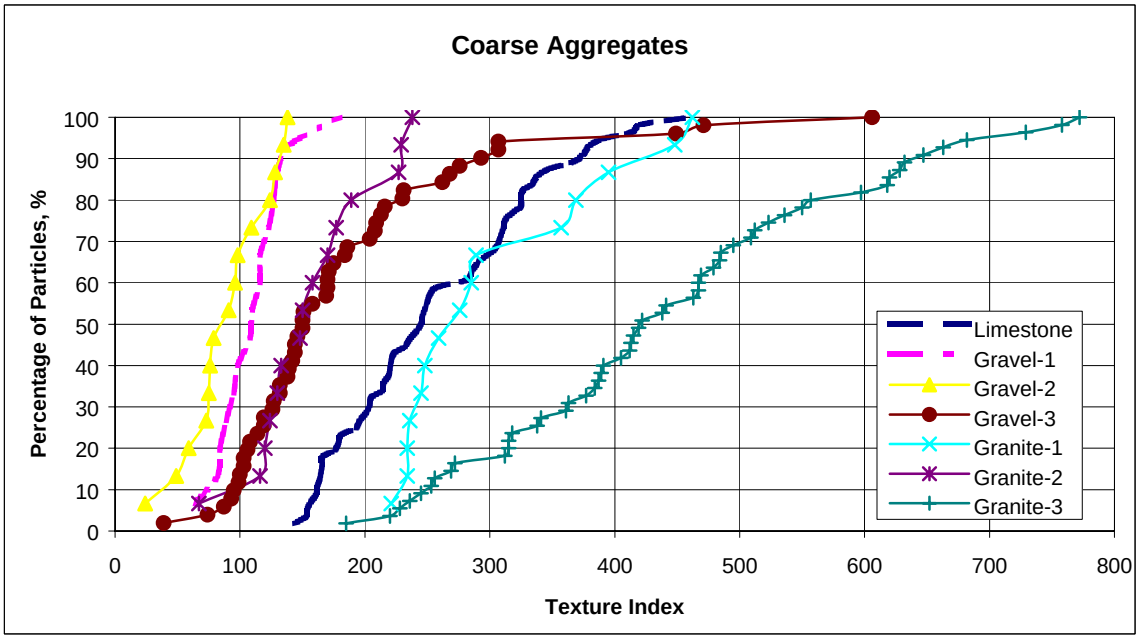

(d) Texture Index

Figure 14. Image Analysis Results: Coarse Aggregates (Continued).

CHAPTER V
PERFORMANCE TESTS

MATERIAL SELECTION

The researchers identified three aggregates for performance tests: a limestone; a granite (Granite-3), and a gravel (Gravel-3). We selected the aggregates on the basis of image analysis results of both coarse and fine aggregates. Brazos river gravel (Gravel-3) was selected because that was the only natural gravel (uncrushed) of the gravel material available, and Georgia granite (Granite-3) was selected because this material covered the entire spectrum of granite results and, hence, could be used as a representative sample from the granite group. On the basis of image analysis results, these three mixtures should exhibit field performance (particularly related to rutting) from excellent to poor, i.e., granite, limestone, river gravel performing as excellent, fair, and poor, respectively. Limestone and gravel are from Texas, but granite is from Georgia.

GRADATION

An aggregate gradation is the distribution of particle size expressed as a percent of the total weight. Gradation is determined by sieve analysis, that is, by passing the material through a series of sieves stacked with progressively smaller openings from top to bottom, and weighing the material retained on each sieve. The gradation of an aggregate is normally expressed as total percent passing various sieve sizes. Gradation of an aggregate can be graphically represented by a gradation curve for which the ordinate is the total percent by weight passing a given size on an arithmetic scale, while the abscissa is the particle size plotted to a logarithmic scale *(4)*.

Nominal Maximum Size

The nominal maximum size is one sieve size larger than the first sieve to retain more than 10 percent *(5)*. Nominal maximum size of limestone and granite is 12.5 mm, whereas that of gravel is 9.5 mm. Type of gradation is well graded or densely graded and the gradation curves are passing below the restricted zone. Table 9 shows percent passing on each sieve size for all three aggregates, and Figure 15 shows all three gradation curves.

Table 9. Gradation of All Three Aggregates.

Sieve Size in mm	Limestone % passing	Granite % passing	Gravel % passing
19	100	100	100
12.5	98.75	98.75	100
9.5	79.52	79.52	91.75
4.75	46.17	46.17	48.22
2.36	31.62	31.62	32.71
1.18	24.46	24.46	27.96
0.6	17.84	17.84	22.26
0.3	11.22	11.22	9.75
0.15	6.26	6.26	3.94
0.075	1.5	1.5	2.95
PAN	0	0	0

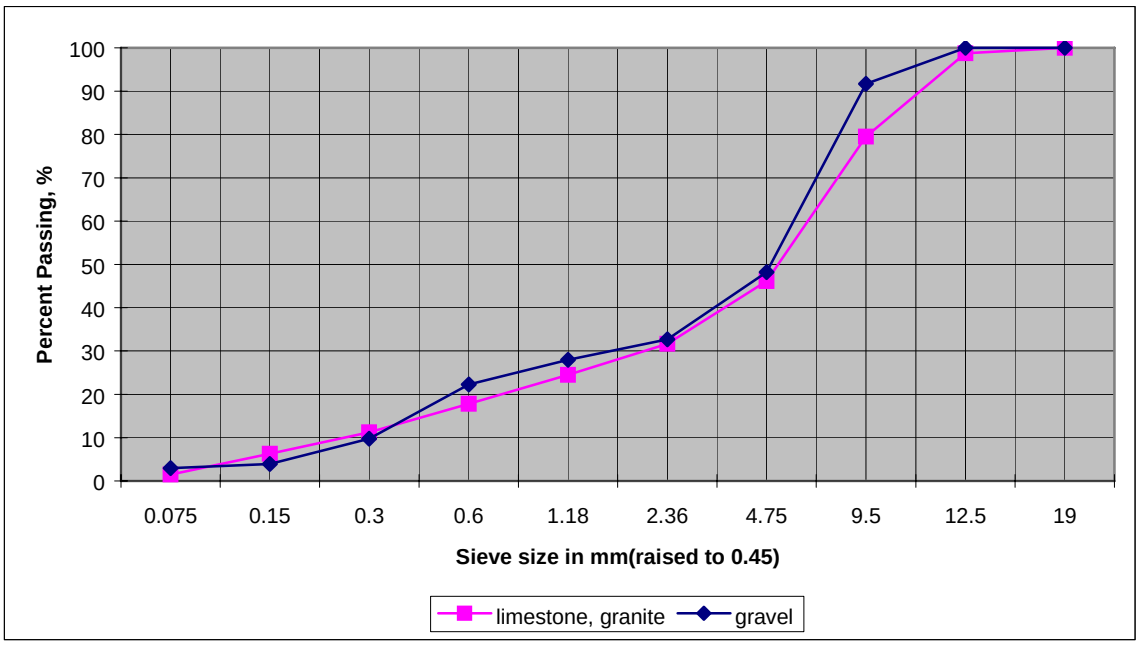

Figure 15. Gradation Curves of Limestone, Granite, and Gravel.

MIXTURE DESIGN

The gradations selected for this project were below the restricted zone. Gradation was kept the same for limestone and granite but different for gravel. Superpave mixture design method was used to find the optimum binder content. The traffic level selected was 10 to 30 million ESALs for design purpose. For the selected traffic level and representative climate site N_{ini}, N_{des}, and N_{max} are 8, 109, 174, respectively for the Superpave gyratory compactor.

Specimens for the volumetric analysis were compacted to 109 gyrations (N_{des}). Table 10 shows the mix design information and all the design criteria were met.

Mixing and Compaction Temperature

Superpave HMA mixtures are mixed and compacted under equiviscous temperature conditions corresponding to 0.17 Pa•s and 0.28 Pa•s, respectively *(1)*. Viscosity of the

asphalt was tested using the Brookfield rotational viscometer at 275 °F (135 °C) and 347 °F (175 °C). Plotting the result on a viscosity versus temperature graph (log-normal), the mixing and compaction temperatures were determined for PG 64-22 asphalt. Table 11 describes the mixing and compaction temperatures for both asphalts.

Table 10. Mixture Design Information.

Mixture Type	Binder Content (%)	Binder Type	Rice Density (gm/cc)	VMA (%)	Aggregate *BSG
Limestone	4.85	PG 64-22	2.478	14.72	2.65
River Gravel	3.60	PG 64-22	2.484	11.44	2.60
Granite	4.46	PG 64-22	2.471	15.14	2.69

**BSG=Bulk specific gravity*.

Table 11. Mixing and Compaction Temperatures.

Asphalt Grade	Mixing		Compaction	
	Temp Range (°F)	Selected Temp, (°F)	Temp Range, (°F)	Selected Temp, (°F)
PG 64-22	317 – 330	320	294 – 306	295

LABORATORY TESTS

APA Test

Asphalt Pavement Analyzer is the most popular and commonly used loaded wheel tester in the U.S. Pavement Technology, Inc. started manufacturing this equipment in the mid-1990s. The APA is capable of evaluating rutting, fatigue, and moisture resistance of HMA mixtures. The fatigue test is performed on beam specimens supported on the two

ends. Rutting and moisture-induced damage evaluations can be performed on either cylindrical or beam specimens. This machine is capable of testing in both dry and wet conditions.

Oscillating beveled aluminum wheels apply a repetitive load through high-pressure hoses to generate the desired contact pressure. The loaded wheel oscillates back and forth over the hose. While the wheel moves in the forward and backward directions, the linear variable differential transducers (LVDTs) connected to the wheels measure the depression at regularly specified intervals. Usually, three replicates of specimens are tested in this machine. Rut evaluation is typically performed by applying 8000 load cycles. The wheel load is usually 100 lb. (445 N), and the hose pressure is 100 psi (690 kPa). Some researchers have successfully used this device with higher wheel load and contact pressure (*19*). APA testing can be performed using chamber temperatures ranging from 41 to 160 °F (5 to 71 °C) (*20*).

Several research projects have been conducted to evaluate performance of the APA. Choubane et al. (*21*) indicated that the APA might be an effective tool to rank asphalt mixtures in terms of their respective rut performance. Kandhal et al. (*22*) reported that the APA has the ability to predict relative rutting potential of HMA mixtures. They also mentioned that the APA is sensitive to asphalt binder and aggregate gradation

Hamburg Test

The Hamburg Wheel-Tracking Device is an accelerated wheel tester. Helmut-Wind, Inc. in Hamburg, Germany, originally developed this device (*23*). It has been used as a specification requirement for some of the most traveled roadways in Germany to evaluate rutting and stripping (*24*). Use of this device in the U.S. began during the 1990s. Several agencies undertook research efforts to evaluate the performance of the

HWTD. The Colorado Department of Transportation (CDOT), FHWA, National Center for Asphalt Technology (NCAT), and Texas Department of Transportation (TxDOT) are among them.

Since the adoption of the original HWTD, significant changes have been made to this machine. A U.S. manufacturer now builds a slightly different device. The basic idea is to operate a steel wheel on a submerged, compacted HMA slab or cylindrical specimen. The original HWTD uses a slab with dimensions of 12.6 inches × 10.2 inches × 1.6 inches (320 mm × 260 mm × 40 mm). The slab is usually compacted at 7 ± 1 percent air voids using a linear kneading compactor. The test is conducted under water at constant temperature ranging from 77 to 158 °F (25 to 70 °C). Testing at 122 °F (50 °C) is the most common practice (*20*). The sample is loaded with a reciprocating motion of the 1.85 inch (47 mm) wide steel wheel using a 158 lb force (705 N). Usually, the test is conducted at 20,000 cycles or up to a specified amount of rut depth (12.5 mm). Rut depth is measured at several locations including the center of the wheel travel path, where usually it reaches the maximum value. One forward and backward motion comprises two cycles.

Tim Aschenbrener (*23*) found an excellent correlation between the HWTD and pavements with known field performance.

RESULTS

The graphs below show the Hamburg and APA test results. Figure 16 shows that all the three aggregates deformed within 20,000 cycles in the Hamburg test. Two replicates of each aggregate type were tested in water. Granite reached maximum rutting depth in 14,200 average cycles, limestone in 5451 cycles, and gravel in 1280 cycles at a temperature of 122 ^{o}F (50 °C).

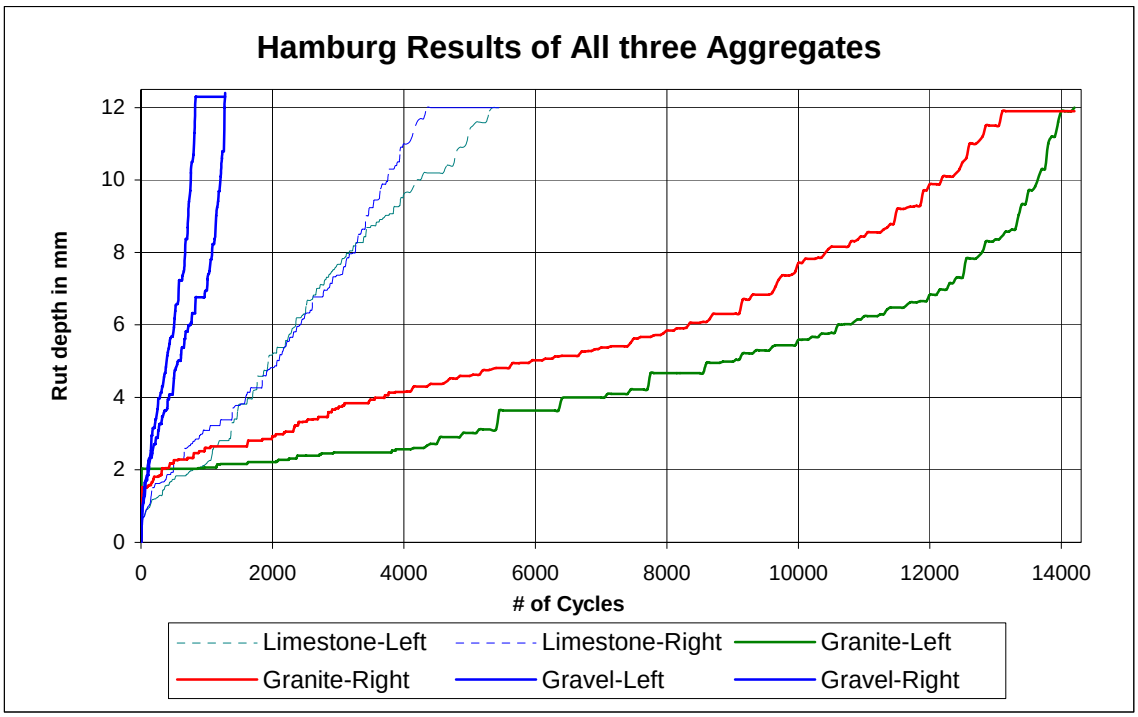

Figure 16. Hamburg Test Results of All Three Aggregates.

Figure 17 shows APA results in which two replicates of each aggregate type were subjected to 8000 cycles, and the damage was observed at a temperature of 131 ^{o}F (55 °C) without water. Average rutting of 0.6 inches (14.6 mm) was observed in the case of gravel material after 8000 cycles, while there was no significant difference observed in the cases of limestone and granite material. Approximately 0.9 inches (2.2 mm) rutting was observed in case of limestone while 0.11 inches (2.8 mm) was observed in the case of granite after 8000 cycles.

The results suggest that the granite mix performance is superior to the limestone mix under moist condition. This can suggest that the granite, which has higher texture and angularity, retained more bonding with binder in the presence of water compared with the limestone aggregate. Of course, the chemical properties of the granite such as surface energy might have contributed to this superior performance (*25*).

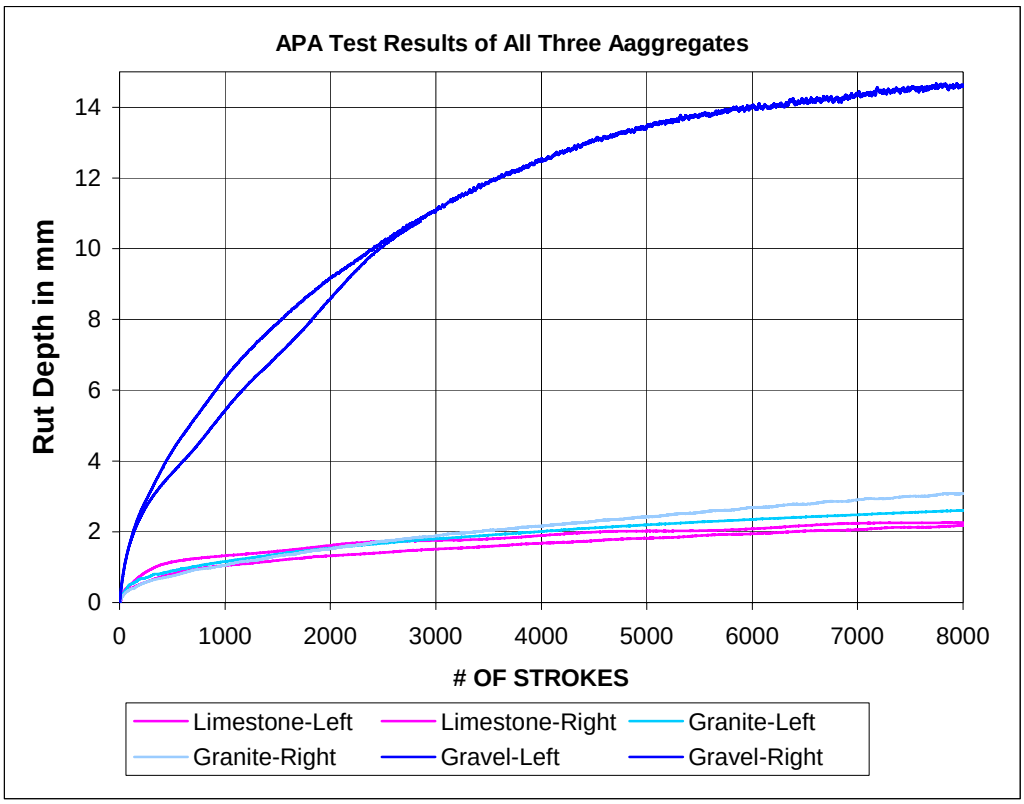

Figure 17. APA Test Results of All Three Aggregates.

RESULTS AND ANALYSIS

Correlation between image analysis and performance tests:

Surface properties such as angularity, form, and texture of limestone, granite and gravel aggregates were found with the aid of image analysis. Angularity was measured both with the gradient and radius methods and form was analyzed by finding the form index, sphericity, and shape factor.

Sphericity and shape factors were included later in the AIMS software and, hence, these indices were found only for three aggregates, which were tested for performance.

It was found from the above results that the APA test could not distinguish clearly between limestone and granite but Hamburg results show that granite, limestone, and river gravel exhibit field performance (particularly related to rutting) from excellent to poor, i.e., granite, limestone, and gravel performing as excellent, fair, and poor, respectively.

Similar observations were made using image analysis as shown in Figures 18 through 23.

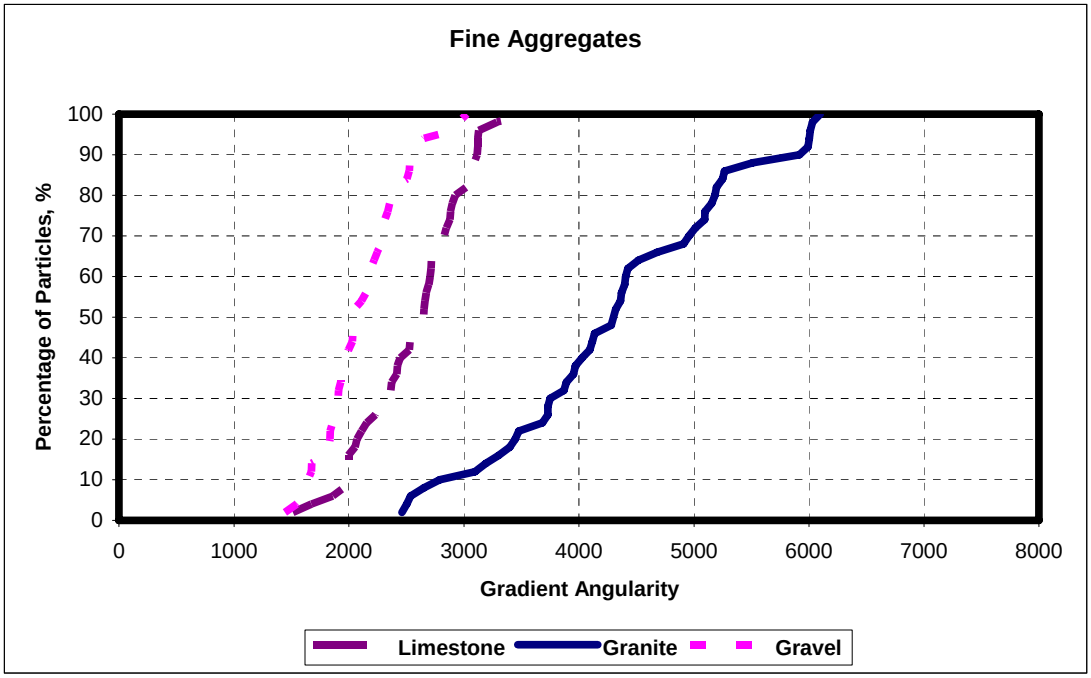

Figure 18. Gradient Angularity Results of Fine Aggregates.

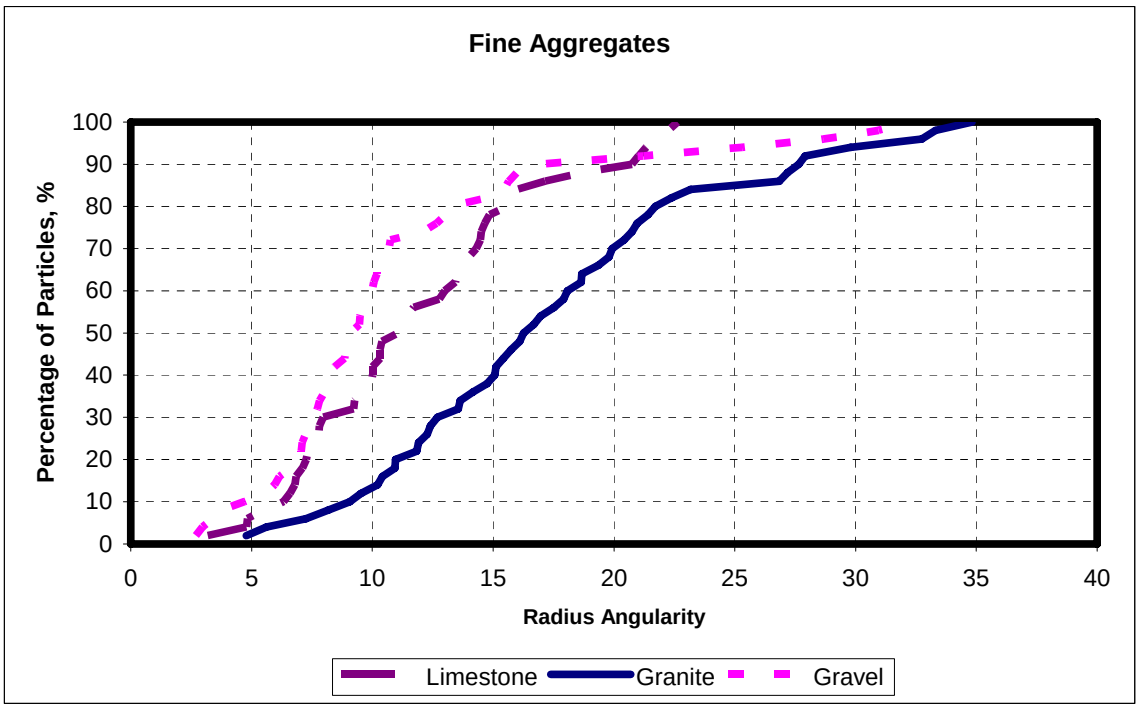

Figure 19. Radius Angularity Results of Fine Aggregates.

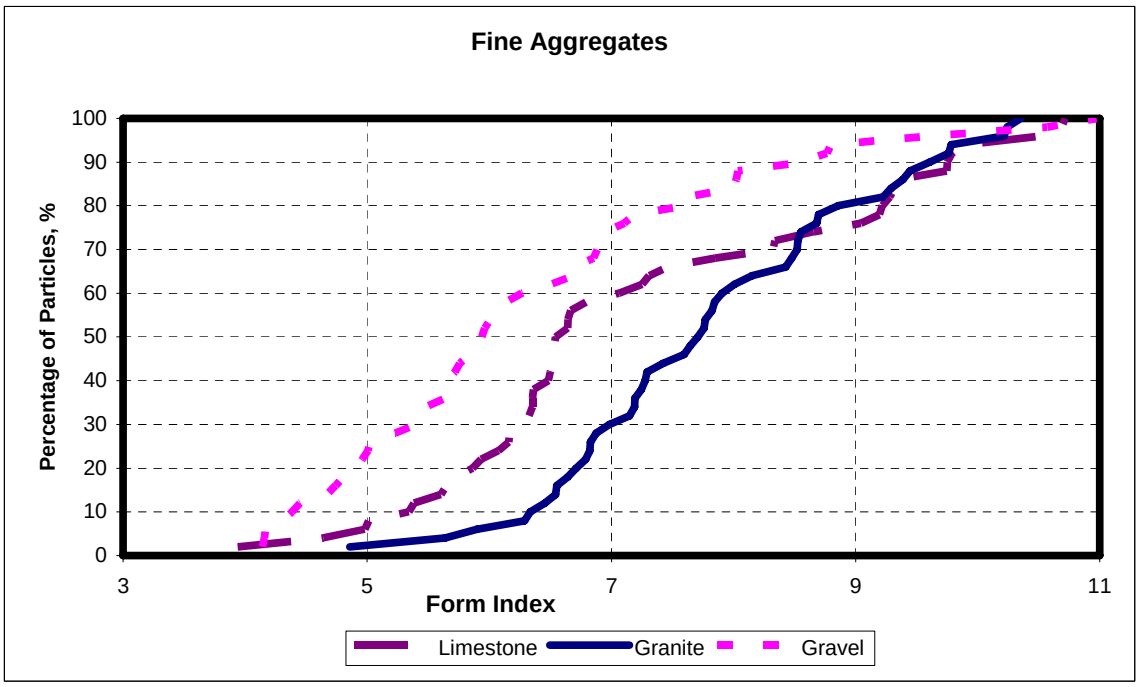

Figure 20. Form Index Results of Fine Aggregates.

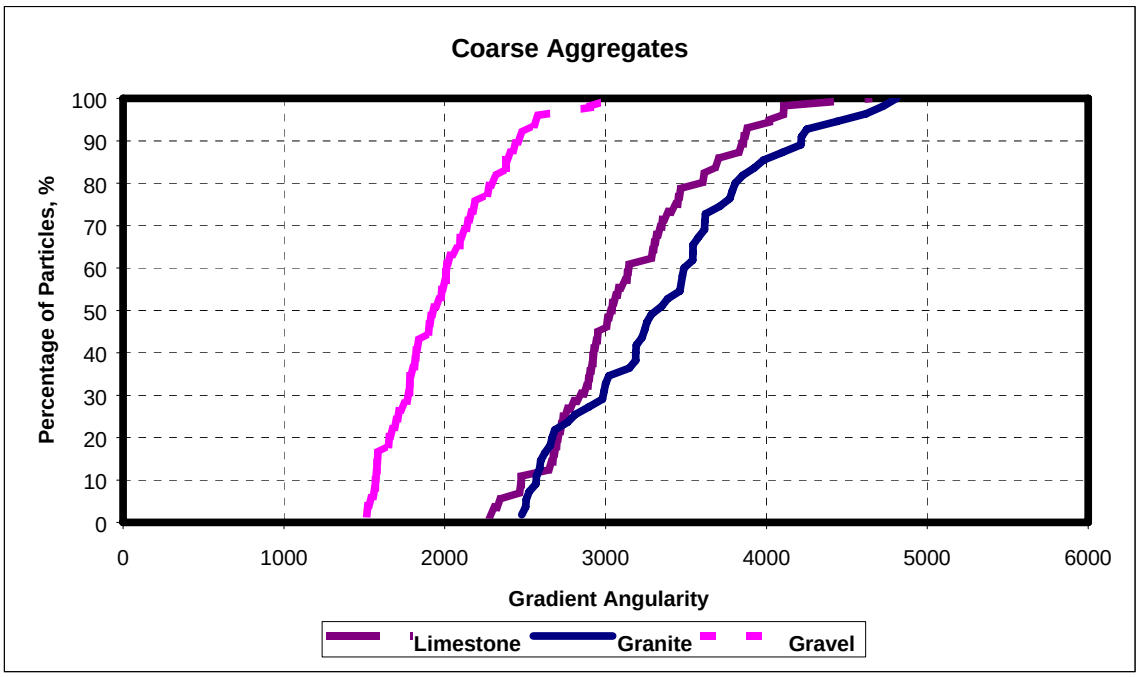

Figure 21. Gradient Angularity Results of Coarse Aggregates.

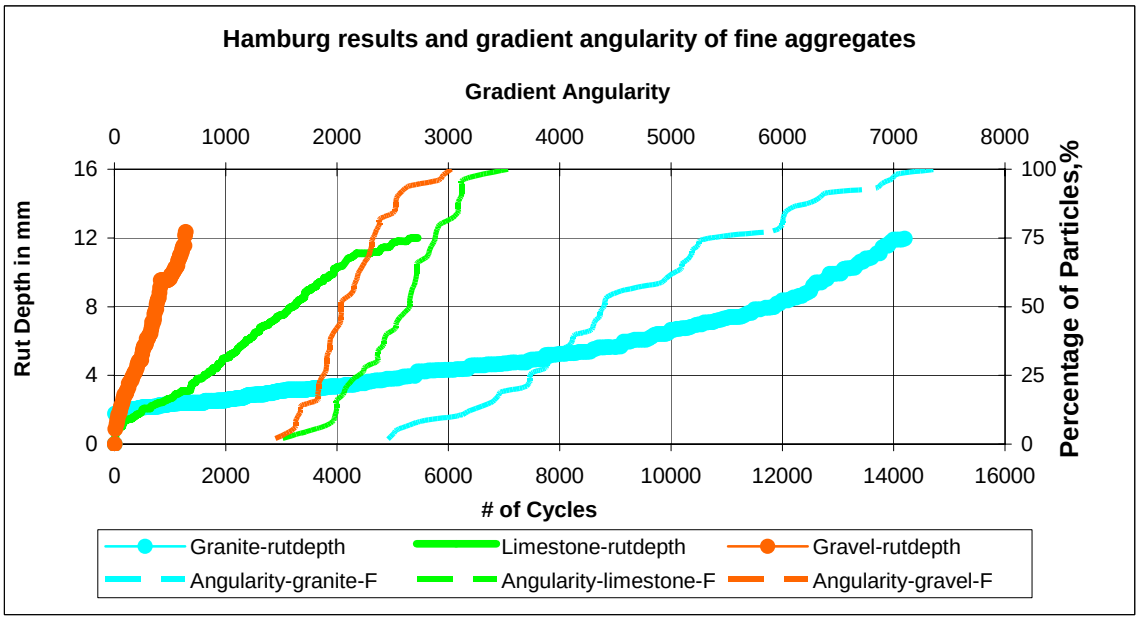

Figure 22. Hamburg Test and Gradient Angularity of Fine Aggregates.

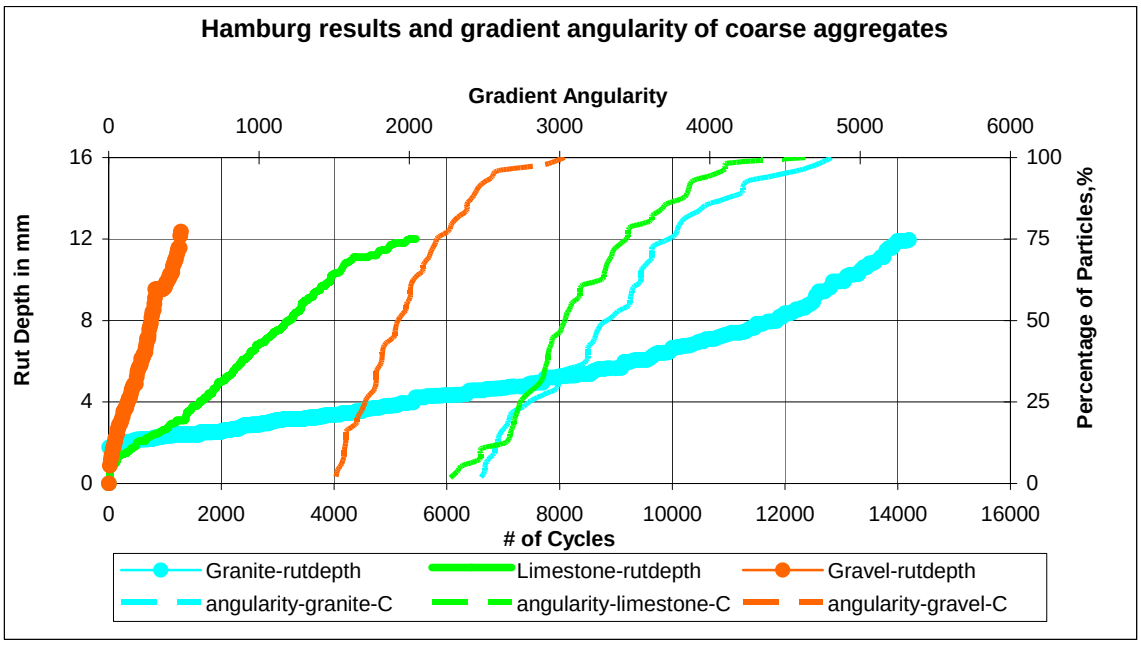

Figure 23. Hamburg Test and Gradient Angularity of Coarse Aggregates.

Both show that granite, limestone and gravel exhibit field performance from excellent to poor.

As shown in Figures 22 and 23, it is obvious that gravel is the weakest of all the aggregates and it has the least angularity, form and texture values.

Only coarse angularity by radius method did not show a similar pattern. According to the radius method, coarse limestone is more angular than coarse granite. This is due to the fact that the radius method considers the elongation of a particle and limestone is more elongated than granite (form value of limestone is about 7.15 and that of the granite is about 6.52) thus, the angularity of limestone as measured by the radius method is higher than granite. On the other hand coarse granite is rough and has small irregularities on its surface due to which angularity of granite as measured by the gradient method is higher than limestone. These irregularities are too small to be captured by the radius method since θ is taken as 5 degrees.

In the case of texture, the coarse aggregate texture chart as shown in Figure 24 follows the same pattern. But in the case of fine aggregate texture, limestone has a higher texture index than granite.

The texture index in Figure 24 shows that granite, limestone, and gravel exhibit field performance from excellent to poor.

The sphericity of coarse aggregates in Figure 25 shows that granite, limestone, and gravel exhibit field performance from excellent to poor.

The shape factor of coarse aggregates in Figure 26 shows that granite, limestone, and gravel exhibit field performance from excellent to poor.

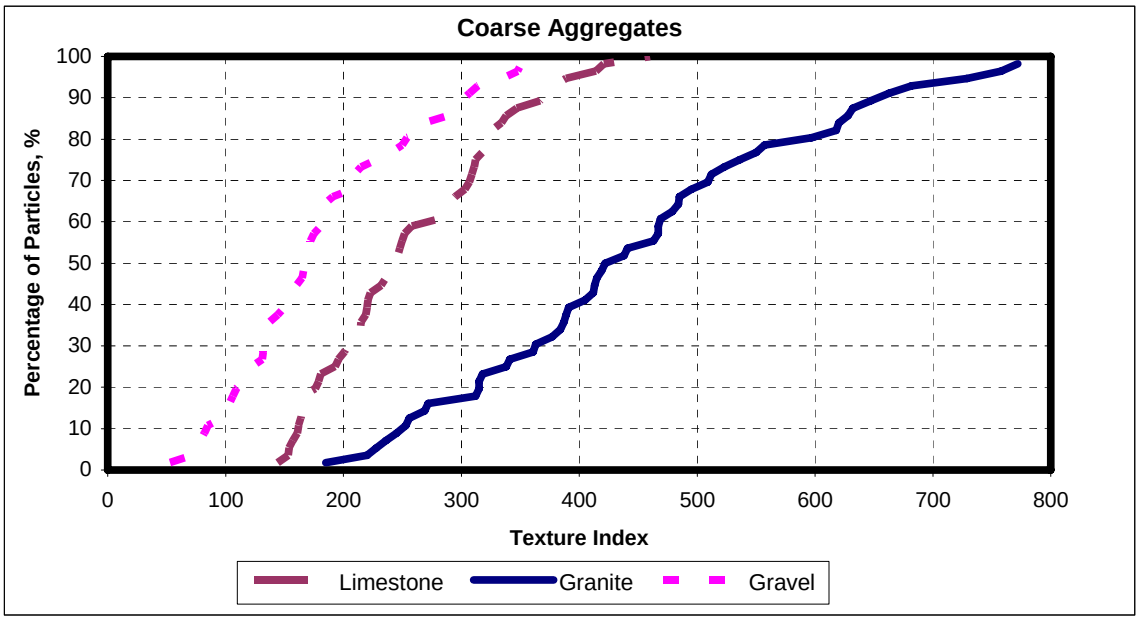

Figure 24. Texture Index of Coarse Aggregates.

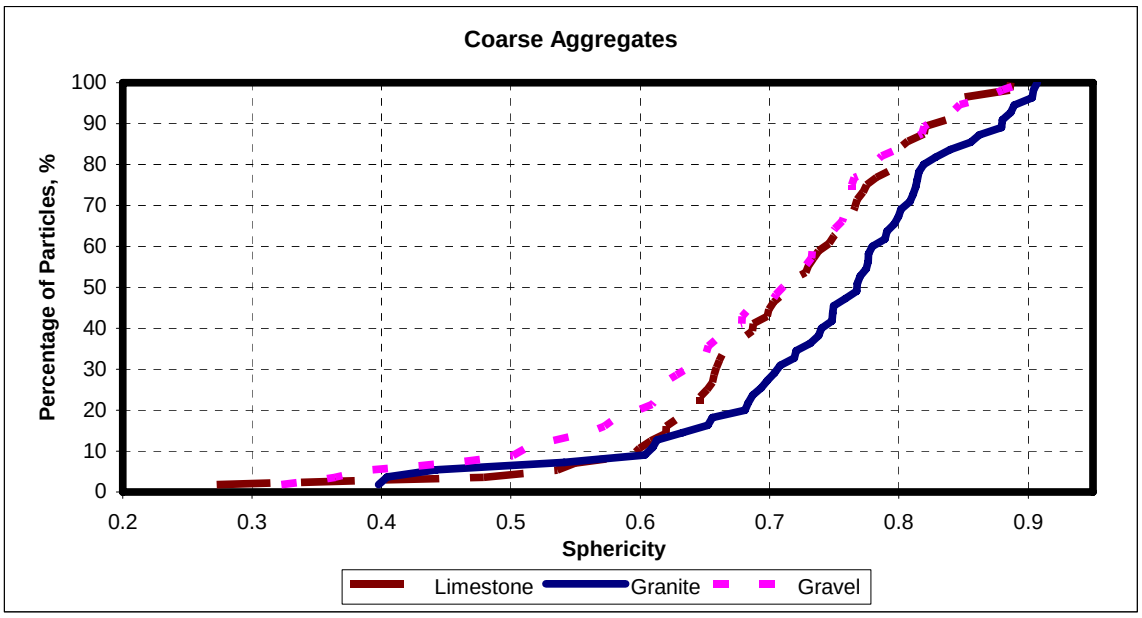

Figure 25. Sphericity of Coarse Aggregates.

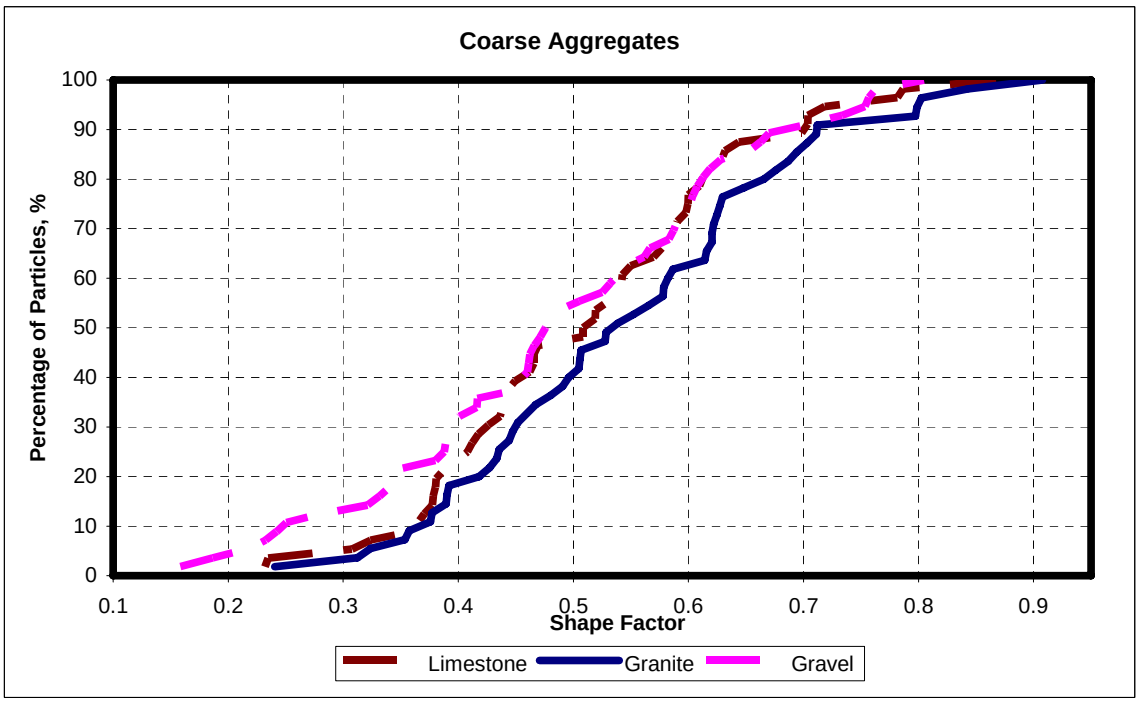

Figure 26. Shape Factor of Coarse Aggregates.

Figures 25 and 26 show the shape factor and sphericity are higher for granite than limestone whereas gravel has the lowest value. Since limestone is more elongated than granite the sphericity and shape factor of limestone should be less than granite. Gravel has the lowest value because gravel material has many flat particles.

Thus, gradient angularity is the best surface parameter to predict performance, especially related to rutting. Also, form parameters such as form index, sphericity, and shape factor correlate well with the performance results.

CHAPTER VI
STATISTICAL ANALYSIS

This chapter presents a general description of all the statistical parameters used in this project followed by analysis and results.

Statistical parameters such as the mean or median can be used to represent the entire distribution. Median of all the values is used as a representative of the entire data set because of the presence of outliers. Complete distribution offers more information when comparing shape properties of different aggregates, as shown in Figures 11 and 14. However, median values, as shown in Tables 5 and 7 briefly describe properties and can be used to distinguish different aggregates. Data transformation (squareroot of original values) has been taken for data analysis as it fits the normal distribution. Here we only consider the aggregates that we selected for performance tests (seven aggregates: one limestone, three gravels, and three granites). The statistical analysis is done in two parts as follows:

- t-test,
- analysis of variance (ANOVA).

Unpaired t-test with unequal variance: The t-test assesses whether the means of two groups are *statistically* different from each other. This analysis is appropriate whenever we want to compare the means of two groups. This test is done to check the effect of crushing on aggregates and to evaluate whether image analysis can effectively monitor change in aggregate properties for different aggregates. Since the variance in the crushed and uncrushed cases is different, we chose the unequal variance option. The t-test tells us if the variation between two groups is "significant." T-test is done in Microsoft Excel.

ANOVA (Analysis of Variance): the t-test can compare two groups, however, when we want to compare many groups together we need to use ANOVA. The one-way analysis of variance allows us to compare several groups of observations, all of which are independent and possibly with a different mean for each group. A test of great importance is whether or not all the means are equal. The test is used to compare angularity, textures, and form of all the aggregates, both coarse and fine, to confirm which aggregate types fall in the same range as identified by ANOVA. The ANOVA test can only tell us whether there is a difference between the groups that we are analyzing or not. Once we have found that there is some difference between the means of these groups, Post Hoc range tests and pair wise multiple comparisons can determine which means differ. Tukey's HSD test is used for this purpose. These tests were done using SPSS software.

Appendix C shows the Normal Probability Plots for Gravel-1 (crushed and as received). An original value does not give a good fit over the normal curve. Data should be normal to be able to use t-tests and ANOVA tests in statistical analysis. So the data are transformed and the square root of the original value is taken. The graphs are shown in Appendix C. As it is obvious from the graphs that data points vary a lot at the two tails, the deviation is minimized by data transformation. After transforming data, deviation is fully minimized at the lower tail but there is some deviation at the upper end. The graph shows the transformation of only one type of material, both crushed and uncrushed. The same trend was observed in the rest of the aggregates.

T-TEST RESULTS

Below are the t-test outputs for rad_ang, grad_ang, form, and texture values.
Ho =μ1 = μ2,. there is no difference in the mean value after crushing
H1= μ1 =/=μ2,. there is difference in the mean value after crushing
α = 0.05, so if p value < α; reject Ho

Limestone

t-test: Two-Sample Assuming Unequal Variances
Radius_Angularity

	crushed	*uncrushed*
Mean	3.806	3.386
Variance	0.939	0.530
Observations	50.000	50.000
Hypothesized Mean Difference	0.000	
df	91.000	
t-stat	2.450	
P(T<=t) one-tail	0.008	
t Critical one-tail	1.662	
P(T<=t) two-tail	0.016	
t Critical two-tail	1.986	

Here p<alpha, reject Ho and since t-stat is positive, there is an increase in angularity value as measured by the radius method.

t-test: Two-Sample Assuming Unequal Variances
Gradient_Angularity

	crushed	*uncrushed*
Mean	54.449	50.466
Variance	23.269	20.499
Observations	50.000	50.000
Hypothesized Mean Difference	0.000	
df	98.000	
t-stat	4.257	
P(T<=t) one-tail	0.000	
t Critical one-tail	1.661	
P(T<=t) two-tail	0.000	
t Critical two-tail	1.984	

Here p<alpha, reject Ho and since t-stat is positive, there is an increase in angularity value as measured by the gradient method.

t-test: Two-Sample Assuming Unequal Variances
Form

	crushed	*uncrushed*
Mean	2.923	2.675
Variance	0.151	0.102
Observations	50.000	50.000
Hypothesized Mean Difference	0.000	
df	94.000	
t-stat	3.496	
P(T<=t) one-tail	0.000	
t Critical one-tail	1.661	
P(T<=t) two-tail	0.001	
t Critical two-tail	1.986	

Here p<alpha, reject Ho and since t-stat is positive, there is an increase in form value as measured by this method.

t-test: Two-Sample Assuming Unequal Variances
Texture

	crushed	*uncrushed*
Mean	14.415	13.836
Variance	2.522	2.043
Observations	15.000	15.000
Hypothesized Mean Difference	0.000	
df	28.000	
t-stat	1.049	
P(T<=t) one-tail	0.152	
t Critical one-tail	1.701	
P(T<=t) two-tail	0.303	
t Critical two-tail	2.048	

Here p>alpha, accept Ho. No significant change observed in case of texture after crushing.

In the case of limestone, according to the t-test, increase in radius angularity, gradient angularity, and form is observed after crushing. In this case gradient angularity shows more increase in angularity as p value for gradient method is 0.00 and that of radius method is 0.008. No significant difference was observed in texture after crushing.

Below are the t-test outputs for rad_ang, grad_ang, form, and texture values.
Ho =$\mu 1 = \mu 2$, there is no difference in the mean value after crushing
H1= $\mu 1 =/= \mu 2$, there is difference in the mean value after crushing
$\alpha = 0.05$, so if p value ,< α: reject Ho

Gravel-1

t-test: Two-Sample Assuming Unequal Variances

Radius_Angularity

	crushed	*uncrushed*
Mean	4.010	3.644
Variance	0.708	0.528
Observations	50.000	50.000
Hypothesized Mean Difference	0.000	
df	96.000	
t-stat	2.329	
P(T<=t) one-tail	0.011	
t Critical one-tail	1.661	
P(T<=t) two-tail	0.022	
t Critical two-tail	1.985	

Here p<alpha, reject Ho and since t-stat is positive there is an increase in the angularity value as measured by the radius method.

t-test: Two-Sample Assuming Unequal Variances

Gradient_Angularity

	crushed	*uncrushed*
Mean	53.870	51.704
Variance	29.326	26.272
Observations	50.000	50.000
Hypothesized Mean Difference	0.000	
df	98.000	
t-stat	2.054	
P(T<=t) one-tail	0.021	
t Critical one-tail	1.661	
P(T<=t) two-tail	0.043	
t Critical two-tail	1.984	

Here p<alpha, reject Ho and since t-stat is positive, there is an increase in angularity value as measured by the gradient method.

t-test: Two-Sample Assuming Unequal Variances
Form

	crushed	*uncrushed*
Mean	3.009	3.006
Variance	0.078	0.095
Observations	50.000	50.000
Hypothesized Mean Difference	0.000	
df	97.000	
t-stat	0.062	
P(T<=t) one-tail	0.475	
t Critical one-tail	1.661	
P(T<=t) two-tail	0.951	
t Critical two-tail	1.985	

Here p>alpha, accept Ho, form values before crushing and after crushing are very close.

t-test: Two-Sample Assuming Unequal Variances
Texture

	crushed	*uncrushed*
Mean	13.388	10.185
Variance	4.319	2.776
Observations	15.000	15.000
Hypothesized Mean Difference	0.000	
df	27.000	
t-stat	4.656	
P(T<=t) one-tail	0.000	
t Critical one-tail	1.703	
P(T<=t) two-tail	0.000	
t Critical two-tail	2.052	

Here p<alpha, so reject Ho and since t-stat is positive, an increase in texture value was observed after crushing.

Thus, in the case of Gravel-1 according to the t-test, angularity and texture values increase after crushing while no difference is observed in the case of form. However, the p value for radius angularity is less than for gradient angularity so increase in angularity in the case of the radius method is more than with the gradient method.

Below are the t-test outputs for rad_ang, grad_ang, form, and texture values.
Ho =$\mu 1 = \mu 2$, there is no difference in the mean value after crushing
H1= $\mu 1 =/= \mu 2$, there is difference in the mean value crushing
$\alpha = 0.05$, so if p value < α : reject Ho

Gravel-2

t-test: Two-Sample Assuming Unequal Variances
Radius_Angularity

	crushed	*uncrushed*
Mean	4.703	3.842
Variance	1.056	0.952
Observations	50.000	50.000
Hypothesized Mean Difference	0.000	
df	98.000	
t-stat	4.299	
P(T<=t) one-tail	0.000	
t Critical one-tail	1.661	
P(T<=t) two-tail	0.000	
t Critical two-tail	1.984	

Here p<alpha, reject Ho and since t-stat is positive, there is an increase in angularity value as measured by the radius method.

t-test: Two-Sample Assuming Unequal Variances
Gradient_Angularity

	crushed	*uncrushed*
Mean	63.290	59.056
Variance	187.489	70.721
Observations	50.000	50.000
Hypothesized Mean Difference	0.000	
df	81.000	
t-stat	1.863	
P(T<=t) one-tail	0.033	
t Critical one-tail	1.664	
P(T<=t) two-tail	0.066	
t Critical two-tail	1.990	

Here p<alpha, reject Ho and since t-stat is positive, there is an increase in angularity value as measured by the gradient method.

t-test: Two-Sample Assuming Unequal Variances

Form

	crushed	*uncrushed*
Mean	3.042	2.773
Variance	0.135	0.135
Observations	50.000	50.000
Hypothesized Mean Difference	0.000	
df	98.000	
t-stat	3.647	
P(T<=t) one-tail	0.000	
t Critical one-tail	1.661	
P(T<=t) two-tail	0.000	
t Critical two-tail	1.984	

Here p<alpha, reject Ho and since t-stat is negative, there is an increase in form value as measured by this method.

t-test: Two-Sample Assuming Unequal Variances

Texture

	crushed	*uncrushed*
Mean	12.164	9.959
Variance	6.547	4.590
Observations	15.000	15.000
Hypothesized Mean Difference	0.000	
Df	27.000	
t -stat	2.559	
P(T<=t) one-tail	0.008	
t Critical one-tail	1.703	
P(T<=t) two-tail	0.016	
t Critical two-tail	2.052	

Here p<alpha, so reject Ho and since t-stat is positive, an increase in texture value was observed after crushing.

In the case of Gravel-2, increase in radius angularity, gradient angularity, and form and texture is observed after crushing. Increase in radius angularity is greater than in gradient angularity since p value is less in the case of the radius method.

Below are the t-test outputs for rad_ang, grad_ang, form, and texture values.

Ho = $\mu 1 = \mu 2$, there is no difference in the mean value after crushing

H1 = $\mu 1 =/= \mu 2$, there is difference in the mean value after crushing

$\alpha = 0.05$, so if p value < α : reject Ho

Gravel-3

t-test: Two-Sample Assuming Unequal Variances

Radius_Angularity

	crushed	*uncrushed*
Mean	5.377	3.209
Variance	3.931	0.787
Observations	50.000	50.000
Hypothesized Mean Difference	0.000	
df	68.000	
t-stat	7.059	
P(T<=t) one-tail	0.000	
t Critical one-tail	1.668	
P(T<=t) two-tail	0.000	
t Critical two-tail	1.995	

Here p<alpha, reject Ho and since t-stat is positive there is an increase in angularity after crushing as measured by the radius method.

t-test: Two-Sample Assuming Unequal Variances

Gradient_Angularity

	crushed	*uncrushed*
Mean	61.074	45.983
Variance	42.095	14.787
Observations	50.000	50.000
Hypothesized Mean Difference	0.000	
df	80.000	
t-stat	14.149	
P(T<=t) one-tail	0.000	
t Critical one-tail	1.664	
P(T<=t) two-tail	0.000	
t Critical two-tail	1.990	

Here p<alpha, reject Ho and since t-stat is positive there is an increase in angularity after crushing as measured by the radius method.

t-test: Two-Sample Assuming Unequal Variances
Form

	crushed	*uncrushed*
Mean	3.082	2.501
Variance	0.218	0.093
Observations	50.000	50.000
Hypothesized Mean Difference	0.000	
df	84.000	
t-stat	7.368	
P(T<=t) one-tail	0.000	
t Critical one-tail	1.663	
P(T<=t) two-tail	0.000	
t Critical two-tail	1.989	

Here p<alpha, reject Ho and since t-stat is positive there is an increase in angularity after crushing.

t-test: Two-Sample Assuming Unequal Variances
Texture

	crushed	*uncrushed*
Mean	11.035	10.055
Variance	3.970	4.334
Observations	15.000	15.000
Hypothesized Mean Difference	0.000	
df	28.000	
t-stat	1.341	
P(T<=t) one-tail	0.095	
t Critical one-tail	1.701	
P(T<=t) two-tail	0.191	
t Critical two-tail	2.048	

Here p<alpha so accept Ho, there is no significant difference because of crushing.

In Gravel-3, no difference is observed in texture after crushing, but angularity and form value increased after crushing.

Below are the t-test outputs for rad_ang, grad_ang, form, and texture values.
Ho =μ1 = μ2, there is no difference in the mean value after crushing
H1= μ1=/= μ2,there is difference in the mean value after crushing
α = 0.05, so if p value < α: reject Ho

Granite-1

t-test: Two-Sample Assuming Unequal Variances
Radius_Angularity

	crushed	*uncrushed*
Mean	4.183	4.190
Variance	1.036	0.843
Observations	50.000	50.000
Hypothesized Mean Difference	0.000	
df	97.000	
t-stat	-0.040	
P(T<=t) one-tail	0.484	
t Critical one-tail	1.661	
P(T<=t) two-tail	0.968	
t Critical two-tail	1.985	

Here p>alpha, so accept Ho. No significant difference is found after crushing.

t-test: Two-Sample Assuming Unequal Variances
Gradient_Angularity

	crushed	*uncrushed*
Mean	58.851	70.984
Variance	15.333	39.049
Observations	50.000	50.000
Hypothesized Mean Difference	0.000	
df	82.000	
t-stat	-11.633	
P(T<=t) one-tail	0.000	
t Critical one-tail	1.664	
P(T<=t) two-tail	0.000	
t Critical two-tail	1.989	

Here p<alpha, so reject Ho. Since t-stat is negative, a decrease in angularity is found after crushing as measured by the gradient method.

t-test: Two-Sample Assuming Unequal Variances

Form

	crushed	*uncrushed*
Mean	3.006	2.952
Variance	0.135	0.082
Observations	50.000	50.000
Hypothesized Mean Difference	0.000	
df	93.000	
t-stat	0.830	
P(T<=t) one-tail	0.204	
t Critical one-tail	1.661	
P(T<=t) two-tail	0.409	
t Critical two-tail	1.986	

Here p>alpha, so accept Ho. No significant difference was found with crushing in the case of form.

t-test: Two-Sample Assuming Unequal Variances

Texture

	crushed	*uncrushed*
Mean	11.336	14.420
Variance	3.818	2.218
Observations	15.000	15.000
Hypothesized Mean Difference	0.000	
df	26.000	
t-stat	-4.861	
P(T<=t) one-tail	0.000	
t Critical one-tail	1.706	
P(T<=t) two-tail	0.000	
t Critical two-tail	2.056	

Here p<alpha so reject Ho, t-stat is negative so that means a decrease in texture.

In the case of Granite-1, no significant difference was found in radius angularity and form after crushing. However, gradient angularity and texture index values decreased after crushing.

Below are the t-test outputs for rad_ang, grad_ang, form, and texture values.
Ho = μ1 = α2,. there is no difference in the mean value after crushing
H1= μ1=/=μ2,. there is difference in the mean value after crushing
α = 0.05, so if p value < α: reject Ho

Granite-2

t-test: Two-Sample Assuming Unequal Variances
Radius_Angularity

	crushed	*uncrushed*
Mean	4.984	4.247
Variance	1.618	0.788
Observations	50.000	50.000
Hypothesized Mean Difference	0.000	
Df	88.000	
t-stat	3.359	
P(T<=t) one-tail	0.001	
t Critical one-tail	1.662	
P(T<=t) two-tail	0.001	
t Critical two-tail	1.987	

Here p<alpha, reject Ho and since t-stat is positive, there is an increase in angularity value as measured by the radius method.

t-test: Two-Sample Assuming Unequal Variances
Gradient_Angularity

	crushed	*uncrushed*
Mean	72.819	57.253
Variance	81.775	52.388
Observations	50.000	50.000
Hypothesized Mean Difference	0.000	
df	94.000	
t-stat	9.503	
P(T<=t) one-tail	0.000	
t Critical one-tail	1.661	
P(T<=t) two-tail	0.000	
t Critical two-tail	1.986	

Here p<alpha, reject Ho and since t-stat is positive, there is an increase in angularity value as measured by the gradient method.

t-test: Two-Sample Assuming Unequal Variances

Form

	crushed	*uncrushed*
Mean	2.882	3.095
Variance	0.080	0.066
Observations	50.000	50.000
Hypothesized Mean Difference	0.000	
df	97.000	
t-stat	-3.947	
P(T<=t) one-tail	0.000	
t Critical one-tail	1.661	
P(T<=t) two-tail	0.000	
t Critical two-tail	1.985	

Here p<alpha, reject Ho and since t-stat is negative, there is a decrease in form value.

t-test: Two-Sample Assuming Unequal Variances

Texture

	crushed	*uncrushed*
Mean	15.123	11.179
Variance	3.111	1.954
Observations	15.000	15.000
Hypothesized Mean Difference	0.000	
df	27.000	
t-stat	6.787	
P(T<=t) one-tail	0.000	
t Critical one-tail	1.703	
P(T<=t) two-tail	0.000	
t Critical two-tail	2.052	

Here p<alpha so reject Ho, t-stat is positive, so that means an increase in texture value was observed after crushing.

In the case of Granite-2, increase in angularity, texture, and decrease in form was observed after crushing.

Below are the t-test outputs for rad_ang, grad_ang, form, and texture values.
Ho = $\mu 1 = \mu 2$ there is no difference in the mean value after crushing
H1= $\mu 1 =/= \mu 2$, there is difference in the mean value after crushing
$\alpha = 0.05$, so if p value < α; reject Ho

Granite-3

t-test: Two-Sample Assuming Unequal Variances
Radius_Angularity

	crushed	*uncrushed*
Mean	4.495	4.585
Variance	1.540	1.726
Observations	50.000	50.000
Hypothesized Mean Difference	0.000	
df	98.000	
t-stat	-0.352	
P(T<=t) one-tail	0.363	
t Critical one-tail	1.661	
P(T<=t) two-tail	0.726	
t Critical two-tail	1.984	

t-test: Two-Sample Assuming Unequal Variances
Gradient_Angularity

	crushed	*uncrushed*
Mean	65.920	68.085
Variance	68.867	84.645
Observations	50.000	50.000
Hypothesized Mean Difference	0.000	
df	97.000	
t-stat	-1.236	
P(T<=t) one-tail	0.110	
t Critical one-tail	1.661	
P(T<=t) two-tail	0.220	
t Critical two-tail	1.985	

Here p<alpha, accept Ho. No change in angularity is observed after crushing as measured by the gradient method.

t-Test: Two-Sample Assuming Unequal Variances
Form

	crushed	*uncrushed*
Mean	3.028	2.899
Variance	0.136	0.103
Observations	50.000	50.000
Hypothesized Mean Difference	0.000	
df	96.000	
t-stat	1.863	
P(T<=t) one-tail	0.033	
t Critical one-tail	1.661	
P(T<=t) two-tail	0.066	
t Critical two-tail	1.985	

Here p-alpha, reject Ho. Form value increased after crushing.

t-Test: Two-Sample Assuming Unequal Variances
Texture

	crushed	*uncrushed*
Mean	11.406	11.424
Variance	3.457	4.110
Observations	15.000	15.000
Hypothesized Mean Difference	0.000	
df	28.000	
t-stat	-0.024	
P(T<=t) one-tail	0.490	
t Critical one-tail	1.701	
P(T<=t) two-tail	0.981	
t Critical two-tail	2.048	

Here p<alpha so accept Ho, there is no significant difference because of crushing

In the case of Granite-3, form index increased after crushing but texture and angularity values did not show much difference after crushing.

ANOVA: ANALYSIS OF VARIANCE

The objective of this analysis was to determine variability in different aggregates on the basis of image analysis results. ANOVA was done separately for fine and coarse aggregate results. All seven groups are as listed in Table 12. Tukey's test was conducted to determine the groups with significant variability as shown in Table 13 – 15.

Table 12. Aggregate Groups for Statistical Analysis.

Aggregate Type	Group	
Gravel-1	1	Gravel-1Beck
Limestone	2	Limestone Martin Marietta
Gravel-2	3	Gravel-2 Trinity
Granite-1	4	Granite-1 Millcreek
Granite-2	5	Granite-2 Davis
Gravel-3	6	Gravel-3 Brazos river gravel
Granite-3	7	Granite-3 Georgia granite

ANOVA: Radius Angularity of Fine Aggregates

Ho = there is no difference in the mean value of all fine aggregates

H1= there is difference in the mean value of all fine aggregates

$\alpha = 0.05$, so if p value < α, reject Ho; multiple comparison tests will be performed
Confidence interval (%): 95.00

Testing at alpha=0.05 significance level, Ho is rejected and the radius angularity values of all the aggregates are significantly different. Thus, multiple comparison tests were performed using Tukey's test.

Table 13. Fine Aggregate: ANOVA for Radius Angularity.

	Sum of Squares	df	Mean Square	F	Significance
Between Groups	50.250	6	8.375	11.329	.000
Within Groups	253.552	343	.739		
Total	303.802	349			

Table 14. Fine Aggregate: Tukey's Test for Radius Angularity.

	N	Subset for alpha = .05			
AGGREGATE		1	2	3	4
6.00	50	3.191			
2.00	50	3.385	3.385		
1.00	50	3.644	3.644	3.644	
3.00	50		3.841	3.841	3.841
7.00	50			4.090	4.090
4.00	50				4.190
5.00	50				4.247
Sig.		.116	.111	.127	.217

Means for groups in homogeneous subsets are displayed.
a Uses Harmonic Mean Sample Size = 50.000.

In the case of radius angularity, Turkey's test results show that four groups are formed and the groups are overlapping.

ANOVA: Gradient Angularity of Fine Aggregates

Ho = there is no difference in the mean value of all fine aggregates

H1= there is difference in the mean value of all fine aggregates

α= 0.05, so if p value < α, reject Ho; multiple comparison tests will be performed

Confidence interval (%): 95.00

Table 15. Fine Aggregate: ANOVA for Gradient Angularity.

	Sum of Squares	df	Mean Square	F	Sig.
Between Groups	23144.856	6	3857.476	95.339	.000
Within Groups	13878.040	343	40.461		
Total	37022.896	349			

Testing at alpha=0.05 significance level, Ho is rejected and the gradient angularity values of all the aggregates are significantly different (Table 16). Thus, multiple comparison tests were performed using Tukey's test (Table 17).

Table 16. Fine Aggregate: Tukey's Test for Gradient Angularity.

	N	Subset for alpha = .05				
AGGREGATE		1	2	3	4	5
6.00	50	45.919				
2.00	50		50.465			
1.00	50		51.703			
5.00	50			57.253		
3.00	50			59.056		
7.00	50				65.365	
4.00	50					70.983
Sig.		1.000	.960	.793	1.000	1.000

Means for groups in homogeneous subsets are displayed.
a Uses Harmonic Mean Sample Size = 50.000.

In the case of gradient angularity, Tukey's test results show that five groups are formed and groups are overlapping less than with radius angularity. Thus, gradient angularity can better distinguish between different aggregates as compared to radius angularity.

ANOVA: Form Index of Fine Aggregates

Ho = there is no difference in the mean value of all fine aggregates

H1 = there is difference in the mean value of all fine aggregates

$\alpha = 0.05$, so if p value < α, reject Ho; multiple comparison tests will be performed

Confidence interval (%): 95.00

Table 17. Fine Aggregate: ANOVA for Form Index.

	Sum of Squares	df	Mean Square	F	Sig.
Between Groups	12.829	6	2.138	23.752	.000
Within Groups	30.876	343	0.09		
Total	43.705	349			

Testing at alpha=0.05 significance level, Ho is rejected and the form indices of all the aggregates are significantly different (Table 18). Thus, multiple comparison tests were performed using Tukey's test (Tables 19 - 20).

Table 18. Fine Aggregate: Tukey's Test for Form Index.

	N	Subset for alpha = .05			
AGGREGATE		1	2	3	4
6.00	50	2.495			
2.00	50		2.675		
3.00	50		2.773		
7.00	50		2.788	2.788	
4.00	50			2.951	2.951
1.00	50				3.005
5.00	50				3.095
Sig.		1.000	.491	.092	.201

Means for groups in homogeneous subsets are displayed.
a Uses Harmonic Mean Sample Size = 50.000.

Form index values of different aggregates have been divided into four groups from low to high.

ANOVA: Texture Index of Fine Aggregates

Ho = there is no difference in the mean value of all fine aggregates

H1 = there is difference in the mean value of all fine aggregates

$\alpha = 0.05$, so if p value $< \alpha$, reject Ho; multiple comparison tests will be performed

Confidence interval (%): 95.00

Table 19. Fine Aggregate: ANOVA for Texture Index.

	Sum of Squares	df	Mean Square	F	Sig.
Between Groups	303.536	6	50.589	16.301	.000
Within Groups	304.146	98	3.104		
Total	607.681	104			

Testing at alpha=0.05 significance level, Ho is rejected and the texture indices of all the aggregates are significantly different. Thus, multiple comparison tests were performed using Tukey's test.

Table 20. Fine Aggregate: Tukey's Test for Texture Index.

	N	Subset for alpha = .05	
AGGREGATE		1	2
3.00	15	9.959	
6.00	15	10.055	
1.00	15	10.185	
5.00	15	11.179	
7.00	15	11.423	
2.00	15		13.835
4.00	15		14.419
Sig.		.266	.970

Means for groups in homogeneous subsets are displayed.
a Uses Harmonic Mean Sample Size = 15.000.

Tukey's test grouped the texture index of fine aggregates into two groups (Table 21).

ANOVA: Radius Angularity of Coarse Aggregates

Ho = there is no difference in the mean value of all fine aggregates

H1 = there is difference in the mean value of all fine aggregates

$\alpha = 0.05$, so if p value $<\alpha$, reject Ho; multiple comparison tests will be performed

Confidence interval (%): 95.00

Table 21. Coarse Aggregate: ANOVA for Radius Angularity.

	Sum of Squares	df	Mean Square	F	Sig.
Between Groups	20.982	6	3.497	5.814	.000
Within Groups	206.322	343	.602		
Total	227.304	349			

Testing at alpha=0.05 significance level, Ho is rejected and the radius angularity values of all the aggregates are significantly different (Table 22).. Thus, multiple comparison tests were performed using Tukey's test (Tables 23-24).

Table 22. Coarse Aggregate: Tukey's Test for Radius Angularity.

	N	Subset for alpha = .05		
AGGREGATE		1	2	3
3.00	50	3.142		
6.00	50	3.335	3.335	
1.00	50	3.520	3.520	
7.00	50	3.557	3.557	3.557
2.00	50	3.567	3.567	3.567
4.00	50		3.690	3.690
5.00	50			3.982
Sig.		.089	.250	.088

Means for groups in homogeneous subsets are displayed.

a Uses Harmonic Mean Sample Size = 50.000.

Tukey's test grouped radius angularity of coarse aggregates into three groups. Groups are overlapping and all three groups have around two aggregates in common.

ANOVA: Gradient Angularity of Coarse Aggregates

Ho = there is no difference in the mean value of all fine aggregates

H1 = there is difference in the mean value of all fine aggregates

$\alpha = 0.05$, so if p value < α, reject Ho; multiple comparison tests will be performed

Confidence interval (%): 95.00

Table 23. Coarse Aggregate: ANOVA for Gradient Angularity.

	Sum of Squares	df	Mean Square	F	Sig.
Between Groups	9593.277	6	1598.879	71.455	.000
Within Groups	7675.006	343	22.376		
Total	17268.283	349			

Testing at alpha=0.05 significance level, Ho is rejected and the gradient angularity values of all the aggregates are significantly different (Table 22). Thus, multiple comparison tests were performed using Tukey's test (Table 23).

Table 24. Coarse Aggregate: Tukey's Test for Gradient Angularity.

	N	Subset for alpha = .05				
AGGREGATE		1	2	3	4	5
3.00	50	41.175				
6.00	50		44.613			
2.00	50			48.318		
5.00	50				53.254	
4.00	50				53.406	
1.00	50				53.762	
7.00	50					56.785
Sig.		1.000	1.000	1.000	.998	1.000

Means for groups in homogeneous subsets are displayed.
a Uses Harmonic Mean Sample Size = 50.000.

Tukey's test results grouped gradient angularity of coarse aggregates into five groups. Groups overlap less compared to radius angularity. Gradient angularity proved to be better compared to radius angularity in distinguishing angularity of different aggregates.

ANOVA: Form Index of Coarse Aggregates

Ho = there is no difference in the mean value of all fine aggregates

H1 = there is difference in the mean value of all fine aggregates

$\alpha = 0.05$, so if p value < α,. reject Ho; multiple comparison tests will be performed

Confidence interval (%): 95.00

Table 25. Coarse Aggregate: ANOVA for Form Index.

	Sum of Squares	df	Mean Square	F	Sig.
Between Groups	27.661	6	4.610	42.299	.000
Within Groups	37.384	343	.109		
Total	65.044	349			

Testing at alpha=0.05 significance level, Ho is rejected and the form indices of all the aggregates are significantly different (Table 25). Thus, multiple comparison tests were performed using Tukey's test (Table 26).

Table 26. Coarse Aggregate: Tukey's Test for Form Index.

	N	Subset for alpha = .05		
AGGREGATE		1	2	3
3.00	50	2.359		
6.00	50	2.382		
1.00	50	2.468		
7.00	50	2.511		
4.00	50		2.864	
2.00	50		2.980	2.980
5.00	50			3.087
Sig.		.241	.585	.667

Means for groups in homogeneous subsets are displayed.
a Uses Harmonic Mean Sample Size = 50.000.

Tukey's test grouped form index of coarse aggregates into three groups.

ANOVA: Texture Index of Coarse Aggregates

Ho = there is no difference in the mean value of all fine aggregates

H1 = there is difference in the mean value of all fine aggregates

$\alpha = 0.05$, so if p value < α, reject Ho; multiple comparison tests will be performed

Confidence interval (%): 95.00

Table 27. Coarse Aggregate: ANOVA for Texture Index.

	Sum of Squares	df	Mean Square	F	Sig.
Between Groups	1669.715	6	278.286	77.448	.000
Within Groups	352.132	98	3.593		
Total	2021.846	104			

Testing at alpha=0.05 significance level, Ho is rejected and the texture indices of all the aggregates are significantly different (Table 27). Thus, multiple comparison tests were performed using Tukey's test (Table 28).

Table 28. Coarse Aggregate: Tukey's Test for Texture Index.

	N	Subset for alpha = .05			
AGGREGATE		1	2	3	4
3.00	15	9.325			
2.00	15	10.767	10.767		
5.00	15		12.445		
6.00	15		12.767		
4.00	15			17.296	
1.00	15			18.728	18.728
7.00	15				20.641
Sig.		.370	.069	.379	.094

Means for groups in homogeneous subsets are displayed.
a Uses Harmonic Mean Sample Size = 15.000.

Tukey's test grouped texture index of coarse aggregates into four groups.

OUTLIERS

This part of the chapter provides a general description of outliers and the reasons why outliers were obtained using AIMS.

Outliers are typically (by definition) infrequent observations. Because of the way in which the regression line is determined (especially the fact that it is based on minimizing not the sum of simple distances but the sum of *squares of distances* of data points from the line), outliers have a profound influence on the slope of the regression line and, consequently, on the value of the correlation coefficient. A single outlier is capable of considerably changing the slope of the regression line and, consequently, the value of the correlation. Just one outlier can be entirely responsible for a high value of the correlation that otherwise (without the outlier) would be close to zero. Needless to say, one should never base important conclusions on the value of the correlation coefficient alone. Thus, outliers are extreme cases on one variable or a combination of variables, and they have a strong influence on the calculation of statistics. The box plot shown in Figure 27 provides an example of outliers. In the figure, the box plot on the left side is with outliers and the box plot on the right side is without outliers. As we can see, the plot with the outliers is a symmetrical with a skew on the higher end. Because of the outlier on the higher end, the mean has shifted toward the higher end and is different from the median. Once we remove the outliers, the box plot on the right side becomes symmetrical with mean and median shown by a single line.

Outliers in the data may be due to recording errors or system noise of various kinds, and as such need to be cleaned as part of the extract, transform, clean and load (ETCL) phase of the data mining. On the other hand, an outlier or small group of outliers may be quite error-free recordings that represent the most important part of your data that deserve further careful attention.

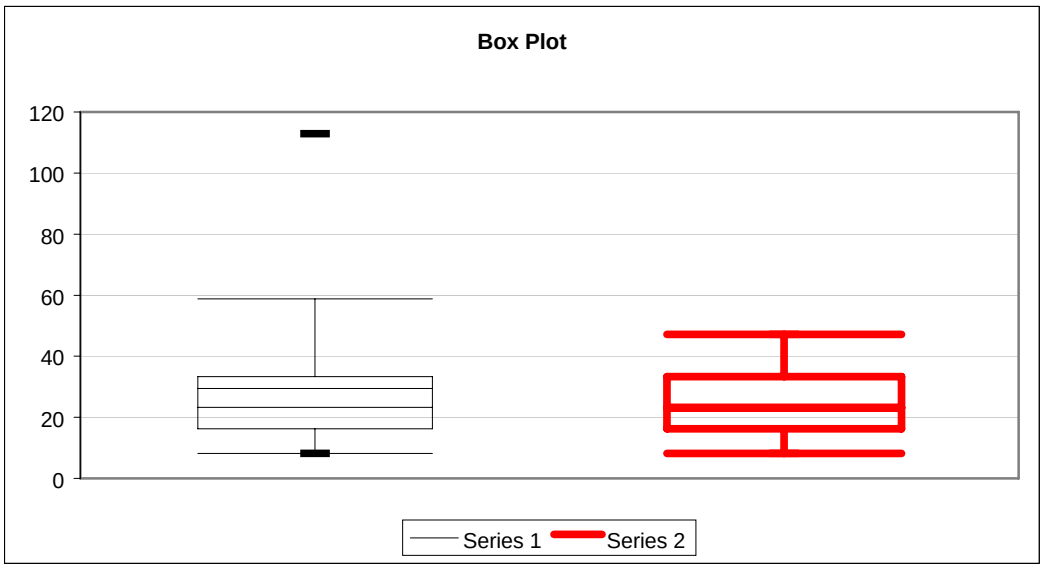

*series 1 = with outliers, series 2 = without outliers.

Figure 27. Box Plot: Angularity Values with and without Outliers.

Following are the reasons for outliers:

- incorrect data entry,
- failure to specify missing value codes,
- case not a member of intended sample population, or
- actual distribution of the population has more extreme cases than a normal distribution.

The influence of outliers can be reduced by checking the following points:

- check the data for the case and ensure proper data entry;
- check if one variable is responsible for most of the outliers and consider deletion of the variable;
- delete the case if it is not part of the population; and
- if variables are from the population, yet to remain in the analysis, transform the variable to reduce influence.

In the case of gradient angularity we can describe angularity as that shape-feature that measures how sharp the corners of a particle are. In order to measure angularity, we must adopt a method that can capture the sharp angular corners of a highly angular particle and at the same time, assign an almost-zero angularity to particles that are rounded. Apart from this fundamental requirement, our method should also have the capability to make fine distinctions between particle shapes that otherwise appear to have similar angularities. The gradient method does possess both of these properties. At sharp corners of the edges of an image, the direction of the gradient vector for adjacent points on the edge changes rapidly. The direction of the gradient vector for rounded particles changes slowly for adjacent points on the edge.

In the case of the gradient method, even though there are very small irregularities on the surface, the vector changes abruptly thus accounting for higher angularity. In Figure 28, the radius angularity for the aggregate is 9.2, and the gradient value is 4088.86. Also, in Figure 29 the gradient angularity of the aggregate is about 6998.44, which is very high. From these two examples it looks as if gradient angularity not only accounts for angularity but also for surface roughness.

Thus, the outliers that were obtained in the case of the gradient method were not faulty values, but they were obtained because of the roughness of the aggregate. These outliers were deleted because they varied a lot compared to sample mean.

Hence, it seems the gradient method is very sensitive to surface irregularities and extreme care should be taken while using images for the gradient method, as the image should be free of all possible noise.

Figure 28. Aggregate with Irregularities on the Surface.

Figure 29. Elongated Aggregate with Very High Angularity and Form Value.

Radius angularity is measured by considering the difference between the radius of a particle in a certain direction and the radius of an equivalent ellipse taken in the same direction. The equivalent ellipse has the same aspect ratios of the particle. Since even AIMS considered the equivalent ellipse as the one that has the same aspect ratio, it was observed that radius angularity of a particle with very high form value was found to be high. The two axes of the equivalent ellipse are defined based on eigenvectors. Equivalent ellipse here is defined by taking the major axis as the maximum height of the particle and the minor axis perpendicular to the height that is passing through the center of gravity of the particle.

Figure 29 shows an example of an aggregate with high form value, which is 18.97, and the radius angularity was found to be 73.30. These values were considered as outliers as detected by statistical software.

Thus, it can be concluded that both methods have their own limitations as described below:

- Radius angularity as obtained from AIMS represents both angularity and forms. A different index can be developed as a combined index representing both radius angularity and form index.

- The radius angularity value is not very sensitive and has a smaller range of values. So, many times if two particles have different angularities they result in almost the same radius angularity value.

- Gradient angularity on the other hand has a bigger spread and larger values. It differentiates angularity of particles in a very precise manner. However, it is so sensitive that any abrupt change in vectors (which measure gradient angularity), due to some noise or any surface irregularity, results in higher gradient values.

- The gradient method considers the effect of roughness along with the angularity of the aggregate.

CHAPTER VII

CONCLUSIONS AND RECOMMENDATIONS

Image analysis was performed on seven aggregates, and three (one limestone, one granite, and one gravel) out of these seven were selected for Performance tests. Two torture-type rutting tests such as Asphalt Pavement Analyzer and Hamburg wheel-tracking tests were performed on these three aggregates to determine if image analysis can predict performance or not. Also, these seven aggregates were correlated with physical test results such as fine aggregate angularity (ASTM C-1252, Method A), compacted aggregate resistance (AASHTO T-193), and flat and elongated test on coarse aggregates (ASTM D-4791-99) to validate the efficacy of image analysis.

The image analysis results were statistically analyzed for seven aggregates. Aggregates were crushed to study the effect of crushing on image analysis parameters. T-test was performed on crushed and uncrushed aggregates to determine the sensitivity of image analysis parameters. Also, ANOVA was done to study the variability in image analysis results.

Based on the findings of test results and data analysis, the following conclusions and recommendations are offered.

CONCLUSIONS

1. Radius angularity obtained by image analysis gives results that have a shorter range as compared to gradient angularity. It is easy to differentiate all seven aggregates using the gradient angularity results. From Tukey's test it can be seen that groups overlap less in the case of gradient angularity as compared to radius angularity.

2. The radius angularity method values highly depend on the way the equivalent ellipse is defined. In AIMS, equivalent ellipse is defined on the basis of the particle controid. So, if in any case a particle controid is toward one end, the equivalent ellipse will be formed with a much bigger size than is needed resulting in a very high and faulty angularity value. In the present project, such values were eliminated, considering them as outliers.

3. Gradient value is very sensitive to the multi-scale surface irregularities.

4. Crushing of the aggregates proved that image analysis parameters are sensitive as values of all the parameters except granite increased after crushing, which is expected as granite comes highly crushed from the source itself.

5. Reasonable correlation was observed between flat and elongated test results and form index values of coarse aggregates.

6. A correlation with $R^2 = 0.5$ was observed between the uncompacted void content values versus radius and gradient angularity values of fine aggregates.

7. No correlation was observed between the compacted aggregate resistance values versus radius and gradient angularity values of fine aggregates.

8. Image analysis of fine aggregates showed that granite has the highest angularity values, followed by crushed gravel, and limestone and river gravel have the least angularity value. Both granite and limestone have high texture values.

9. For the three aggregates selected for performance tests, the image analysis could very well predict the performance results.

RECOMMENDATIONS

1. CAR test samples need to be tested at much higher compression loading than currently specified in order to effectively differentiate between aggregates exhibiting high stability values.

2. In the case of radius angularity, the equivalent ellipse needs to be defined properly.

3. Since gradient angularity is very sensitive to any surface irregularity, the image analysis system should be such that it eliminates any surface noise.

4. Instead of doing image analysis for only one sieve size, it should be done for the entire gradation.

5. Performance tests should be done on an additional material (such as Gravel-1, which is crushed gravel).

6. Different aggregate combinations should be selected as limestone coarse and granite fines or gravel fines and vice versa to study the effect of fine and coarse aggregate image analysis parameters on performance.

REFERENCES

1. McGennis R.B., R.M. Andersen, T.W. Kennedy and M. Solaimanina. *Background of SUPERPAVE Asphalt Mixture Design and Analysis.* Final Report No. FHWA-SA-95-003, Federal Highway Administration, U.S. Department of Transportation, Washington, D. C., February 1995.
2. Rao, C., and E. Tutumluer. *A New Image Analysis Approach for Determination of Volume of Aggregates.* Transportation Research Record 1721, Washington, D.C., 2000, pp 73-80.
3. Masad E., *The Development of A Computer Controlled Image Analysis System for Measuring Aggregate Shape Properties.* Project 77, IDEA program attachment to final report, Pullman, Washington, Oct 2000-2002.
4. Roberts, F., P. Kandhal, R.Brown, L.Lee, and T. Kennedy, *Hot Mix Asphalt Materials, Mixture Design and Construction.* National Center for Asphalt Technology, NAPA Education Foundation, Baltimore, Maryland, Second Edition, 1996.
5. *SuperPave Mix Design Guide*. Superpave Series SP-2, Asphalt Institute. Lexington, Kentucky, 1997.
6. Bedi, H., *Development of Statistical Wet Weather Model to Evaluate Frictional Properties at the Pavement-Tire Interface on Hot Mix Asphalt Concrete.* Master's Thesis, Texas A&M University, College Station, Texas, December 2001.
7. American Society for Testing and Materials *(ASTM),* Annual Book of ASTM Standards, Vol. 04.02, ASTM, Philadelphia, Pennsylvania, 2000, pp. 664-668.
8. Chowdhury, A., *Evaluation of Superpave Fine Aggregate Specification.* Master's Thesis, Texas A&M University, College Station, Texas, May 1999.
9. American Society for Testing and Materials *(ASTM),* Annual Book of ASTM Standards, Vol. 04.08, ASTM, Philadelphia, Pennsylvania, 2000, pp 492-495.

10. Park D., C. Arif, J. Button, D.N. Little, and E. Masad. *Effects of Fine Aggregates on Rutting Resistance* (CD-ROM), Proceedings of 9th International Conference of Asphalt Pavement, Copenhagen, Denmark, August 2002.
11. Kandhal, P.S., and F. Parker, *Aggregate Tests Related to Asphalt Concrete Performance in Pavements.* Research Report 405, National Cooperative Highway Research Program, National Research Council, Washington, D.C., 1998.
12. Masad, E., *Review of Imaging Techniques for Characterizing the Shape of Aggregates Used in Asphalt Mixes.* Proc., 9th Annual Symposium, International Center for Aggregate Research, Austin, Texas, April 22-25, 2001.
13. Jahn, D.W., *Evaluation of Aggregate Particle Shapes through Multiple Ratio Analysis.* Proc., 8th Annual Symposium, International Center for Aggregate Research, Denver, Colorado, April 12-14, 2000.
14. Masad, E., D. Olcott, T. White, and L. Tashman. *Correlation of Fine Aggregate Imaging Shape Indices with Asphalt Mixture Performance.* Transportation Research Record 1757. Transportation Research Board, Washington, D.C., pp. 148-156. Geomaterials 2001.
15. Chandan, T., T. Fletcher, K. Sivakumar, and E. Masad., *Geometry Analysis of Aggregate Particles Using Imaging Techniques*, Department of Civil and Environmental Engineering, Washington State University, Pullman, Washington. June 2002.
16. Goldstein J., D. Newbury, P. Echlin, J. David, A. D. Romig, C. Fiori, and E. Lifshin, *Scanning Electron Microscopy and X-Ray Microanalysis.* A Text for Biologists, Materials Scientists and Geologists, Kluwer Academic Publishers, New York, February 2003.
17. JNNIE, The Joint NSF-NASA Initiative on Evaluation. *Report GA-A22123, B-108.* July 1995.
http://sdcd.gsfc.nasa.gov/ESS/annual.reports/ess95contents/app.inhouse.jnnie.html
18. Williams, C.R., and B.D. Prowell, *Comparison of Laboratory Wheel-Tracking Test Results with WesTrack Performance*, Transportation Research Record 1681,

Transportation Research Board, National Research Council, Washington, D.C., 1999.

19. *Asphalt Pavement Analyzer User's Guide*. Pavement Technology, Inc., Covington, Georgia, 1998.
20. Choubane, B., G.C. Page, and J. A. Musselman, *Suitability of Asphalt Pavement Analyzer for Predicting Rutting*. Transportation Research Record 1723, Transportation Research Board, National Research Council, Washington, D.C., 2000.
21. Kandhal, P.S. and R.B Mallick, *Evaluation of Asphalt Pavement Analyzer for HMA Design,* NCAT Report No. 99-4, National Center for Asphalt Technology, Auburn University, Alabama, 1999.
22. Aschenbrener T., *Evaluation of Hamburg Wheel-Tracking Device to Predict Moisture Damage in Hot-Mix Asphalt,* Transportation Research Record 1492, Transportation Research Board, National Research Council, Washington, D.C., 1995.
23. Cooley, Jr. L.A., P.S. Kandhal, M.S. Buchanan., F. Fee, and A. Epps, *Loaded Wheel Testers in the United States: State of the Practice,* Transportation Research E-Circular No. E-C016, Transportation Research Board, National Research Council, Washington, D.C., July 2000.
24. Shah, B., *Evaluation of Moisture Damage within Asphalt Concrete Mixes,* Master's Thesis, Texas A&M University, College Station, Texas, August 2003.

APPENDIX A

CORRELATION BETWEEN IMAGE ANALYSIS RESULTS AND PHYSICAL TEST RESULTS

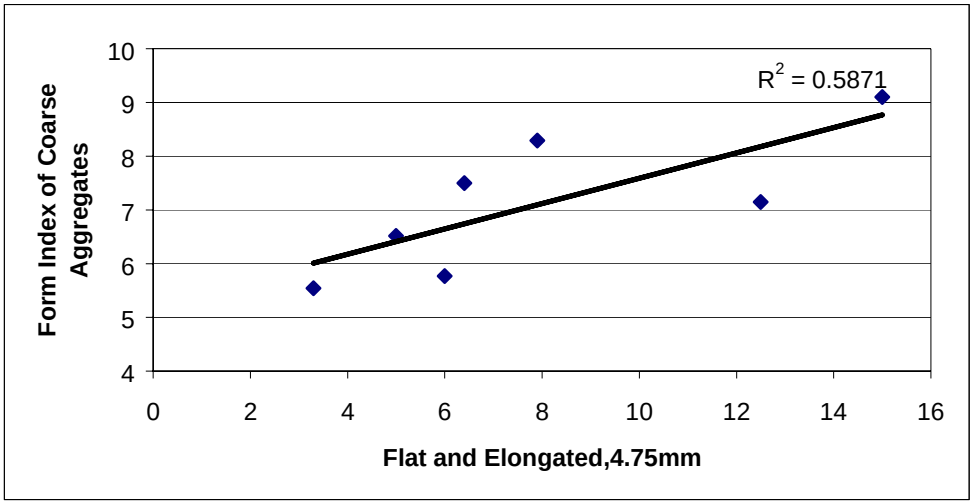

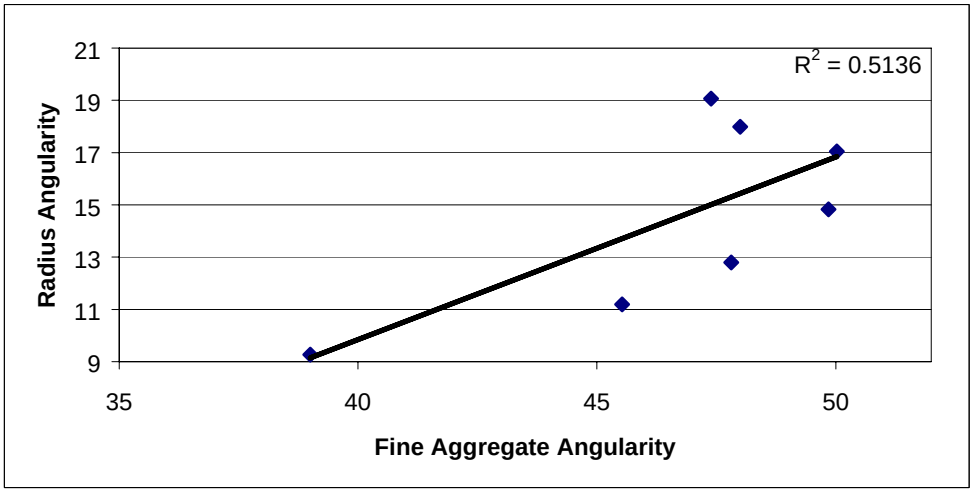

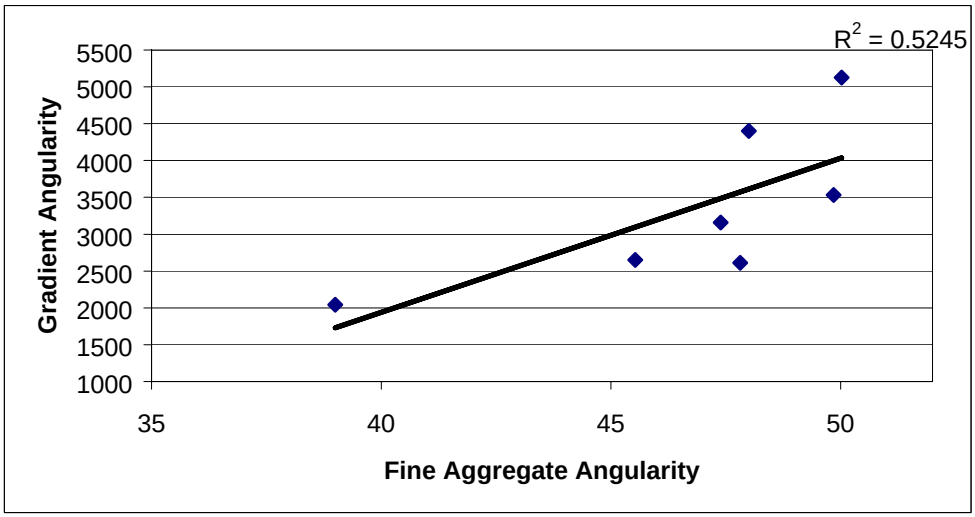

Figure A1. Correlation between Fine Aggregate Angularity, Flat and Elongated Results, and Image Analysis Results.

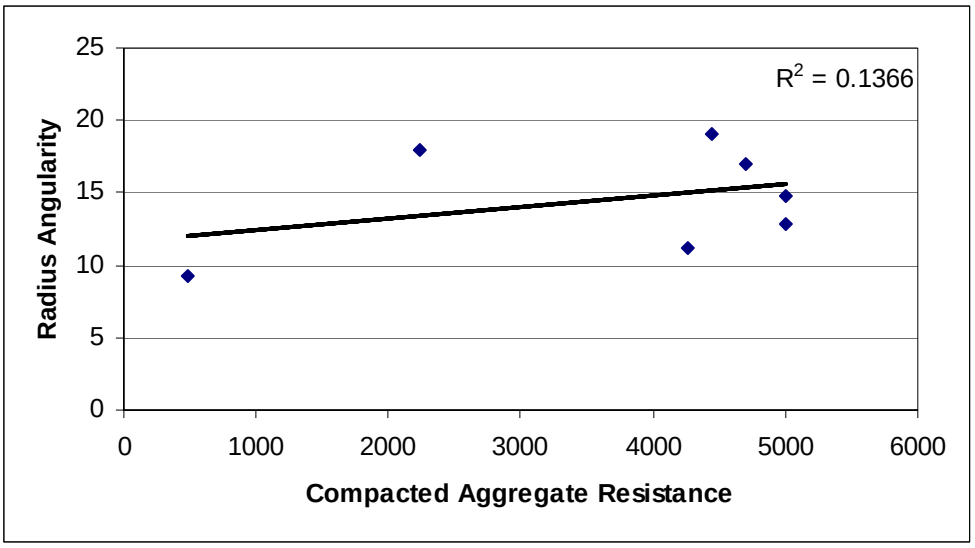

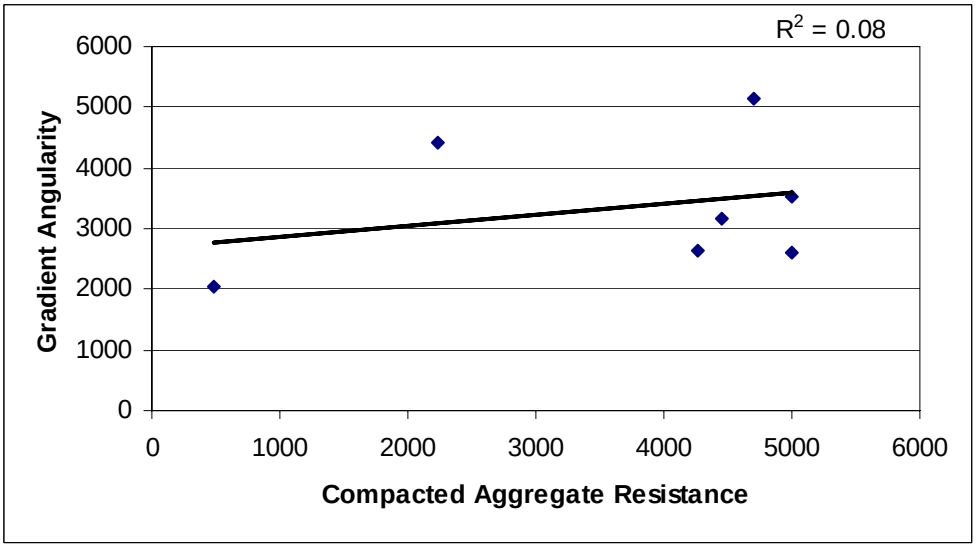

Figure A2. Correlation between Compacted Aggregate Resistance and Image Analysis Results.

APPENDIX B

EFFECT OF CRUSHING ON IMAGE ANALYSIS RESULTS

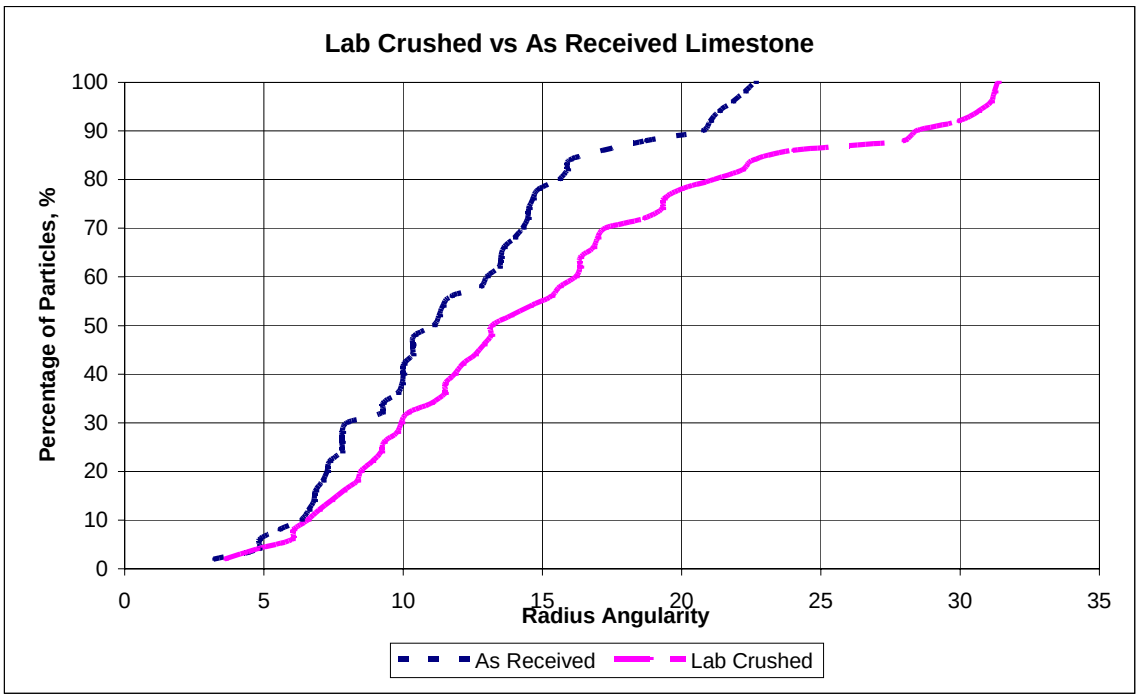

Figure B1. Effect of Crushing on Radius Angularity of Limestone Aggregate.

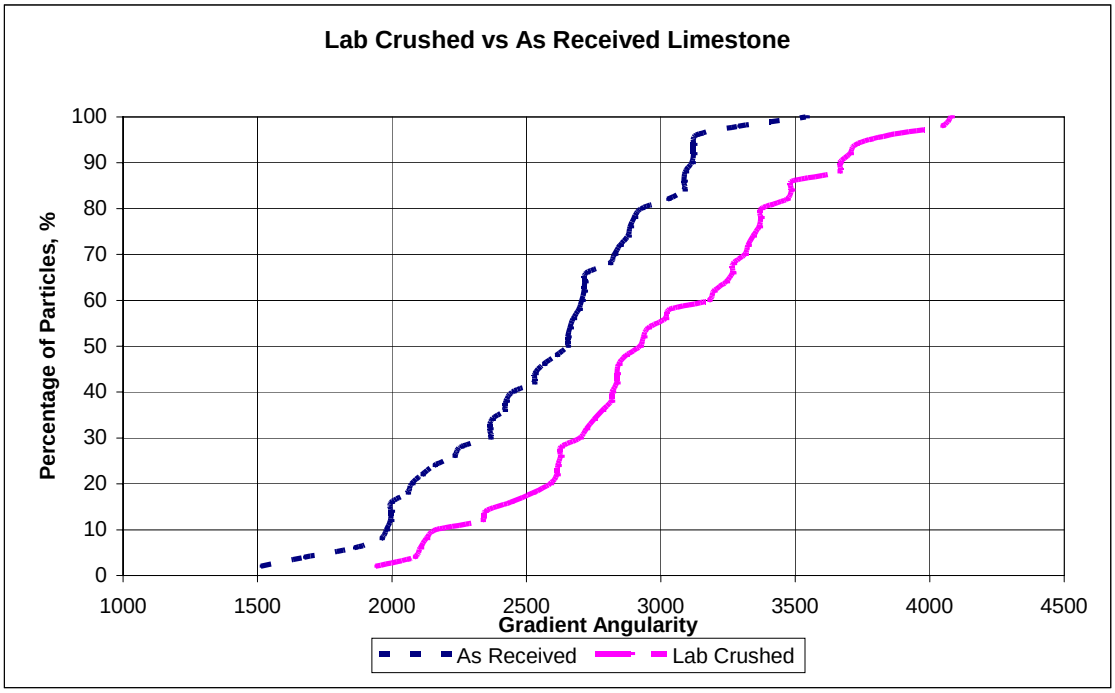

Figure B2. Effect of Crushing on Gradient Angularity and Radius Angularity of Limestone Aggregate.

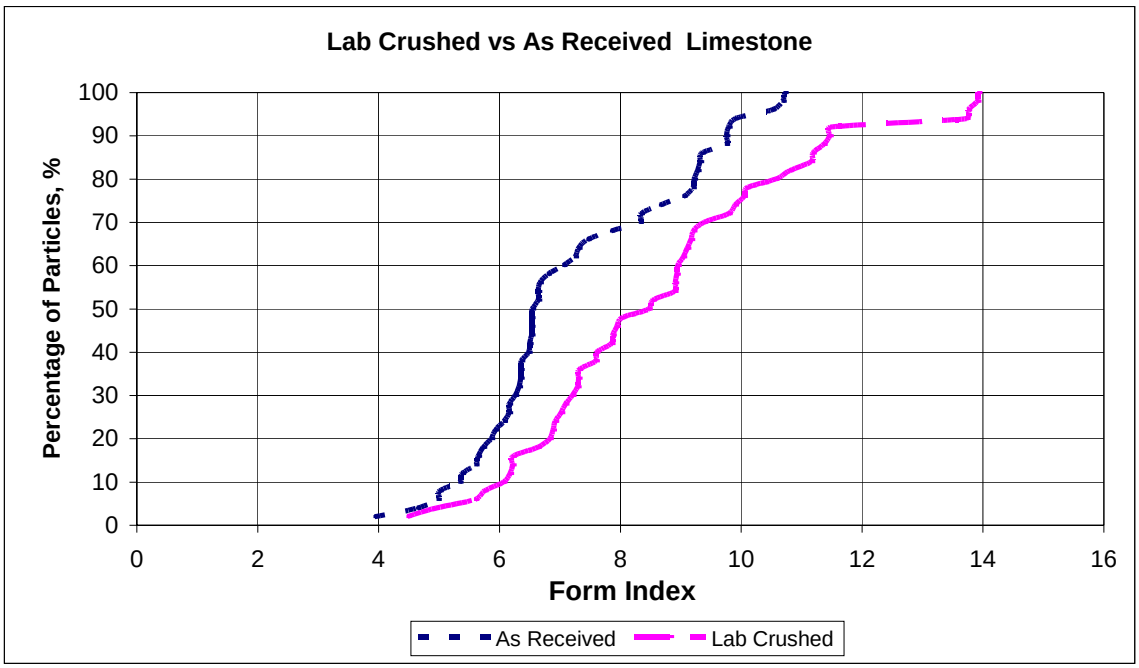

Figure B3. Effect of Crushing on Form Index of Limestone Aggregate.

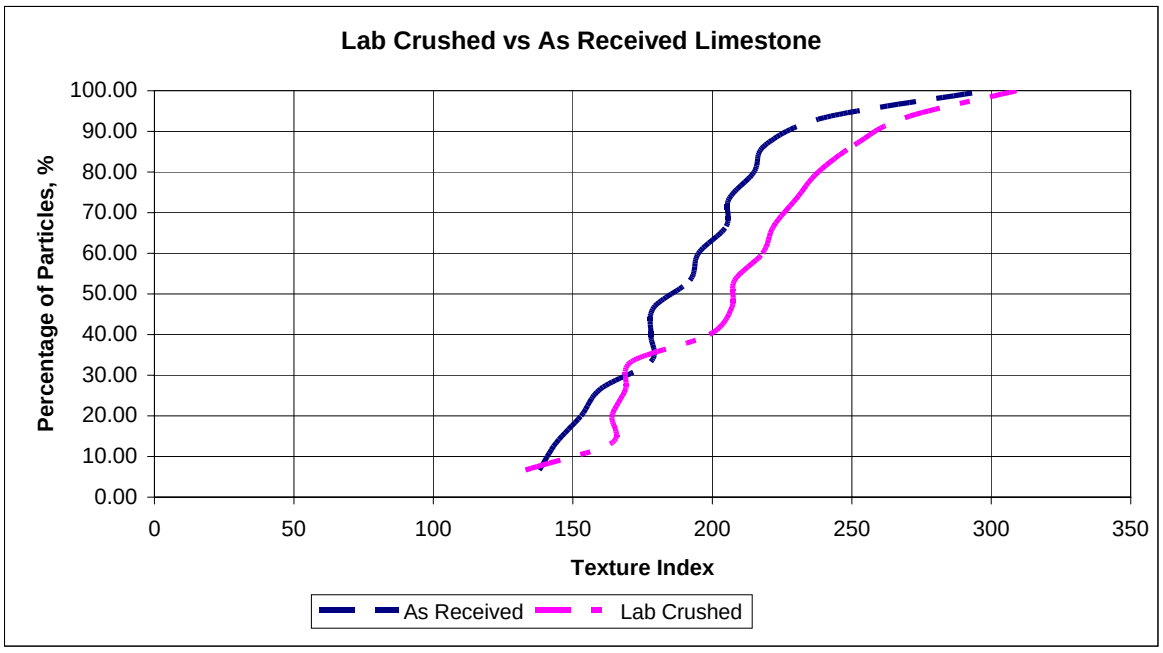

Figure B4. Effect of Crushing on Texture Index of Limestone Aggregate.

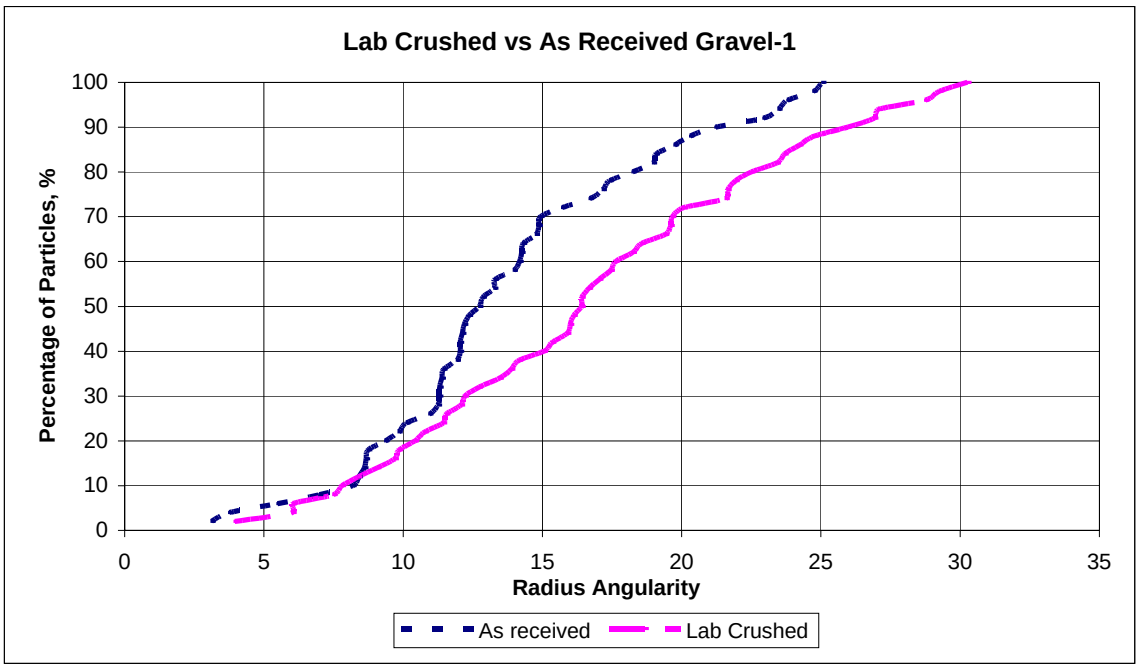

Figure B5. Effect of Crushing on Radius Angularity of Gravel-1 Aggregate.

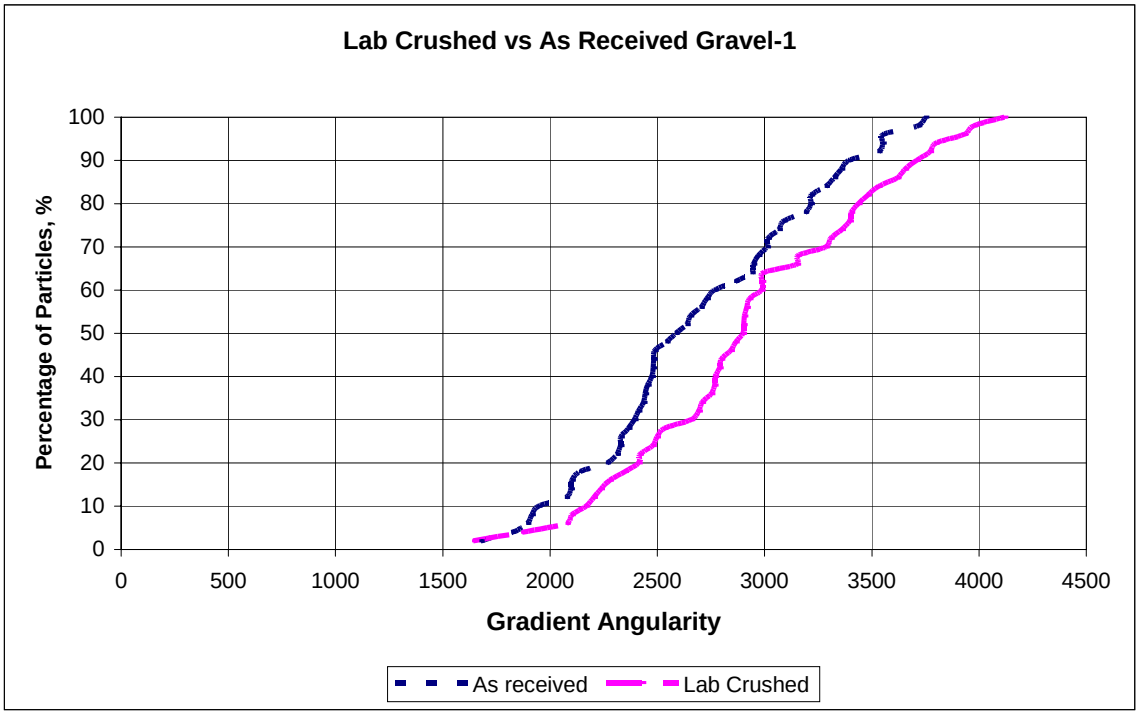

Figure B6. Effect of Crushing on Gradient Angularity of Gravel-1 Aggregate.

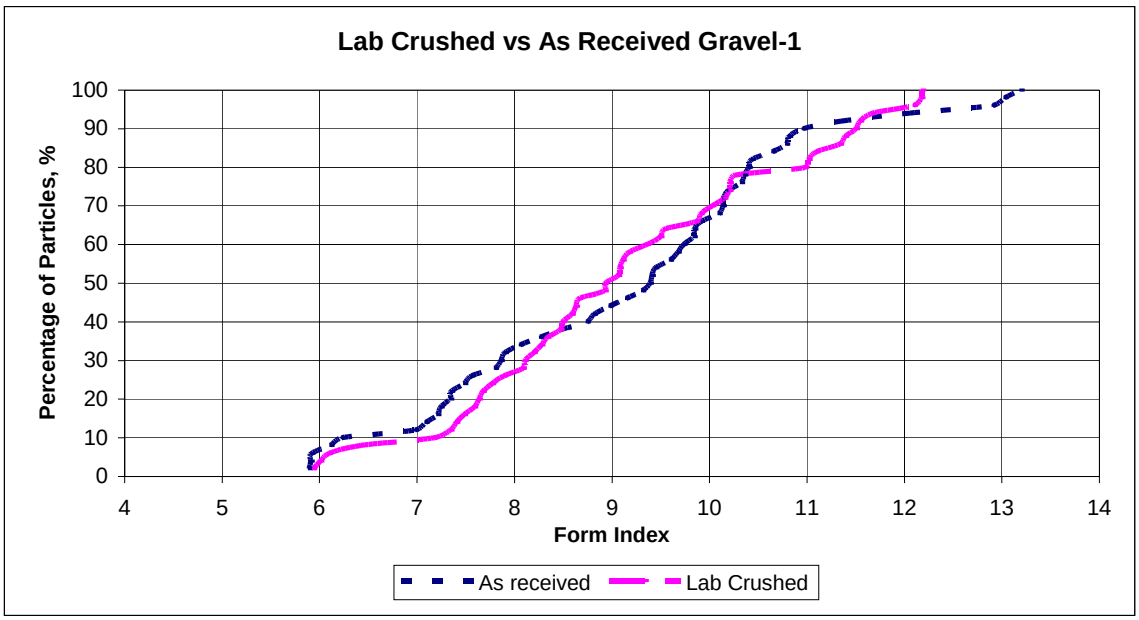

Figure B7. Effect of Crushing on Form Index of Gravel-1 Aggregate.

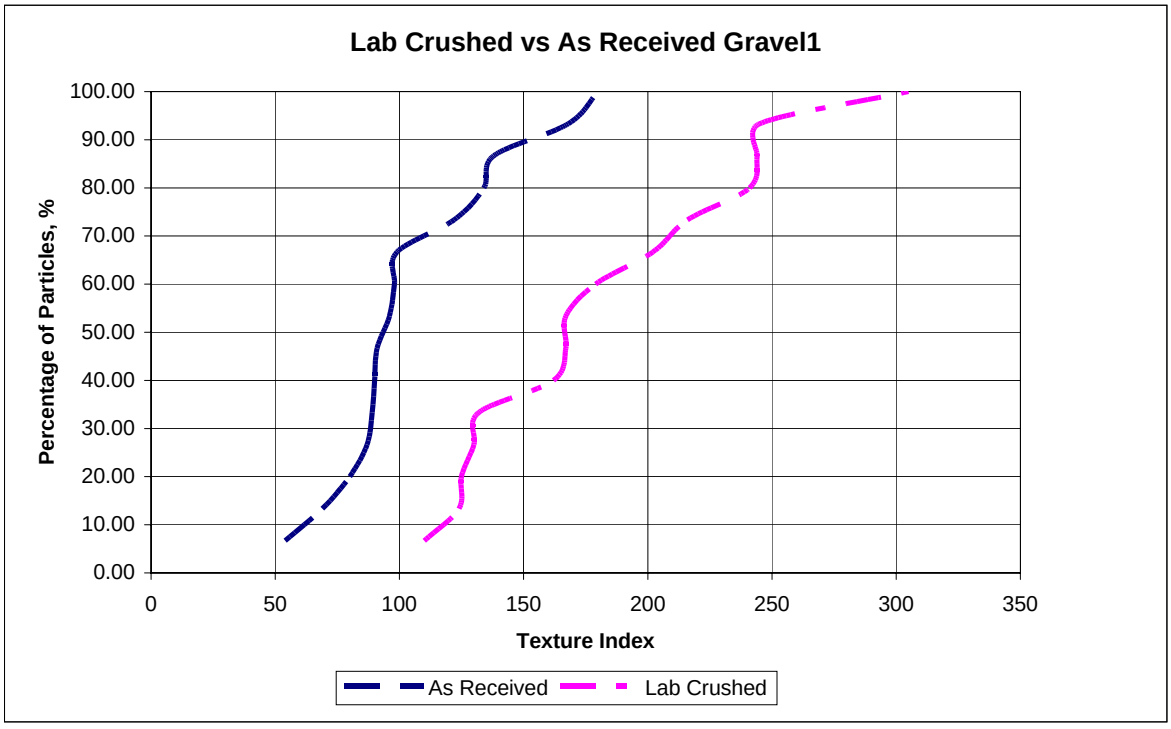

Figure B8. Effect of Crushing on Texture Index of Gravel-1 Aggregate.

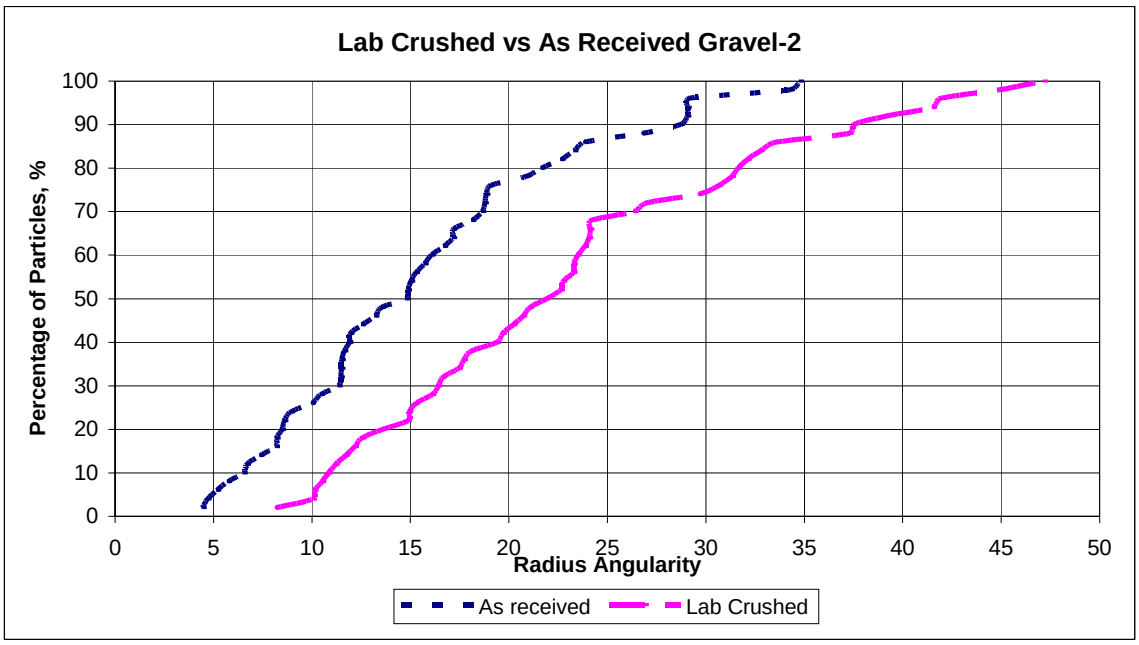

Figure B9. Effect of Crushing on Radius Angularity of Gravel-2 Aggregate.

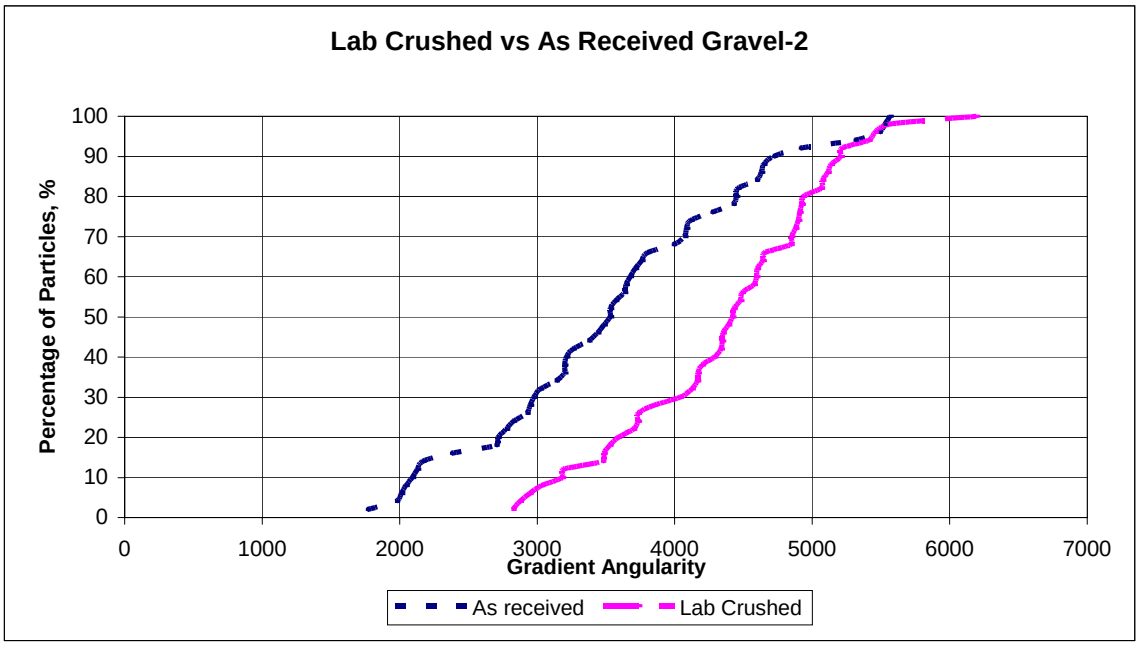

Figure B10. Effect of Crushing on Gradient Angularity of Gravel-2 Aggregate.

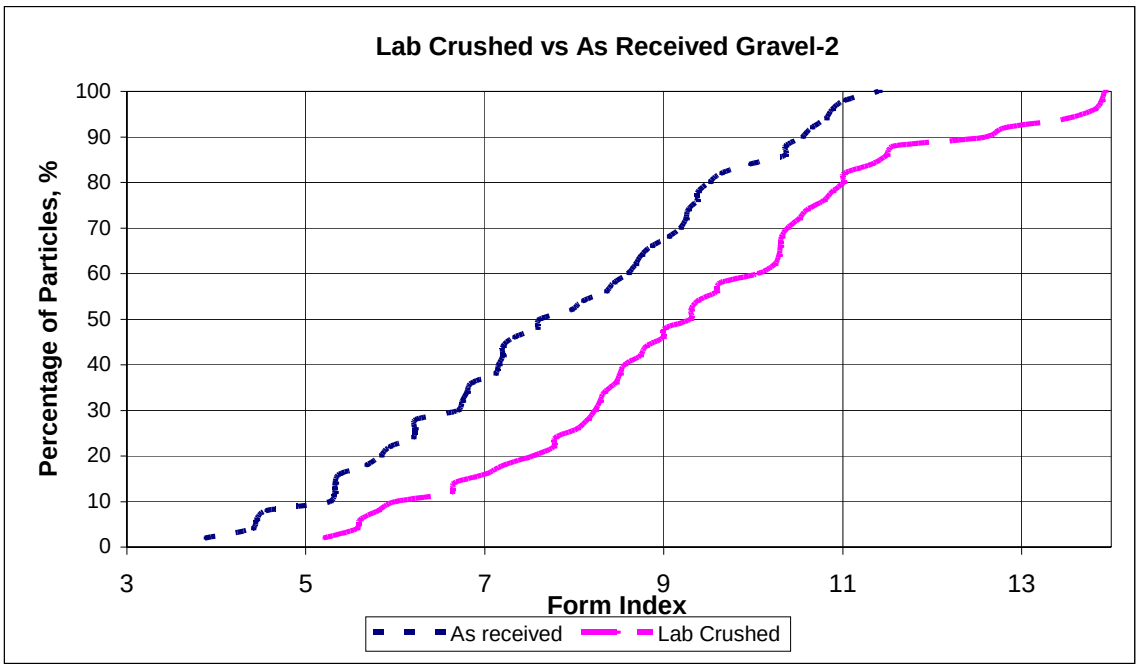

Figure B11, Effect of Crushing on Form Index of Gravel-2 Aggregate.

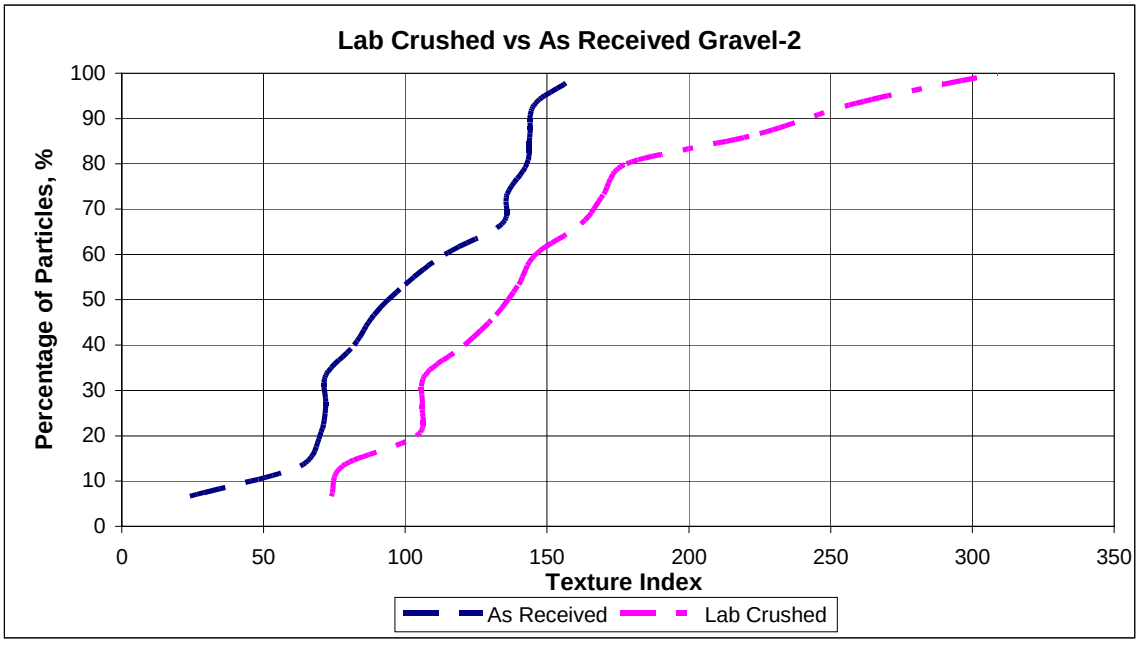

Figure B12. Effect of Crushing on Texture Index of Gravel-2 Aggregate.

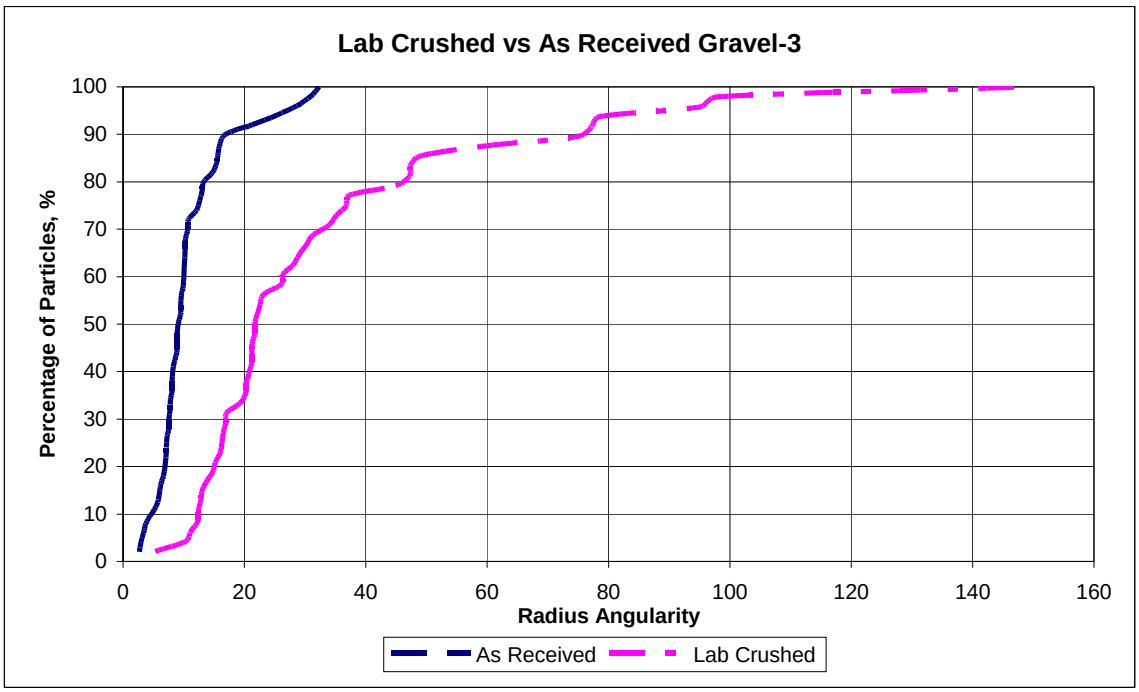

Figure B13. Effect of Crushing on Radius Angularity of Gravel-3 Aggregate.

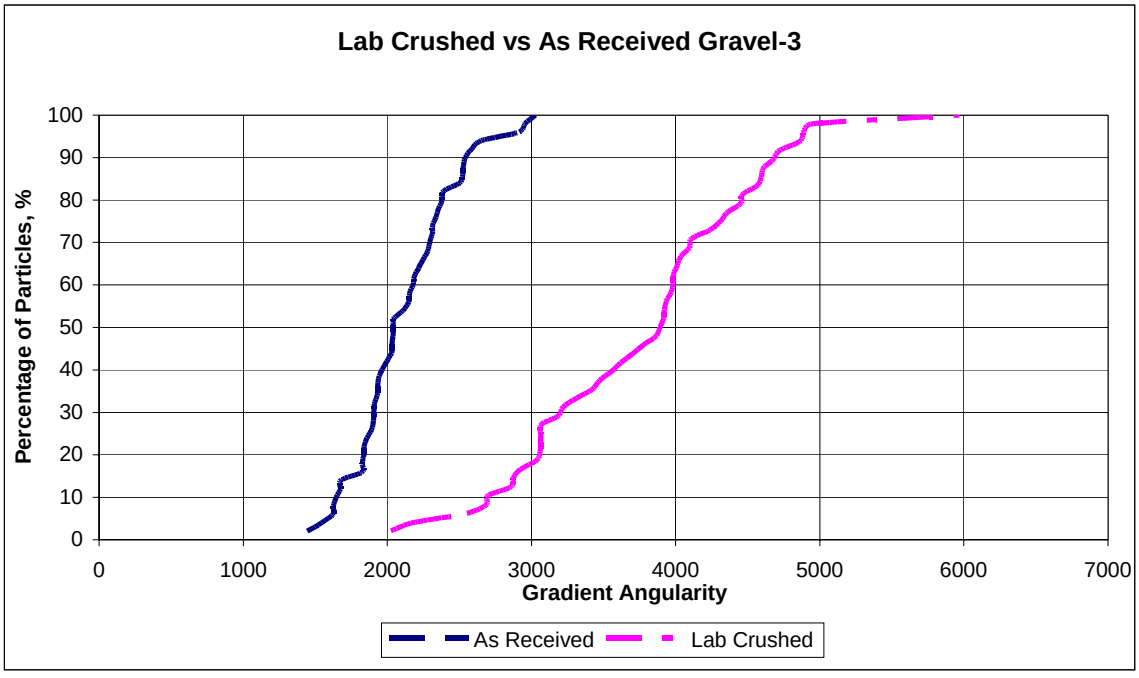

Figure B14. Effect of Crushing on Gradient Angularity of Gravel-3 Aggregate

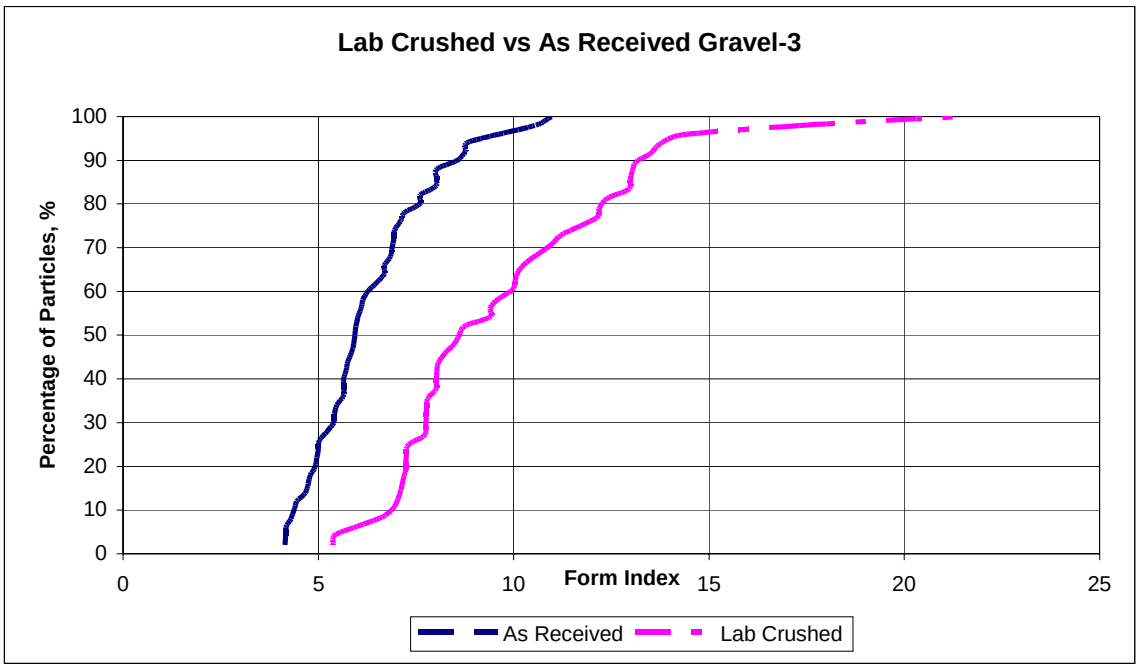

Figure B15. Effect of Crushing on Form Index of Gravel-3 Aggregate.

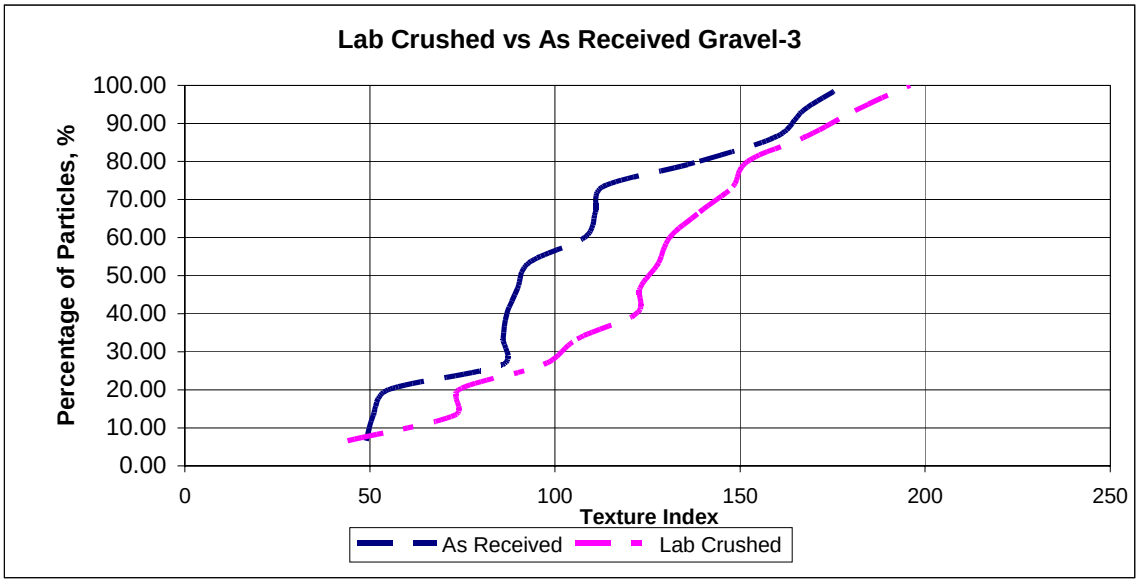

Figure B16. Effect of Crushing on Texture Index of Gravel-3 Aggregate.

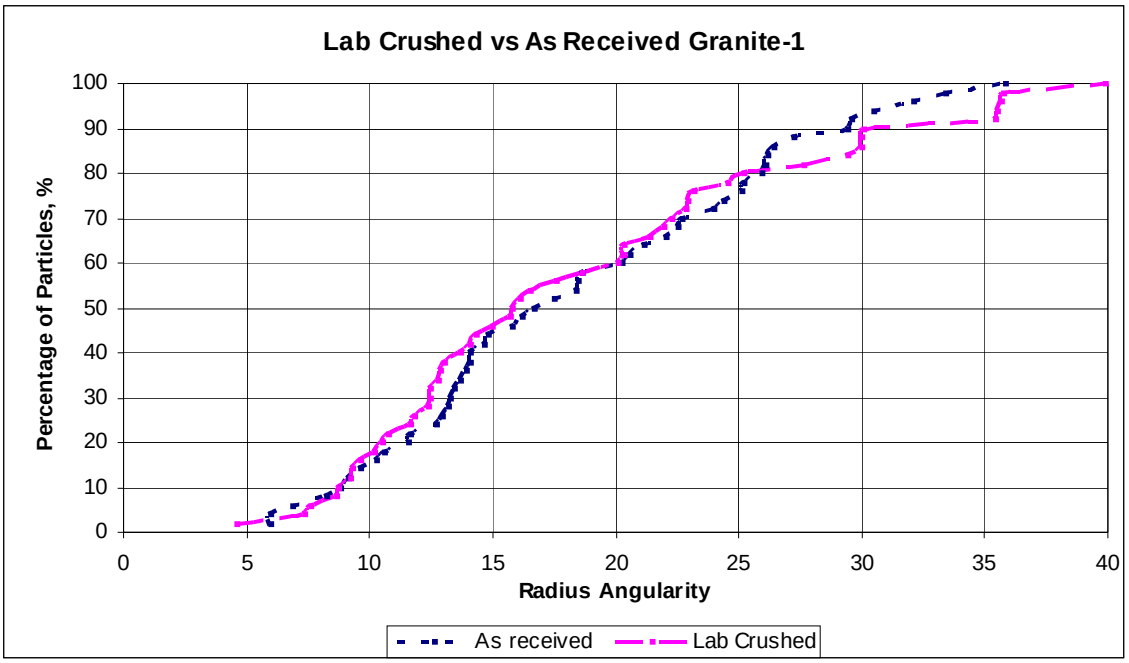

Figure B17. Effect of Crushing on Radius Angularity of Granite-1 Aggregate.

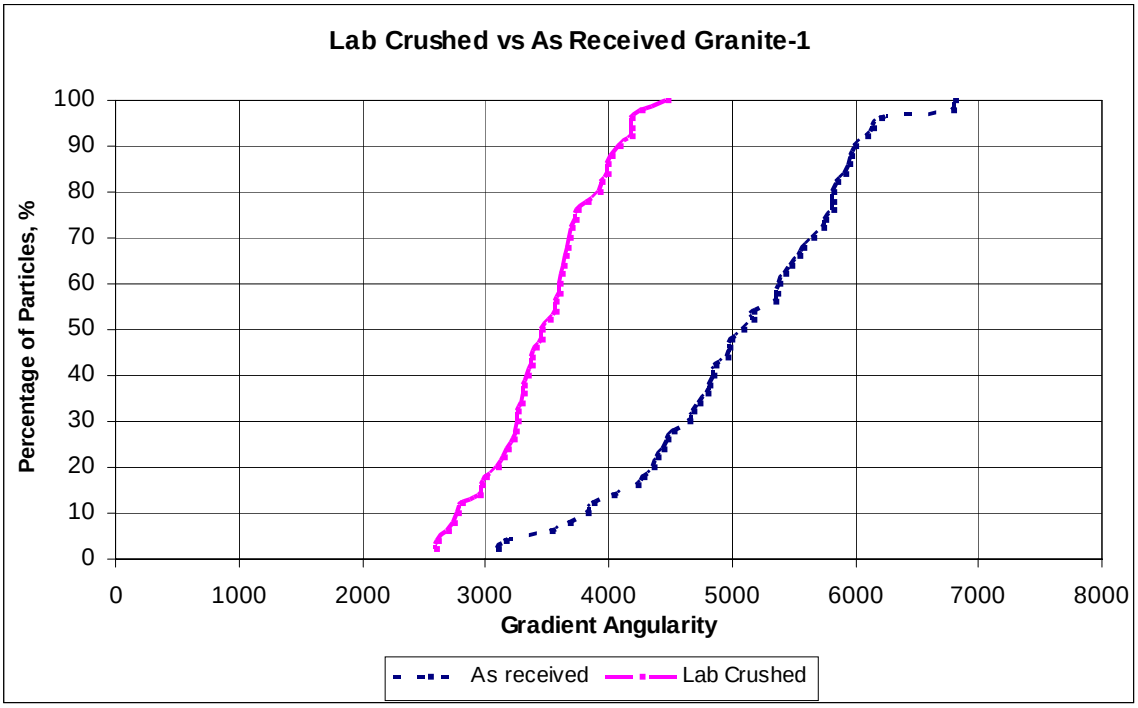

Figure B18. Effect of Gradient Angularity on Granite-1 Aggregate.

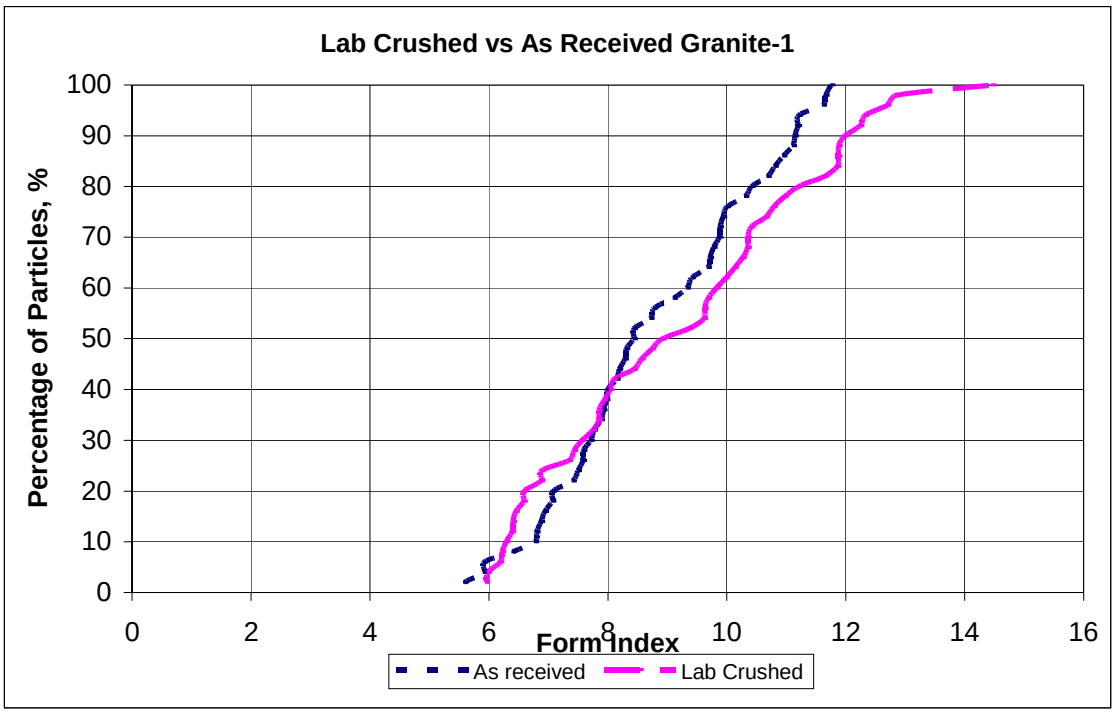

Figure B19. Effect of Form Index on Granite-1 Aggregate.

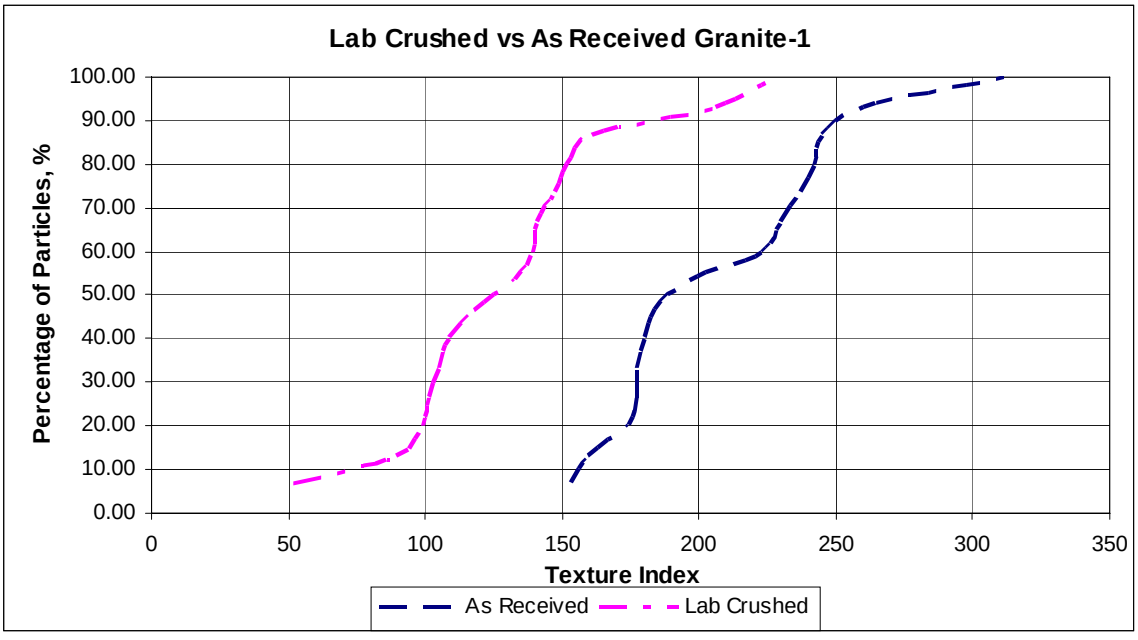

Figure B20. Effect of Texture Index on Granite-1 Aggregate.

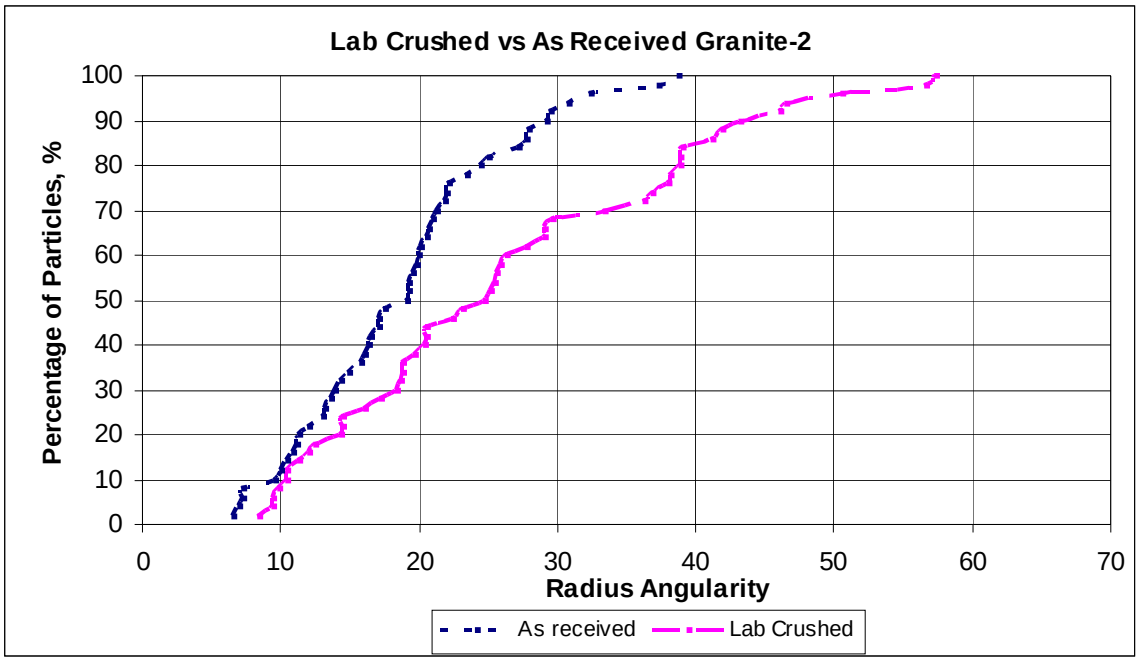

Figure B21. Effect of Crushing on Radius Angularity on Granite-2 Aggregate.

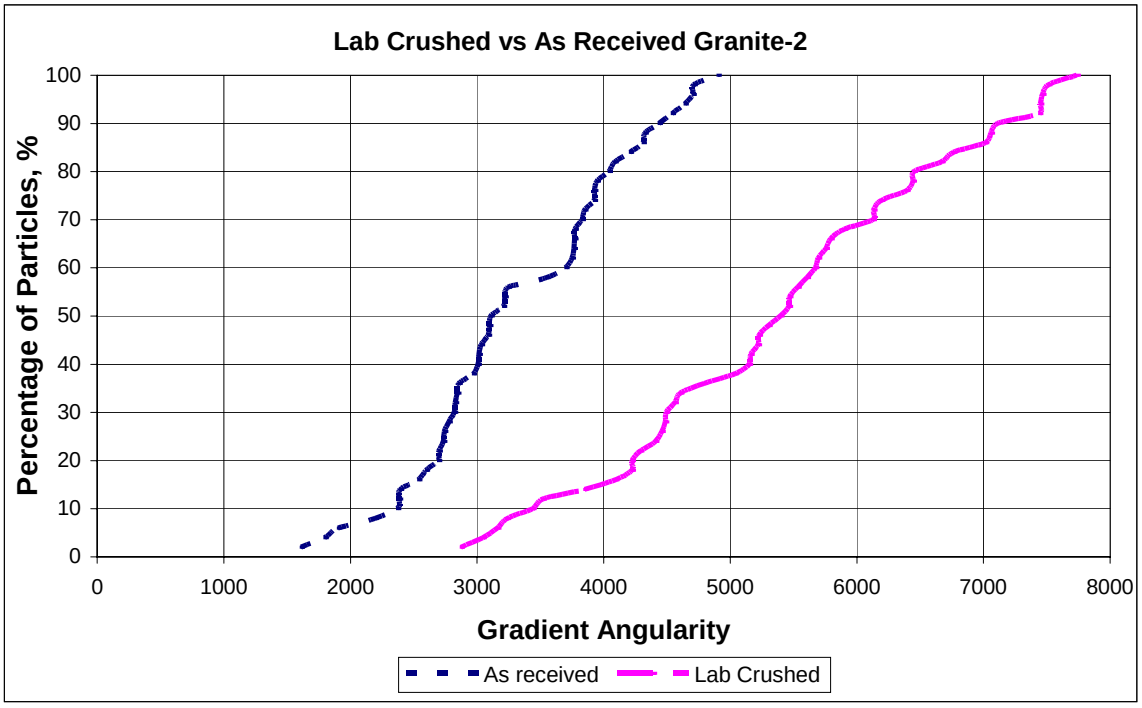

Figure B22. Effect of Crushing on Gradient Angularity on Granite-2 Aggregate.

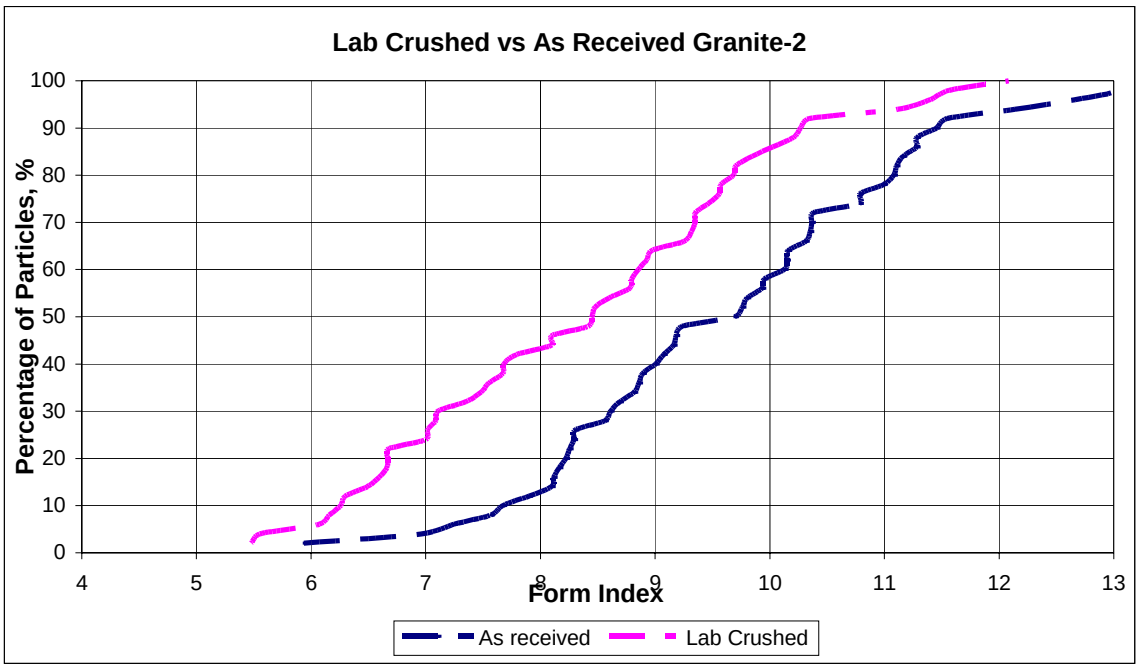

Figure B23. Effect of Crushing on Form Index of Granite-2 Aggregate.

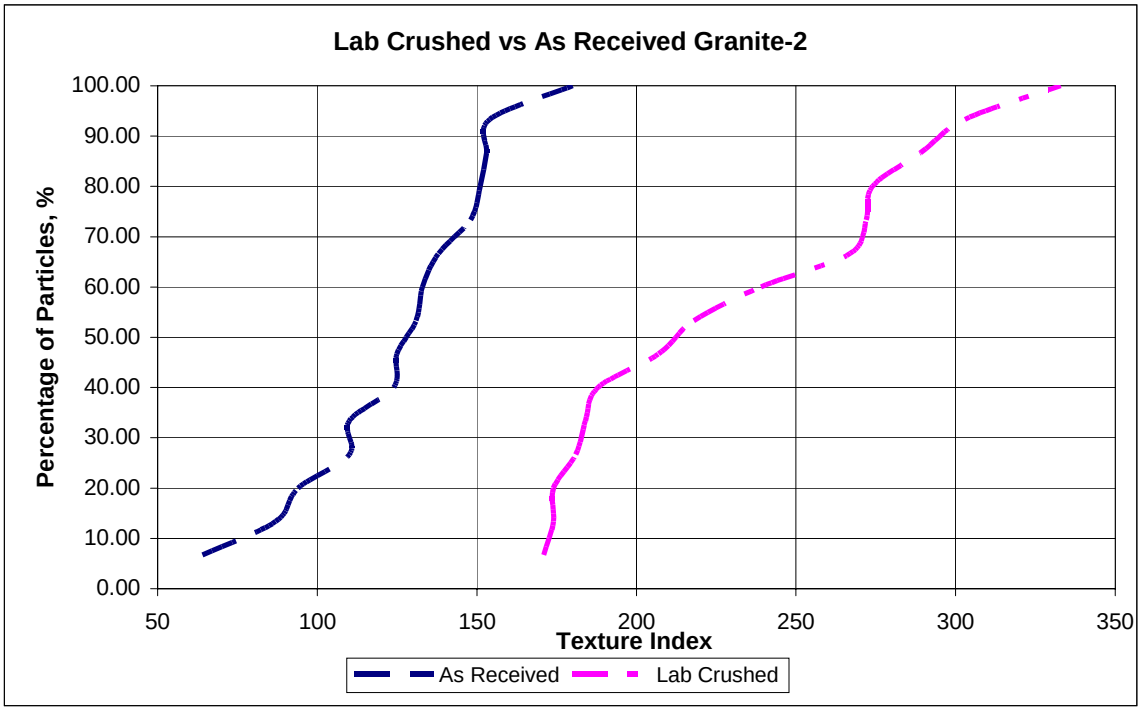

Figure B24. Effect of Crushing on Texture Index of Granite-2 Aggregate.

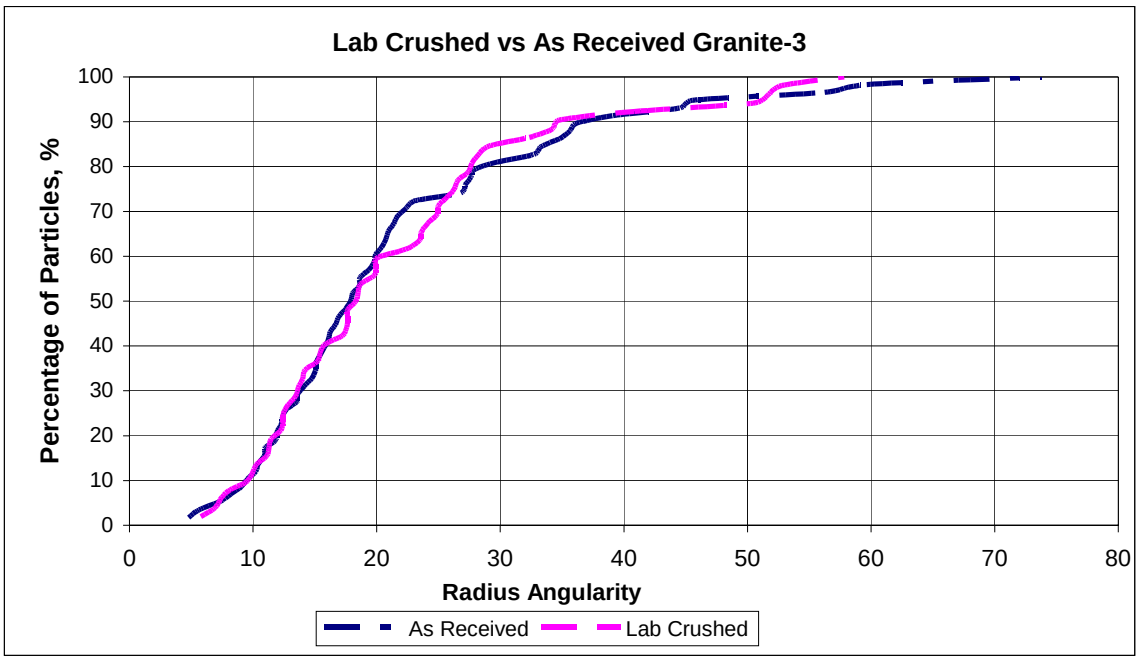

Figure B25. Effect of Crushing on Radius Angularity of Granite-3 Aggregate.

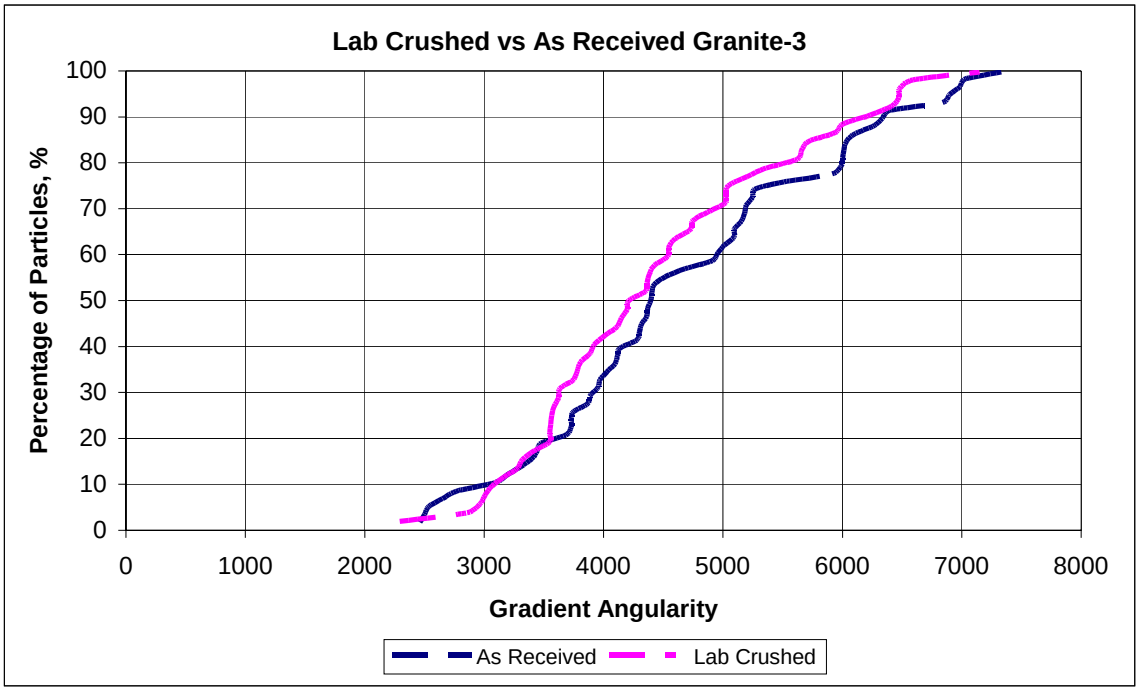

Figure B26. Effect of Crushing on Gradient Angularity of Granite-3 Aggregate.

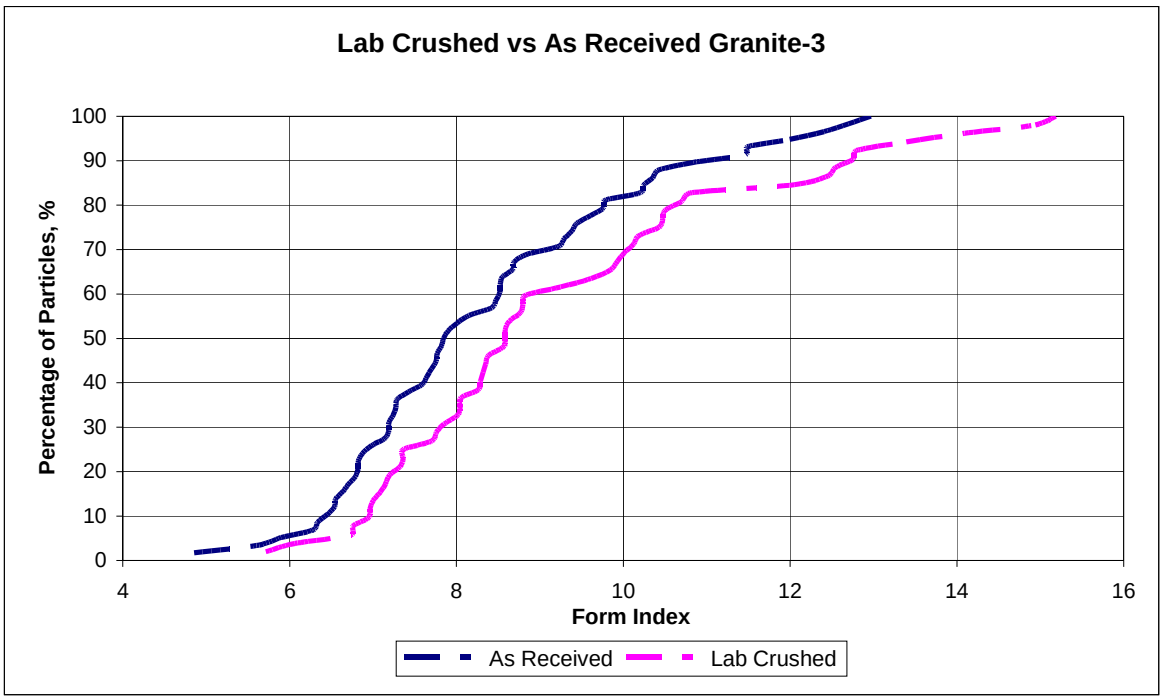

Figure B27 Effect of Crushing on Form Index of Granite-3 Aggregate.

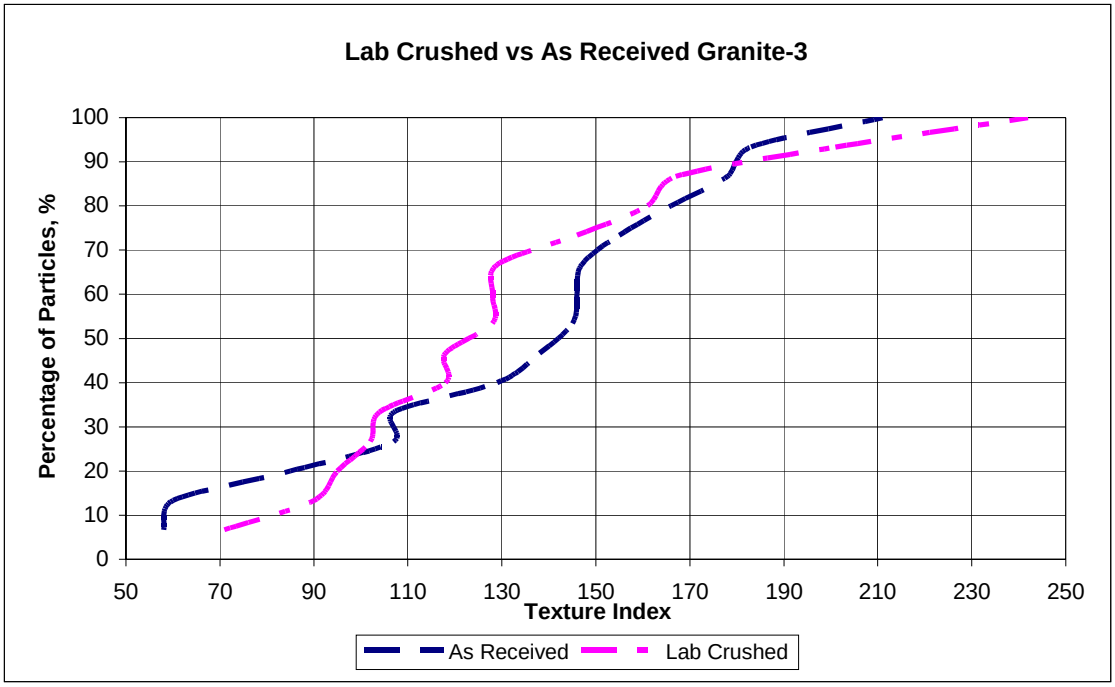

Figure B28. Effect of Crushing on Texture Index of Granite-3 Aggregate.

\

APPENDIX C

NORMAL PROBABILITY PLOTS OF CRUSHED AND AS RECEIVED FINE AGGREGATES

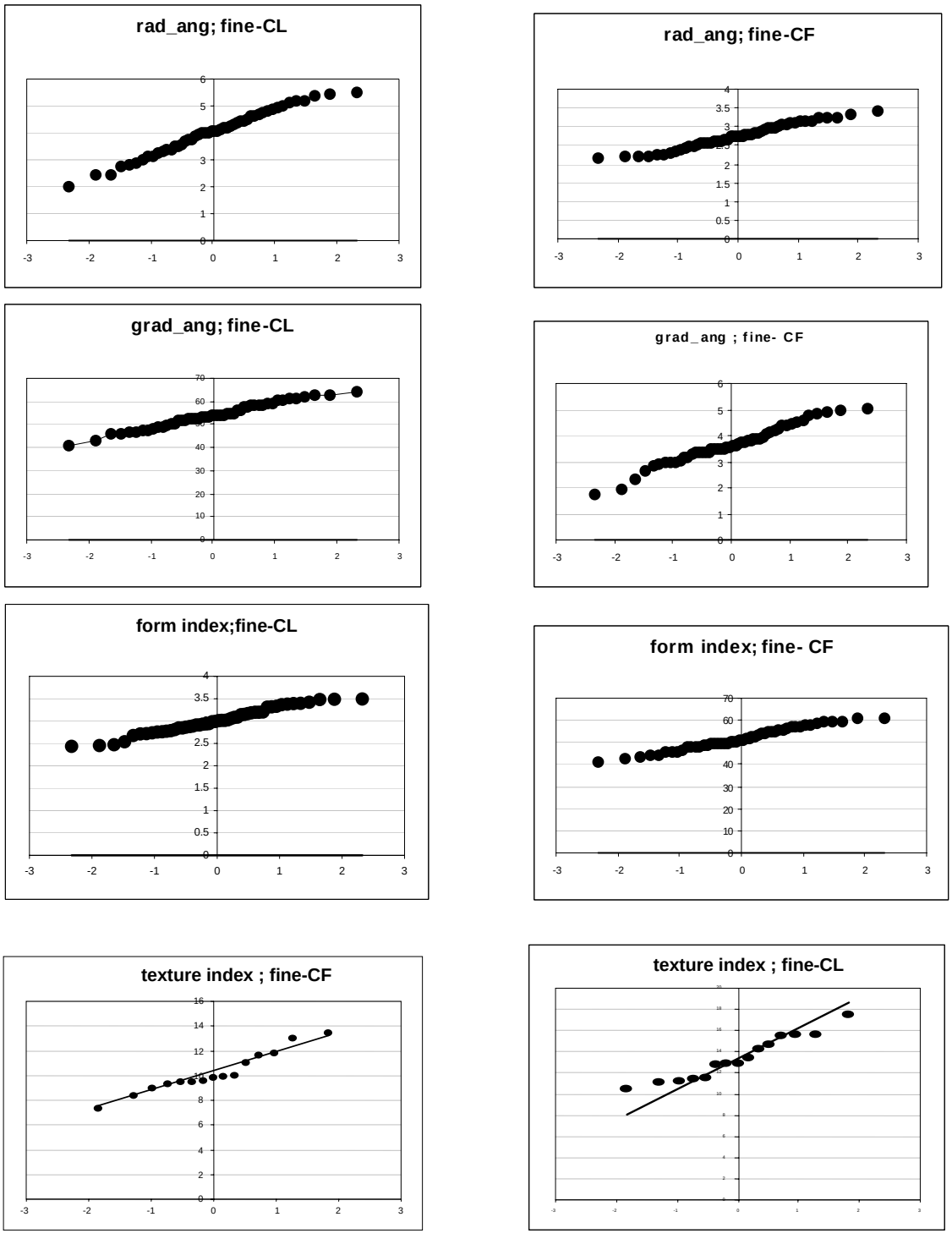

Figure C1. Gravel-1 -Square Root of Original Values which Fits the Normal Curve.

CL = crushed lab, CF = crushed field.

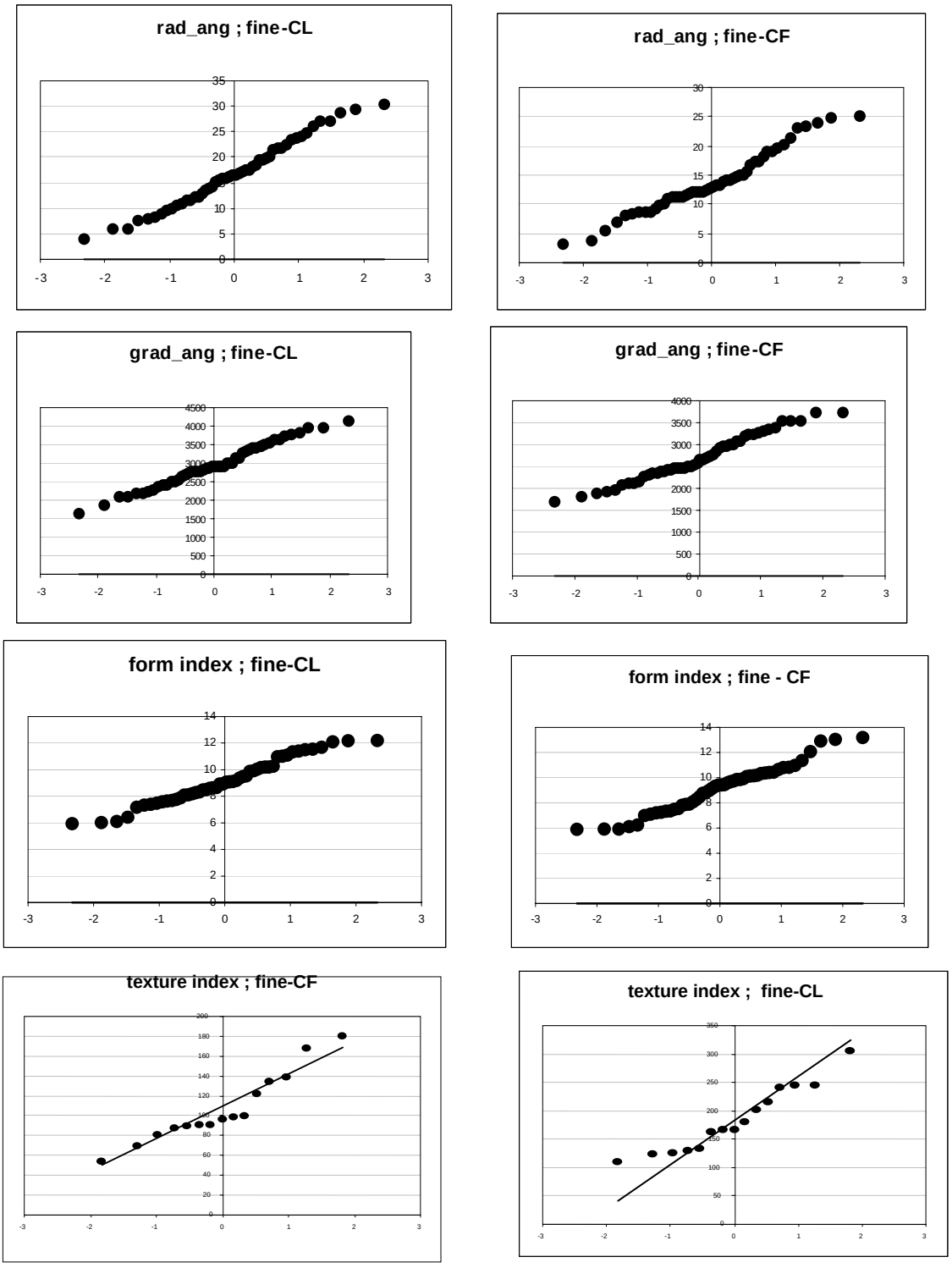

Figure C2. Gravel-1 - Original Values which Do Not Fit the Normal Curve and Are Deviating at Tails. ***CL = crushed lab, CF = crushed field.***

APPENDIX D

LIMESTONE, GRANITE AND GRAVEL SELECTED FOR PERFORMANCE TESTS

Figure D1. Georgia Granite Aggregate Particles-Granite-3 Passing 25 mm and Retained on 12.5 mm Sieve.

Figure D2. Martin Marietta Limestone Aggregate Particles, Texas Passing 25 mm and Retained on 12.5 mm Sieve.

Figure D3. Brazos River Gravel Aggregate Particles, Texas-Gravel-3 Passing 12.5 mm and Retained on 9.5 mm Sieve Size.